universität wien

MASTERARBEIT / MASTER'S THESIS

Titel der Masterarbeit / Title of the Master's Thesis

"The NFκB/STAT3/PD-L1 network and its impact on the tumor aggressiveness of *TERT* promoter wild-type versus mutated Glioblastoma"

verfasst von / submitted by

Lisa Gabler, BSc

angestrebter akademischer Grad / in partial fulfilment of the requirements for the degree of

Master of Science (MSc)

Wien, 2016 / Vienna 2016

Studienkennzahl lt. Studienblatt / degree programme code as it appears on the student record sheet:	A 066 830
Studienrichtung lt. Studienblatt / degree programme as it appears on the student record sheet:	Molecular Microbiology, Microbial Ecology and Immunobiology
Betreut von / Supervisor:	Univ. Prof. Dr. Walter Berger

INSTITUTE OF CANCER RESEARCH
MEDICAL UNIVERSITY OF VIENNA

This Master's Thesis was conducted at the

Medical University of Vienna

Department of Medicine I

Institute of Cancer Research

Applied and experimental oncology

And was supervised by

Univ. Prof. Dr. Walter Berger

Daniela Loetsch, PhD

“There is nothing like looking,

if you want to find something”

J.R.R. Tolkien

Danksagung

"Live as if you were to die tomorrow; learn as if you were to live forever"

Mahatma Gandhi

Zu allererst möchte ich meiner Familie ein riesiges Dankeschön aussprechen; durch sie wurde mir dieses Studium erst ermöglicht. Allen voran gilt mein Dank meinen Eltern *Eva und Rudi*, die seit meiner Kindheit meine Wissbegierde und Neugierde förderten und mich ständig vor neue Herausforderungen stellten. Danke für eure Liebe und Geborgenheit. Meiner Schwestern *Ines* danke ich für ihre unendliche Geduld und enge Freundschaft die sie mir zu jeder Zeit schenkt. Ebenso gilt mein Dank meinen Großeltern *Heidi und Rudi*, sowie meinem Onkel *Markus*, die unerschütterlich an meiner Seite stehen und unsere Familie zusammenhalten. Bedanken möchte ich mich außerdem bei meiner besten Freundin *Resi*. Danke für dein offenes Ohr, deine starke Schulter und die vielen Stunden die wir lachend, weinend, tanzend und laufend zusammen verbracht haben.

Mein besonderer Dank gilt außerdem all jenen, die mir mit Rat und Tat bei der Durchführung der praktischen Arbeit, sowie beim Verfassen dieser Masterarbeit zur Seite standen. Insbesondere bedanke ich mich daher sehr herzlich bei:

Univ. Prof. Dr. Walter Berger, für die Ermöglichung dieses Projekts und seine unterstützende und motivierende Betreuung besonders in der Endphase. Danke, dass ihr mich so freundschaftlich und familiär in deiner Forschungsgruppe aufgenommen habt.

Daniela Lötsch, PhD, für ihre fachlich kompetente und freundschaftliche Betreuung. Danke für die geduldige Einschulung, die genauen und zahllosen Entwurfskorrekturen, die vielen Ideen und die andauernde Unterstützung während des gesamten Projektes.

Der gesamten Berger-Gruppe, insbesondere jedoch bei *Sushilla van Schoonhoven, Bernhard Englinger, PhD, Dominik Kirchhofer* und *Mirjana Stojanovic* für stundenlange Erklärungen, inspirierende Daten-Diskussionen und für ihre stetige Hilfsbereitschaft.

Sabine Spiegl-Kreinecker und ihrem Team vom Neuromed Campus des Kepler-Universitäts-Klinikums Linz, für die Ermöglichung des Forschungsstipendiums, für die Zurverfügungstellung einiger Zelllinien sowie für die Durchführung der TRAP-Assays.

Table of contents

1 Introduction

1.1 Cancer incidence and mortality

In 2012, 39,014 new cases of malignant cancer were diagnosed and around 315,000 people are currently suffering from malignancies in Austria *(1)*. The incidence of cancer has been continuously increasing in the last decades *(2)*. In the year 2015, cancer deaths accounted for about one fourth of all deaths in Austria (20,349 vs. 83,073), making cancer the second leading cause of death (grey line) after cardiovascular diseases (orange line) with a slight increase in males compared to females (259 vs. 213 per 100,000 people) (Figure.1) *(1).* With respect to the incidence and the mortality rates, cancer constitutes one of the most devastating diseases nowadays *(3)*.

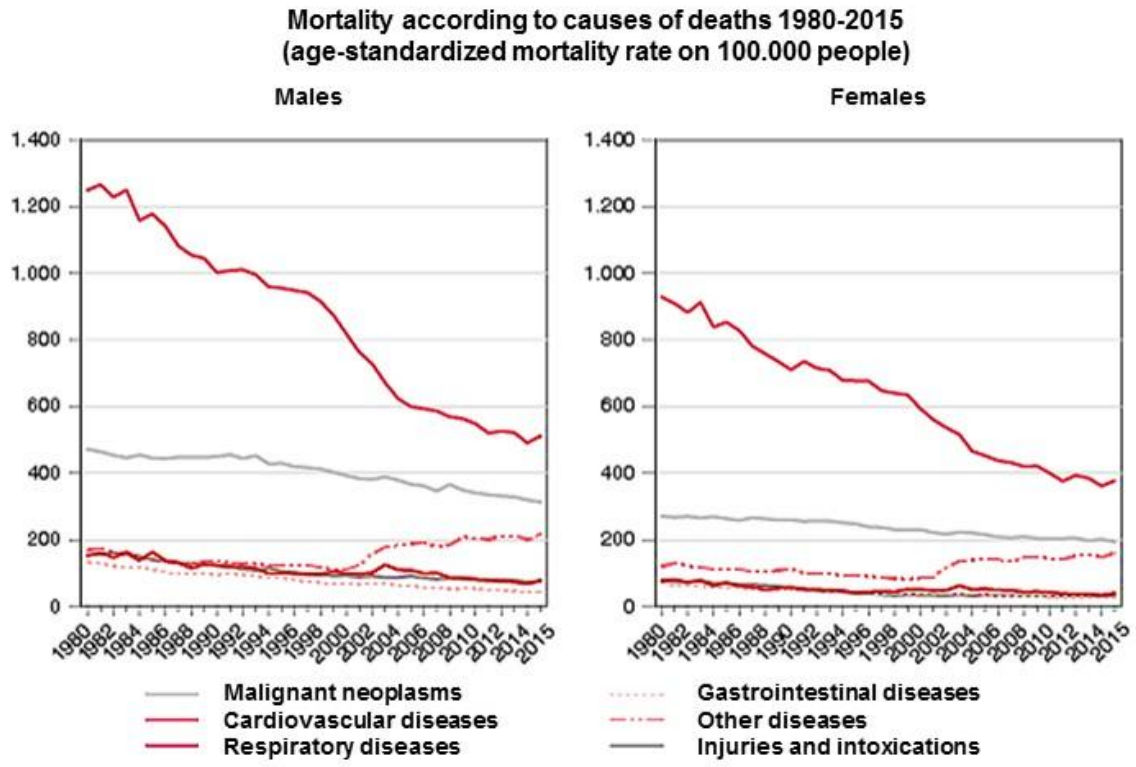

Figure 1. Mortality rate according to causes of deaths in Austria from 1980-2015 (age-standardized mortality rate on 100,000 people). Cancer is the second leading cause of death after cardiovascular diseases (grey vs. orange line). In 2015, the mortality rate for malignancies (grey line) in males (left diagram) was about 1.2 times higher than in females (right diagram) (259 vs. 213 per 100,000 people). (adapted from *(1)*)

1.2 Etiology of cancer

In general, tumors are sub-classified into benign and malignant neoplasias. Benign tumors are characterized by their localized and non-invasive growth pattern, whereas malignant tumors, casually referred to as cancer, are invasive and metastatic neoplasias. *(4)* Although a multitude of various impact factors exists increasing the probability for cancer generation and development, the existence of a common driver for all types of malignancies has not been confirmed yet and hence is rather questionable.

Cancer arises from endogenous somatic cells or from germ cells by a mechanism called malignant transformation. Malignant transformation can have various reasons, however, it is often caused by genomic alterations or dysregulated cellular processes leading to an intracellular imbalance. *(4)* Gene mutations can result in upregulation or downregulation/ silencing of genes, however, they always lead to altered gene expression profiles in cells *(5)*. If proto-oncogenes acquire an activating mutation, they turn into oncogenes *(6)*. In contrast, mutations in tumor suppressor genes cause loss of function due to downregulation and silencing of gene expression or translation of a non-functional protein *(5)*. Although, oncogenes as well as suppressor genes have a completely different way of acting, both have the potential to cause cancer. Important hallmarks of cancer in this context are reduced self-limiting potential and increased proliferation rate, both enabling growth and spreading of this devastating disease *(4)*.

1.3 The hallmarks of cancer

In 2000, Hanahan and Weinberg postulated the six hallmarks of cancer (Figure 2), defining the multi-step process of cancer development, aggressiveness, maintenance and progression *(4)*. These hallmarks include sustaining proliferative signaling, evading growth suppressors, resisting cell death, enabling replicative immortality, inducing angiogenesis and activating invasion, and metastasis (Figure 2). Furthermore, a variety of factors influencing these hallmarks and/or underlying their functions were characterized. As an example, the proliferative signaling like autocrine stimulation is for example sustained via platelet derived growth factor (PDGF) or epidermal growth factor (EGF). The transforming growth factor β (TGF-β) is crucial in evading growth suppressors. Anti-apoptotic factors or apoptotic antagonists like B-cell lymphoma 2 (Bcl-2) are essential factors in resisting cell death. The maintenance of the telomeric function by upregulation of the telomerase activity avoids shortening of the telomeres, thus preventing senescence. This mechanism is underlying the hallmark of enabling replicative

immortality, which is crucial in more or less all malignant tumors including glioblastoma multiforme (GBM). Moreover, inducing angiogenesis by expression of vascular endothelial growth factor (VEGF), thus enabling an improved blood supply to the tumor center, is an indispensable hallmark of solid tumors. Invasion and metastases needs to be activated, for example by epithelial-mesenchymal transition (EMT). *(4)*

However, the original hallmarks described in the year 2000 were updated in 2011 and four additional hallmarks of cancer were included *(7)*. First, reprograming of energy metabolism in order to support tumor proliferation is one emerging hallmark. Evading immune destruction by decreasing B- and T-cell action defines another new hallmark. Furthermore, genomic instability is one driving factor for tumor progression and inflammation caused by the innate immune system and its resulting environmental changes can promote tumor growth. Recently, the tumor microenvironment came into focus, representing the first tumor-promoting factor not entirely mediated by a cellular compartment. Overall, until today the list of cancer hallmarks has been extended from original six to ten. *(7)*

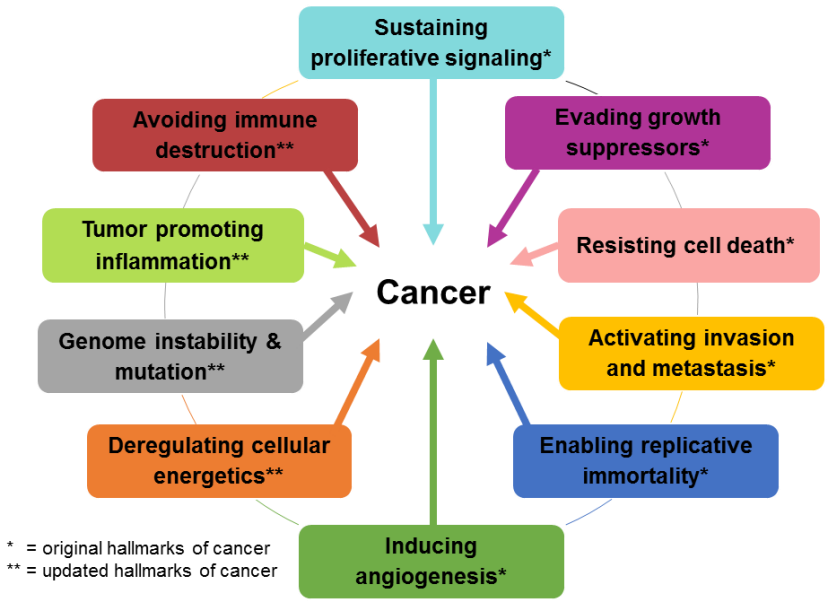

Figure 2. The hallmarks of cancer. The original six hallmarks of cancer include sustaining proliferative signaling, evading growth suppressors, resisting cell death, enabling replicative immortality, inducing angiogenesis and activating invasion, and metastasis. The updated version added four additional hallmarks including deregulating cellular energetics, genome instability and mutation, tumor promoting inflammation and avoiding immune destruction. (Adapted from *(4, 7)*)

1.4 Glioblastoma multiforme (GBM)

GBM is the most common and aggressive malignant brain tumor in adults, representing 55% of all gliomas and 15% of all primary brain tumors *(8)*. The mean age at diagnosis is 64 years and men are 1.35-times more likely to be affected than women *(9)*. In Austria, approximately 350 new cases are reported per year and the incidence rate is 3.4/100,000 inhabitants *(10)*, which is higher as compared to the global incidence rate accounting for 3.19/100,000 people *(11)*. Furthermore, GBM is one of the deadliest types of cancer in humans with a median survival of three months if untreated *(12)*. Nevertheless, the five-year survival rate post diagnosis is limited to 5% of the patients *(11, 13)* and can only slightly be prolonged by use of gold standard therapy (see chapter 1.8.1). According to the World Health Organization (WHO), GBM are characterized as astrocytic gliomas grade IV *(14)*. GBM arise from glial precursor cells, therefore belong to the group of glial tumors and can further be divided into primary and secondary tumors. With respect to histopathological criteria, it is not possible to differentiate between primary and secondary GBM. Secondary GBM are defined as tumors arising from previously diagnosed lower-grade glioma. *(14)* In contrast, primary GBM are those without an antecedent clinical history at the time of diagnosis. Since primary high-grade GBM do not have any tumor-causing precursor lesions, they are also referred to as *de novo* tumors. *(15, 16)*

1.4.1 WHO classification and prognostic factors in GBM

In the fourth edition of the central nervous system (CNS) tumor classification published in 2007, GBM was histologically assigned into the group of astrocytic tumors and subdivided into small cell GBM, giant cell GBM and gliosarcoma (GS). All these subgroups were characterized by WHO grade IV *(17)*. Besides morphological cell descriptions, GBM are further classified by *epidermal growth factor receptor (EGFR)* amplification, *EGFR* alterations, homozygous *p16INK4a* deletion, *phosphatase and tensin homolog (PTEN)* mutations and loss of heterozygosity (LOH) 10q. (reviewed and summarized in *(17)*)

Very recently an updated version of CNS tumor classification was published, characterizing GBM not only by histological parameters, but also according to the *isocitrate dehydrogenase (IDH)* mutation status and other genetic parameters (Figure 3). *(14)*

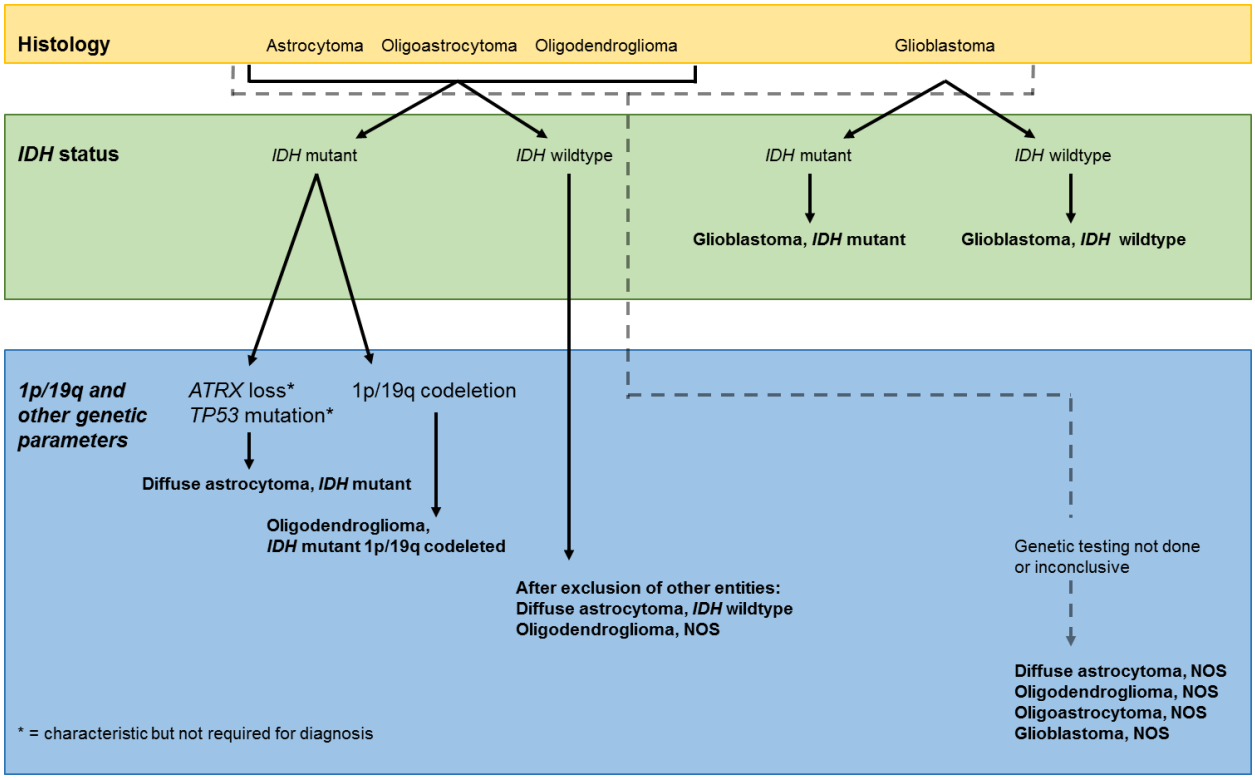

Figure 3. Summary of classification guidelines for diffuse gliomas. According to newest guidelines, diffuse gliomas are classified according to their histological and genetic features. Chronologically, diagnosis starts with histological sample evaluation followed by molecular testing (*IDH* status and other genetic parameters). However, hierarchical order does not necessarily need to be followed. In case of convergence, the molecular result is higher weighted. (adapted from *(14)*)

According to the latest update of the CNS tumor classification guidelines, diffuse gliomas can histologically be sub-grouped into astrocytoma, oligoastrocytoma, oligodendroglioma and GBM. Furthermore, these tumor subgroups are classified according to their genetic features, especially according to their *IDH* status as well as to other genetic parameters, like 1p/19q alterations. *IDH* wild-type (WT) GBM, however, correspond to primary or *de novo* GBM and are mainly found in patients older than 55 years. Within this subgroup, tumors are often characterized by *EGFR* amplifications and chromosome 10 losses. *IDH* mutated (MUT) GBM, in contrast, correspond to secondary GBM originating from a low grade diffuse glioma predominating in patients of younger age. Moreover, the group of not otherwise specified (NOS) GBM is included. All tumors, which cannot be specified according to their *IDH* status, or patients with inconclusive or not available genetic testing, are assigned to the group of NOS GBM. Furthermore, a new variant of GBM is added, named epithelioid GBM, which merges the prior groups of giant cell GBM and GS. A hallmark of this group is the presence of a murine leukemia viral oncogene homolog 1 (C-Raf-1=BRAF) V600E mutation. (reviewed and summarized in *(14)*)

1.4.2 Prognostic and predictive factors in GBM

One important prognostic parameter for GBM not mentioned in the WHO classification, but even though a crucial factor in the choice of treatment for GBM patients, is the methylation of the *O6-methylguanine-DNA methyltransferase* (*MGMT*) promoter *(18)*. The *MGMT* gene encodes for a DNA repair enzyme that removes alkyl groups from the O6-position of guanines, thus restores the normal base structure *(19-21)*. Alkyl groups at this position cause base-mispairing and DNA double-strand breaks. *MGMT* promoter methylation occurs in 40-60% of GBM, leading to gene silencing, hence the alkyl groups are not removed *(22-24)*.

The gold standard care for GBM includes application of the small lipophilic chemotherapeutical drug temozolomide (TMZ), a DNA-alkylating agent of the imidazotetrazine class *(25)*. TMZ adds methyl groups to purine bases of the DNA, namely O^6-guanine, N^7-guanine and N^3-adenine. In patients with a *MGMT* promoter WT sequence, these methyl groups can be removed by the intact MGMT, a part of the DNA repair enzyme family *(19-21)*. Therefore, patients harboring *MGMT* promoter methylation respond much better to TMZ treatment as compared to *MGMT* promoter unmethylated GBM patients. *(26-28)*. Figure 4 outlines the connection between *MGMT* promoter methylation, mismatch repair machinery (MMR) and TMZ response.

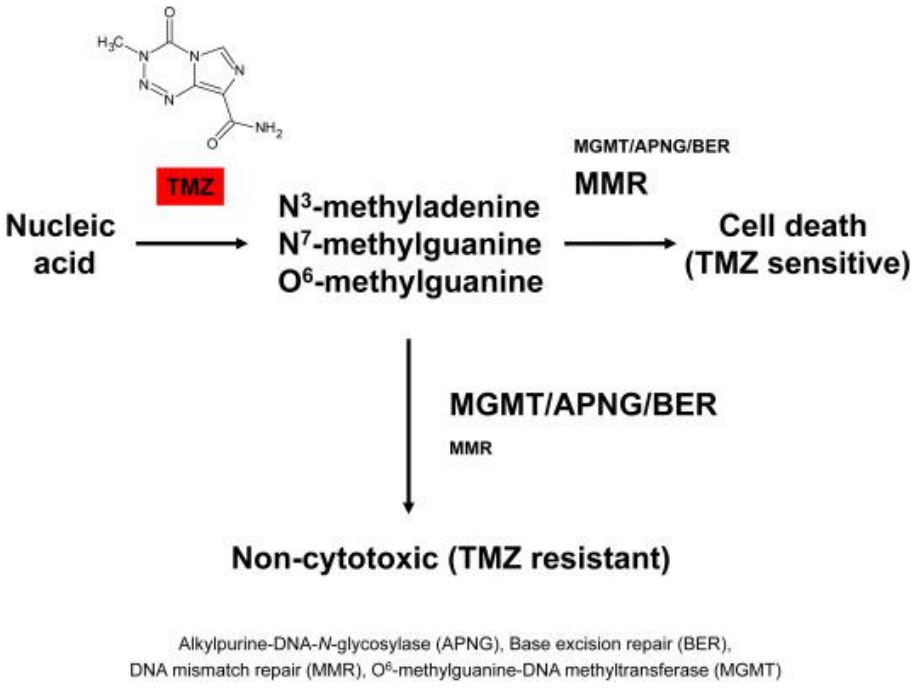

Figure 4. Mechanism of TMZ resistance. TMZ adds methyl groups to the DNA on position N^3 of adenine or on N^7 or O^6 on guanine. An intact mismatch repair (MMR) machinery can restore the original DNA sequence, hence patients harboring a *MGMT* promoter WT are resistant to TMZ. On the contrary, patients harboring a *MGMT* promoter

methylation resulting in silencing of the gene and deficiencies in MMR machinery are more sensitive to the drug. *(29)*

The data concerning a prognostic or predictive quality of the *MGMT* promoter methylation are somewhat contradictory. In 2013, Zhang *et al.* defined the *MGMT* promoter methylation as a prognostic factor in GBM *(18)*. Before it was postulated that *MGMT* promoter methylation is a prognostic as well as a predictive factor *(30-32)*. However, the latest information on that confusion was published in 2014, when it was stated that the *MGMT* promoter methylation strongly correlates with better outcome after TMZ treatment, whereas *MGMT* promoter unmethylated patients do not benefit substantially from the therapy *(26-28)*. Thus, it was again postulated that *MGMT* promoter methylation is a strong predictive, but not prognostic factor in GBM *(33)*.

Parsons *et al.* identified a somatic mutation in the *IDH1* gene in 12% of GBM. *(34)* A study from Yan *et al.* revealed that five out of six secondary GBM harbor this genetic alteration at codon 132 in the *IDH1* gene, suggesting that the mutation drives the progression from a low-grade glioma to a secondary GBM and may represent a biomarker for secondary GBM. Mutations in the *IDH* gene result in loss of enzymatic activity, therefore loss of function of the corresponding proteins. Moreover, GBM harboring either an *IDH1* or an *IDH2* mutation are characterized by significantly better outcome than those lacking these mutations (31 versus 15 months, $p=0.002$). Interestingly, the patients' age is significantly lower in *IDH* MUT GBM compared to WT tumors (median age 32 versus 59 years, $p<0.001$). *(34, 35)*

Another recently discussed feasible biomarker in GBM is the presence of mutations in the telomerase reverse transcriptase *(TERT)* promoter resulting in telomerase reactivation *(36-38)*. Spiegl-Kreinecker *et al.* postulated a prognostic impact of *TERT* promoter mutations compared to *TERT* promoter WT tumors on the overall survival of patients suffering from primary GBM (11.5 vs 23.1 months, $p<0.0001$) *(38)*. Furthermore, researchers described that a certain single nucleotide polymorphism (SNP), namely rs2853669, located in the *TERT* promoter has an impact on the patients' prognosis *(38-40)*. No significant difference was identified regarding overall and progression-free survival in SNP carriers and non-carriers *(38)*. Interestingly, homozygous carriers (CC) displayed a significantly worse prognosis than heterozygous carriers (CT) and non-carriers (TT). Surprisingly, SNP carriers with a WT *TERT* promoter showed enhanced overall survival, while SNP carriers with a MUT *TERT* promoter in contrast, tended to have a tremendously shortened overall survival. *(38)*

1.5 Telomeres

Telomeres are heterochromatic structures located at the ends of human chromosomes and composed of TTAGGG tandem repeats *(41)*. They protect the chromosomal coding sequences from continuous degradation during the replication cycles and therefore ensure chromosomal stability and integrity *(42, 43)*. The 3'-end of a eukaryotic telomere is characterized by a G-rich single-stranded overhang, which is essential for telomere maintenance *(44)* (Figure 5a). The telomeric sequence can perform self-pairing and is folded to secondary structures, protected by various proteins and molecules together forming the Shelterin complex *(45, 46)*. Telomeres form large telomeric loops (T-loops). For this purpose, the single stranded DNA builds a long circle also stabilized by protective proteins *(41)* (Figure 5b). At the end of that circle, the single-stranded DNA binds to one of the disrupted strands of the double-strand, building a triple-stranded structure, called D-loop *(47)* (Figure 5b). Newly generated double-strands can undergo self-pairing again and a four-stranded G-quadruplex is generated. The G-quadruplex is bound by the Shelterin complex, which protects the chromosomal ends from degradation. *(48, 49)* (Figure 5c).

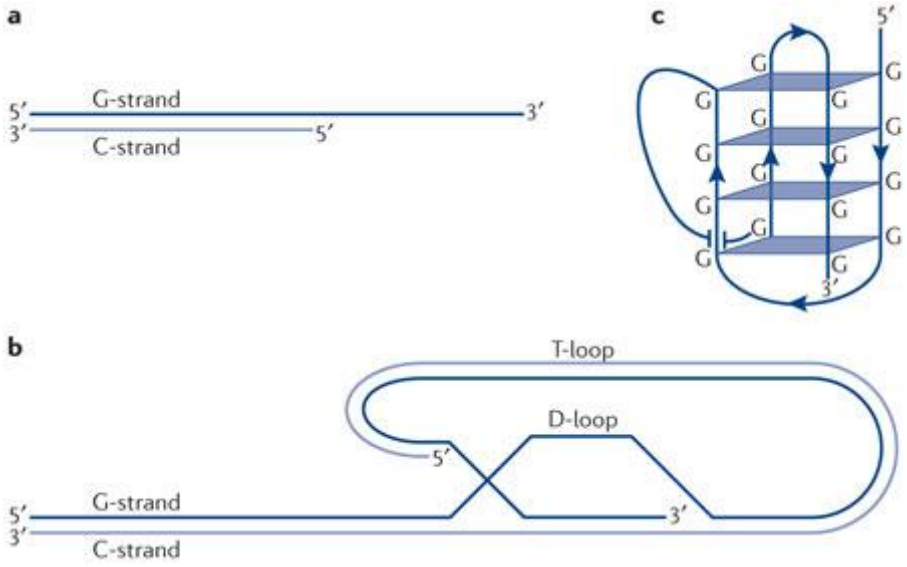

Figure 5. Telomeric DNA structures in eukaryotes. (a) Telomeres harbor a G-rich 3'-end, which can perform self-base-pairing. **(b)** Such secondary structures can form double-stranded telomeric (T) loops or triple stranded D-loops. **(c)** Newly generated GG self-paired double-strands can perform self-pairing again and a four-stranded G-quadruplex is generated. *(50)*

1.5.1 Telomere shortening and replicative senescence

The chromosomal ends are shortened with every cell division. The deterioration of telomeres is caused by the fact that the Okazaki fragments cannot attach their primers at the chromosomal ends, thus the DNA-polymerase cannot continue its action. This is referred to as end replication problem *(51)*. In order to prevent genomic instability and cancer, a physiological somatic cell has self-limiting potential and therefore limited proliferation ability *(51)*. Hence, in case of critically short telomeres, the cell stops the cell cycle progression, ending in replicative senescence *(52-54)*. The number of times a cell can undergo cell division correlates with the length of the telomeres and is defined as Hayflick limit. *(55, 56)*

The word senescence originates from the Latin word *senescere,* which means „to grow old“. Replicative or cellular senescence does not cause immediate cell death, but it is defined by progressive cell cycle arrest. Thereby, the cell stops its proliferation and ends in an arrest at the G0/G1 checkpoint *(57)*. Senescence can have multiple reasons including cellular stress caused by reactive oxygen species, uncommon growth conditions like hyper-proliferative signals common in cell culture conditions, or telomere shortening also leading to DNA damage signals *(52, 58, 59)*.

1.5.2 Telomerase and telomere elongation

In postnatal somatic cells, telomerase expression is repressed resulting in progressive telomere shortening *(60)*. In stem cells, TERT is stably expressed, representing a landmark for pluri- and multipotency in embryonic and adult stem cells. Furthermore, TERT has been identified to be reactivated in various cancer cells, including GBM. Thus, TERT is highly associated with cancer and cellular immortalization. *(61)*

Telomere lengthening is executed by the telomerase holoenzyme that adds *de novo* tandem repeats after each replication cycle *(62)*. Telomerase is composed of the enzymatic protein telomerase reverse transcriptase (TERT), the telomerase RNA (*hTR=TERC*) component representing the primer sequence, as well as a number of cofactors *(63)* (Figure 6). Besides TERT and *TERC*, also the accessory proteins dyskerin (DKC1), Neurospora crassa 10 (NOP10), NHP2 and GAR1 are needed for fully functional telomerase enzyme activity *(64)*. The *TERC* structure is composed of four functional domains including the template for reverse transcription, the pseudoknot domain, a stem-loop for TERT interaction and a 3’ element required for RNA stability *(65)*. The accessory proteins DKC1, NOP10, NHP2 and GAR1 bound

to the chaperone Nuclear Assembly Factor 1 (NAF1) form a tetrameric complex and bind to *TERC (64, 66)*. (Figure 6)

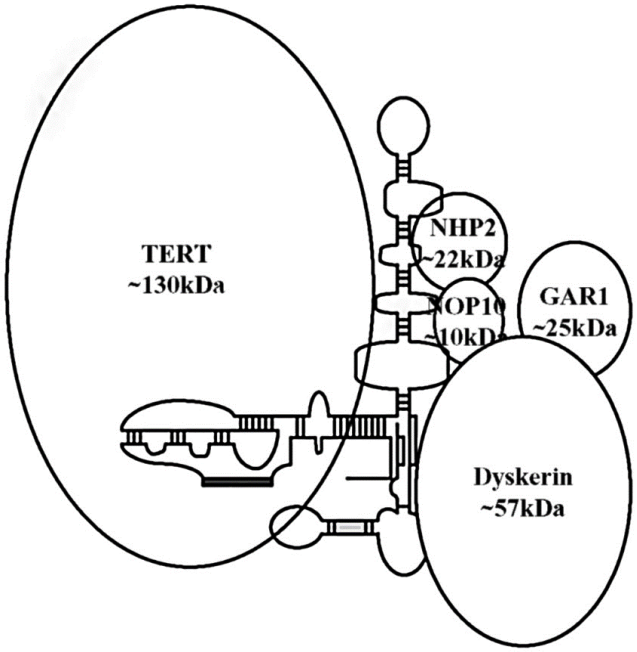

Figure 6. **The telomerase ribonucleoprotein complex** contains the catalytic TERT enzyme as well as the accessory proteins Dyskerin, NHP2, NOP10 and GAR1 bound to the RNA primer sequence *hTR=TERC*. (adapted from *(67)*)

TERT represents the catalytic subunit of the ribonucleoprotein complex and is built of four functional domains, namely telomerase N-terminal (TEN) domain, TR-binding domain (TRBD), reverse transcriptase domain (RT) and C-terminal extension domain (CTE) *(68)* (Figure 7). TEN is necessary for telomerase recruitment to telomeres as well as for catalyzing the telomeric repeat synthesis *(69-71)*. TRBD and RT harbor interaction sites for TERC binding *(72)*. The active site of the RT domain is homologous to retroviral and retrotransposon RT domains *(73)*.

Figure 7. **Functional domains of human TERT (hTERT).** TERT protein comprises four functional domains, namely telomerase N-terminal (TEN) domain, (h)TR-binding domain (TRBD), reverse transcriptase domain (RT), and C-terminal extension domain (CTE). *(74)*

1.5.3 The non-canonical functions of telomerase

Besides elongation of the telomeres, telomerase has a multitude of non-canonical second line functions. For example, TERT modulates the WNT-β-catenin signaling and induces stem cell characteristics in GBM. Moreover, TERT affects nuclear factor 'immunoglobulin κ-light-chain-enhancer' restricted to activated B-cells (NFκB), a central transcription factor important in a multitude of cellular functions. *(75-79, 80*) NFκB directly binds to the *TERT* promoter activating as transcription factor in mice *(76)*. Moreover, an interaction between TERT and the p65 subunit of NFκB was illuminated. This binding was supposed to modulate nuclear translocation of TERT. The dimer translocates to promoters of a subset of NFκB target genes like IL6 and TNFα that are important in cell proliferation and therefore cancer progression. *(81)* Ghosh *et al.* revealed that abrogation of TERT significantly represses the tumor growth, but that this repression could be reversed by overexpression of p65. This leads to the suggestion that the p65 dependent canonical NFκB pathway can compensate the TERT function when it is abrogated. *(75)* Furthermore, it can be concluded that overexpression of TERT resulting from activating *TERT* promoter mutations correlates with NFκB pathway activation. One important target gene of NFκB is *IL6,* representing the main trigger for the Janus kinase (JAK)-signal transducer and activator of transcription (STAT) pathway. Besides this indirect link between the two pathways via IL6 *(82-84)*, STAT3 was also found to be directly interconnected with TERT *(85)*. STAT3 plays a critical role in the regulation *TERT* expression *(85)*. Moreover, TERT is an important effector of STAT3 promoting cell survival and antagonizing apoptosis. *(86, 87)*

1.5.4 *TERT* promoter

The *TERT* gene is located on chromosome 5p15.33 and consists of 16 exons and 15 introns spanning 35kbp *(61, 88)*. The core promoter of *TERT* is located 330bp upstream of the translation starting site and the second part lies 37bp upstream of exon 2 of *TERT (88)*. There are multiple binding sites for transcription factors on the *TERT* promoter which have gene-activating function. Tumor suppressor genes like p53 can repress *TERT* transcription and activity in a specificity protein 1 (Sp1)-dependent manner *(61, 88, 89)*. Furthermore, the transcription factor c-Myc binds to the E-boxes located on the *TERT* promoter which *per se* activates *TERT* transcription *(90)*. On the contrary, if c-Myc forms a complex with BRCA1 and N-Myc, the *TERT* promoter activity is inhibited. *(91, 92)*.

1.5.5 *TERT* promoter mutations and cancer promotion

90% of all cancers show reactivation of telomerase leading to increased telomere elongation *(93-95)*. Overexpression of *TERT* mRNA expression in somatic cells can be caused by epigenetic dysregulation and genetic amplification of the *TERT* gene*,* but also by mutations in the *TERT* promoter *(80, 96-99)*. Especially with respect to *TERT* promoter mutations, *TERT* overexpression results in a variety of cellular functions including enhanced cell proliferation, decreased apoptosis, regulation of DNA damage responses, chromatin state and increased cellular proliferation and life span (reviewed in *(80)*). Killela *et al.* identified *TERT* promoter mutations in 81.8% of tumors from various entities. The most abundant *TERT* promoter alterations are characterized as the somatic point mutations C228T and C250T, accounting for 77.5% and 20.8% of all *TERT* promoter mutations, respectively. Interestingly, *TERT* promoter alterations are not only restricted to somatic cells, because in melanoma also germline mutations are found. With respect to GBM in adults, *TERT* promoter mutations are found in 83% of the cases, whereas the prevalence of such mutations in pediatric patients is significantly lower (83% vs. 11%) *(100)*.

C228T and C250T mutations located at positions -124bp (C228T) and -146bp (C250T) from the ATG start codon of *TERT*. These particular mutations result in cytosine to thymine (C>T) transitions *(101, 102)*. This base-exchange creates novel CCGGAA/T motifs, representing consensus sequences for *de novo* binding of E-twenty six/ternary complex (ETS/TCF) but also NFκB transcription factors (Figure 8) *(101-105)*. Therefore, C228T and C250T mutations can be characterized as activating mutations in the *TERT* promoter, leading to increased *TERT* gene expression *(80)*.

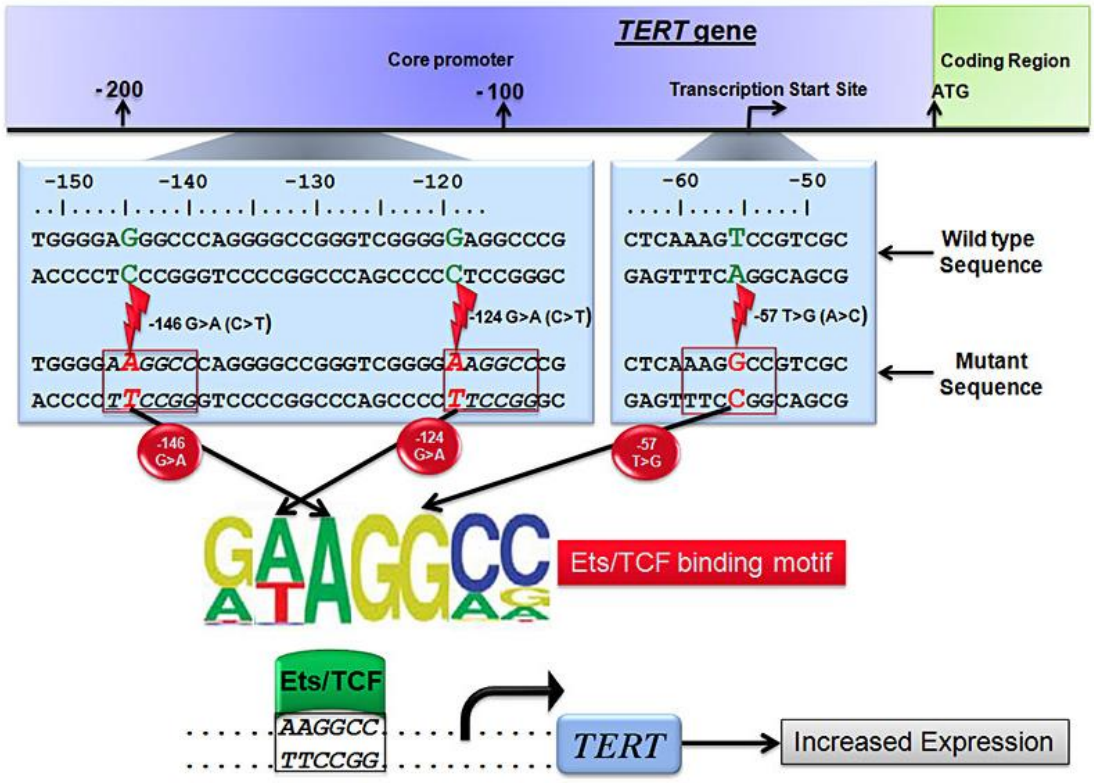

Figure 8. ***TERT* promoter mutations.** The two most common point mutations in the *TERT* promoter are located on positions -124bp and -146bp downstream from the start codon. These mutations result in cytosine to thymine (C>T) transitions representing *de novo* binding sites for Ets/TCF transcription factors. Transcriptional promoter activation causes increased *TERT* expression in this subgroup of tumors. *(106)*

Activating mutations in the *TERT* promoter are often associated with *BRAF* mutations. This coincidence can be explained by genetic stabilization. Accordingly, *BRAF* mutations are stabilized in the genome because of a concomitantly present *TERT* promoter mutation. *(80)* Interestingly, *EGFR* amplifications occur exclusively in primary GBM harboring a *TERT* promoter mutation. Cells harboring *TERT* promoter mutations are characterized by elongated telomeres, thus decreased apoptotic potential. Hence, previously occurred mutations, such as *BRAF* mutations, are more likely to be persistently integrated into the genome. *(107, 108)*

1.6 Signaling pathways

The evaluation and development of malignancies is often associated with genomic mutations, resulting in altered protein structures and activities. In many cases, mutated proteins act in various intracellular signal transduction pathways. Hence, such alterations can cause cancer-associated overexpression of certain pathway members, resulting in constant activation of those signaling cascades. *(4, 7)*

1.6.1 EGFR and MAP kinase pathway

The EGFR and its downstream signaling networks are crucial factors in GBM initiation, progression and therapy. Since the EGFR pathway has main impact on cell proliferation and growth, it is altered in a multitude of tumor entities, including GBM. EGFR belongs to the superfamily of receptor tyrosine kinases (RTK) and is one of the four ErbB family members. EGFR is located on the cellular membrane and harbors a ligand-binding extracellular domain, a hydrophobic transmembrane domain and an intracellular domain with tyrosine-kinase activity. *(109-111)*

Around 40% of all GBM harbor an *EGFR* gene amplification and approximately half of those tumors express the MUT variant EGFRvIII *(109-111)*. EGFRvIII is the most common variant of EGFR and is usually coexpressed with the WT receptor in GBM *(111)*. *EGFRvIII* originates from alternative splicing of exons 2-5, leading to a deletion of 276 amino acids in the extracellular domain of the receptor *(111)*. Thus, the EGFRvIII has an altered protein conformation and is unable to bind to a ligand. The changed conformation leads to a constant activation of the EGFR-associated downstream pathways. This subsequently results in overexpression of EGFR target genes that are mostly involved in pro-survival signal circuits of the malignant cell *(111)*. The main signal transduction pathways downstream of EGFR are the STAT3, the phosphatidylinositol bisphosphate 3 kinase (PI3K) and the mitogen activated protein kinase (MAPK) pathways (Figure 9). The MAPK pathway regulates cellular functions like proliferation and cell survival (Figure 9).

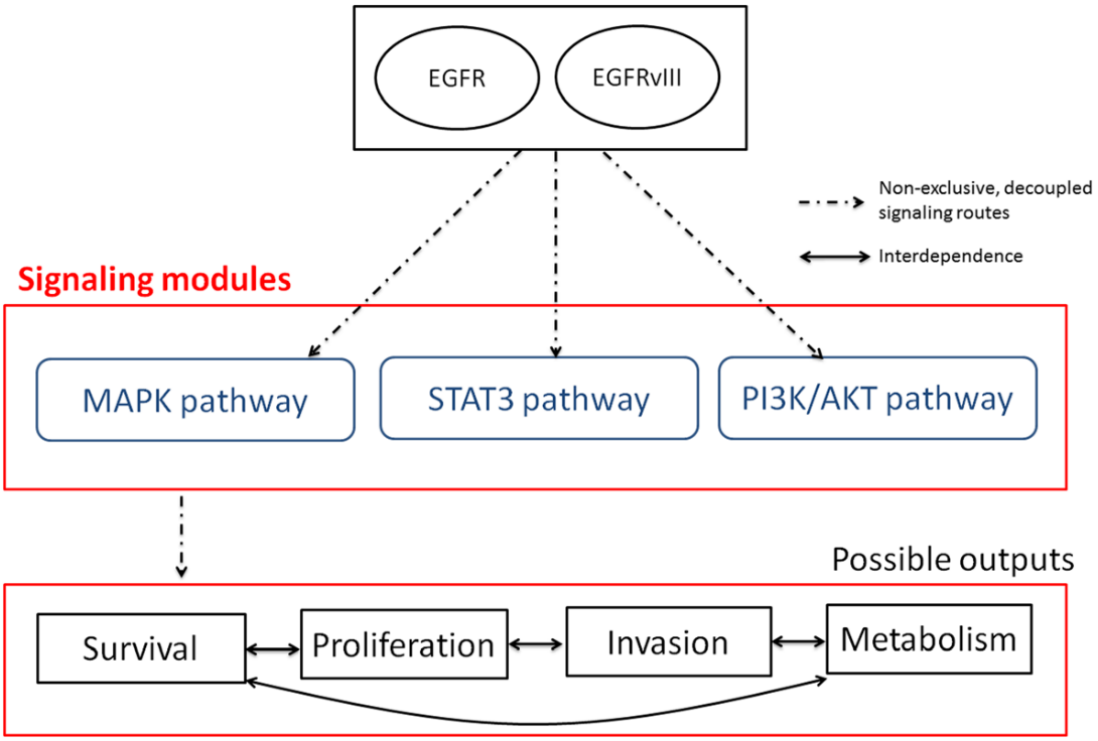

Figure 9. EGFR downstream signal transduction pathways. EGFR and EGFRvIII activation leads to induction of different signaling modules, including MAPK, STAT3 and PI3K/AKT pathways. Target genes of these pathways affect positive regulatory cellular mechanisms including survival, proliferation, invasion and metabolism. *(112)*

In the WT state, EGFR gets activated by binding one out of six ligands including transforming growth factor α (TGF-α), amphiregulin, epigen, heparin-binding EGF-like growth factor (HB-EGF), epiregulin and betacellulin *(113)*. Binding of a ligand leads to dimerization of two EGFR molecules, hence either EGFR homodimerization or heterodimerization with one of the other ErbB family members. *(114)* Thus, the receptor gets phosphorylated and activated and proteins containing Src homology domain 2 (SH2) regions are recruited and bind to the cytoplasmic domain of the receptor-dimer. An example for such an adapter protein is the growth factor receptor-bound protein 2 (GRB2), leading to a recruitment and complexing with the protein son of sevenless (SOS). SOS itself is capable of activating the G-protein rat sarcoma (RAS) by exchanging GDP with GTP, resulting in RAS phosphorylation and activation. *(115, 116)* In an active state, RAS recruits various effector protein kinases of the RAF-family and activates them by phosphorylation. These effector protein kinases are proteins including BRAF homodimers or murine leukemia viral oncogene homolog 1 (C-Raf-1)-BRAF heterodimers, also referred to as mitogen activated protein kinase kinase kinase (MAPKKK). MAPKKK phosphorylate and activate MEK1 and MEK2 (MAPKK) which themselves phosphorylate and activate extracellular (signal-) regulated kinase 1 and 2 (ERK1 and ERK2).

Finally, activated ERK translocates into the nucleus where it activates transcription factors of the activator protein 1 (AP-1) family, which promote EGFR target gene transcription. *(117, 118)*

1.6.2 NFκB signaling pathway

NFκB was first described in 1986 by Sen and Baltimore as DNA-binding protein. *(119)* Today, NFκB is known as one of the major transcription factor families in all vertebrate organisms and is involved in basal regulatory functions like cardiovascular growth, stress response and inflammation. NFκB family members are omnipresent in some low-developed animals like cnidaria and porifera as well as in some insects like the mosquitoes *A.aegypti and A.gambiae*, and the fly *D.melanogaster. (120, 121)*

The NFκB pathway is one of the main intracellular stress-response pathways. Besides inflammation, the NFκB signaling cascade is also involved in the regulation of the adaptive immunity as well as in cell adhesion, cell growth, differentiation, vasoregulation, apoptosis and tumorigenesis *(122-124)*. Although NFκB subunits are ubiquitously expressed, they need an external stimulus to form dimers. Since NFκB is involved in a variety of functions, the induction molecules and their receptors are variable *(122-124)*. Accordingly, the pathway can be activated by a panoply of stimuli including proinflammatory cytokines like tumor necrosis factors (TNF) or IL-1, reactive oxygen species (ROS), bacterial cell wall products like lipopolysaccharide (LPS), vasopressors, viral infection products like double-stranded RNA, lack of major histocompatibility complex (MHC), or DNA damage induced by UV-light. *(124, 125)*

The mammalian NFκB family is composed of five structurally homologous proteins including NFκB1 (p50/p105), NFκB2 (p52/p100), Rel (c-Rel), RelA (p65) and RelB *(126)*. The two subfamilies NFκB (NFκB1 and NFκB2) and Rel (RelA, RelB, c-Rel) share a highly conserved N-terminal DNA binding domain, the Rel homology domain (RHD). However, clustering occurs according to their diverse C-termini. While members of the Rel subfamily display a transactivation domain (TAD), NFκB proteins harbor a death domain (DD) and ankyrin repeats (ANK) with inhibitory domains on their C-termini followed by a glycine rich region (GRR) in the center of the protein (Figure 10) *(121, 126-128)*. RelB harbors an N-terminal leucine zipper (LZ) additionally to the TAD in order to get completely activated *(129)*. In contrast to Rel proteins, NFκB members are synthesized as large precursors and must be proteolytically processed to gain full functionality. As such, p105 is processed to p50 and p100 to p52. Neither NFκB precursor proteins, nor mature proteins p50 and p52, are capable to activate transcription as monomers. Thus, they form heterodimers with members of the Rel subfamily to gain

transcription-promoting potential. On the contrary, p50 or p52 homodimers act as repressors of transcription when they bind to κB elements. *(128)*

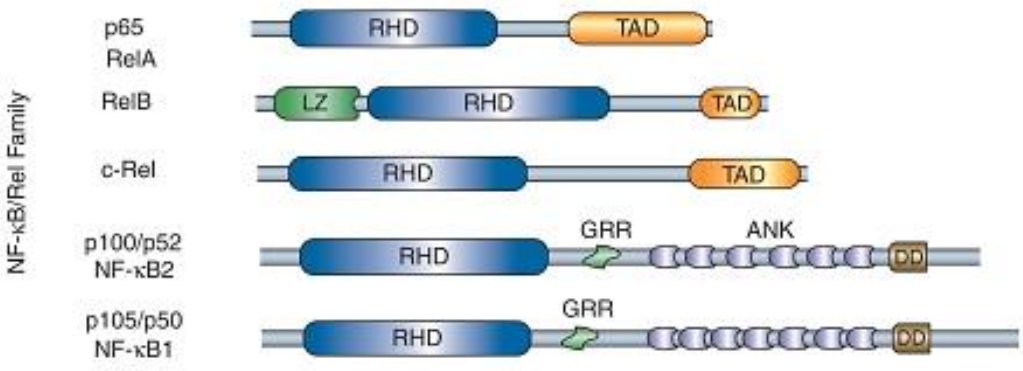

Figure 10. Functional domains of NFκB/Rel family members. The NFκB family is characterized by an N-terminal RHD domain. Solely RelB molecules have an additional LZ domain at the N-terminus followed by the RHD. The NFκB family is divided into two subfamilies, the NFκB and the Rel subfamily. The two protein subgroups display structural differences. The Rel subfamily harbors a TAD domain on the C-terminus. In contrast, the NFκB subfamily exhibits a GRR domain followed by ankyrin repeats and a DD domain at the very C-terminus. RHD = Rel homology domain, LZ = leucine zipper, GRR = glycine rich region, TAD = transactivation domain, ANK = ankyrin repeats, DD = death domain (adapted from *(130)*)

1.6.2.1 The canonical NFκB pathway

NFκB signaling is triggered via two main pathways, namely the so-called canonical and non-canonical/alternative pathway. For a long time, the canonical NFκB signaling was thought to be the only pathway involved in NFκB-mediated transcription regulation. The canonical NFκB pathway is characterized by the molecules NFκB1 and RelA building the core unit of the NFκB transcription factor. *(131, 132)*

As already described above, the pathway activation starts by the binding of various signal molecules to their receptors, mainly Toll-like receptors (TLRs) *(133, 134)*. In general, NFκB-activating signals bind to their receptors, which get activated by mechanisms like dimerization or (auto-) phosphorylation *(135)*, and further adapter molecules bind to trigger the signal transduction *(136, 137)* (Figure 11).

The first common step of all initiator molecules triggering the signal transduction in the NFκB pathway is the activation of the inhibitor of kappa B (IκB) kinase (IKK) complex, a 700kDa

multiprotein complex. The IKK ‘core’ complex comprises the catalytic kinases IKKα, IKKβ and the non-catalytic IKKγ, which is often referred to as NFκB essential modulator (NEMO). The non-catalytic scaffold protein IKKγ is responsible for IKKβ regulation, which itself phosphorylates IκB. (Figure 11) *(131, 138)*

Under resting conditions, unphosphorylated IκBα binds to NFκB subunits. This inactive IκBα-NFκB complex can shuttle between cytoplasm and nucleus, however, the nuclear import has to be catalyzed by importin molecules. Usually, the nuclear export is faster than the import, thus, more IκBα-NFκB complexes remain in the cytoplasm. *(139)* Stimulation of the pathway results in activation of the IKK complex. IKK double-phosphorylates IκBα resulting in IκBα poly-ubiquitination and degradation in the degradosome. Hence, the NFκB proteins are released and translocated into the nucleus where they regulate gene transcription via binding to various κB sites *(140, 141)*. (Figure 11)

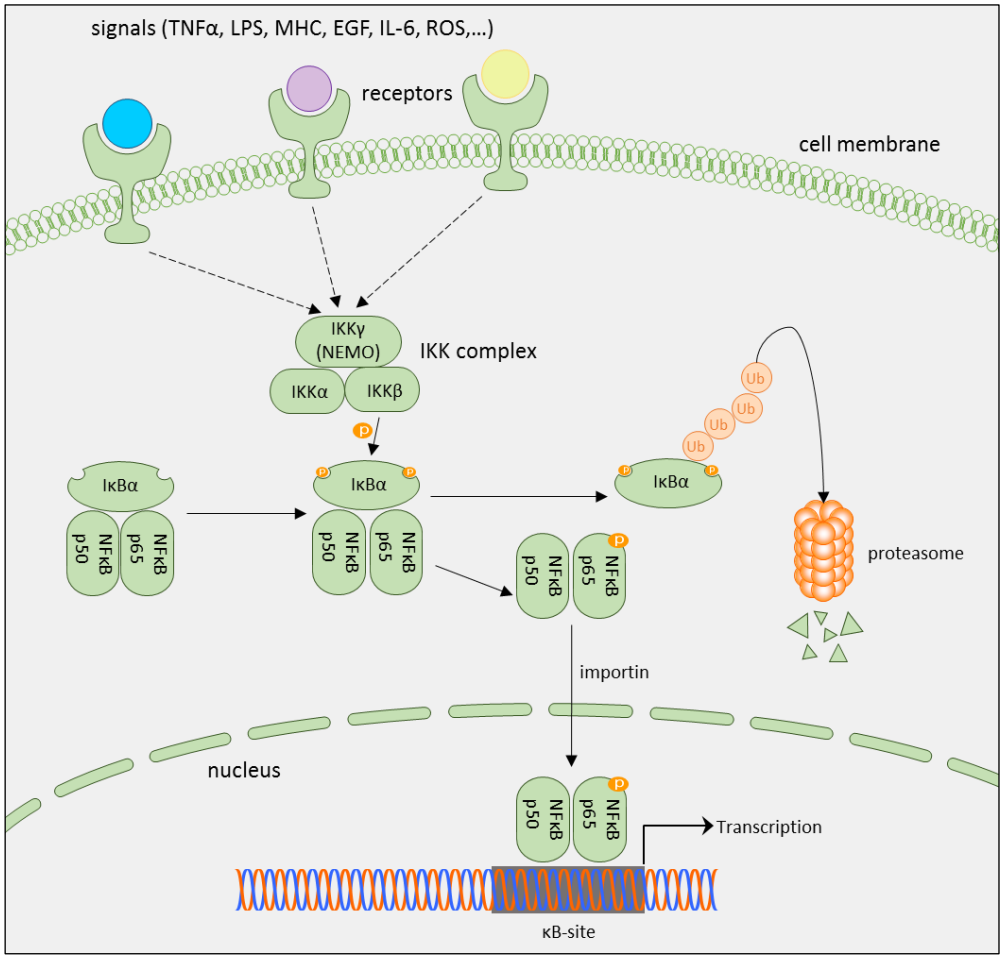

Figure 11. The canonical NFκB signal transduction pathway. Activation of the classical NFκB signaling can be excited by various extracellular signal molecules binding to cell membranous receptors. The signals are transduced via receptor-related adapter

molecules and end with the activation of the IKK complex, composed of IKKα, IKKβ and IKKγ (NEMO). The kinase complex then double-phosphorylates IκBα which is in a complex with an NFκB1 (p50)-RelA (p65) heterodimer. Phosphorylated IκBα is separated from the NFκB heterodimer and marked with ubiquitin for degradation in the proteasome. Furthermore, the p65-p50 heterodimer gets active, probably by phosphorylation of the p65 subunit, and translocates into the nucleus guided importin proteins. Inside the nucleus, NFκB binds to the κB binding sites of various genes and acts as a transcription factor.

1.6.2.2 The non-canonical NFκB pathway

In contrast to the canonical NFκB signaling, the existence of the non-canonical pathway was described much later. The core unit of the non-canonical NFκB transcription factor comprises the homologs NFκB2 and RelB *(131, 132)*. Moreover, the non-canonical signaling axis focuses on the action of IKKα, more than on the canonical IKKβ. IKKα is an independently acting enzyme and does not need any external stimulus from IKKβ or IKKγ *(132, 133)*.

1.6.2.3 NFκB phosphorylation and activation

NFκB phosphorylation is a major part of the activation of NFκB transcription factor, nevertheless it is not fully understood yet. Most of the data regarding NFκB phosphorylation and the fate of NFκB after splitting apart from IκBα until binding to the DNA and performing its transcriptional activity are derived from *in vitro* experiments. Nonetheless, it is known that NFκB cannot reveal its function as a transcription factor directly after its release from IκBα, but there must be various activating signals, most probable phosphorylation events. *(142-144)* Furthermore, it is assumed that this part of the NFκB signaling pathway is highly stimulus- and cell type-specific. *(139)*

Different *in vitro* studies revealed that various kinases are involved in RelA (p65) subunit phosphorylation. These include glycogen synthase kinase 3β (GSK3β) and TRAF-associated NFκB activator (TANK) binding kinase (TBK/ T2K/ NAK). *(142-144)* However, there are a variety of other kinases that are assumed or proven to be involved in the phosphorylation of RelA (p65) on diverse positions, mostly serines. Ser536 on the C-terminal TAD seems to be of crucial importance in the NFκB activation. Interestingly, various kinases target this serine residue including IKKα, IKKβ, protein kinase B (PKB=AKT), ribosomal S6 kinase 1 (RSK1), glycogen synthase kinase 3β (GSK3β), TBK1 and IKKε (reviewed in *(139)*).

1.6.3 Wnt signaling

The Wnt signaling pathway is involved in the regulation of multiple cellular functions like self-renewal, differentiation, regulation of cell-cell interactions, cell fate and migration. Wnt proteins are highly conserved, secreted signaling molecules. The signaling cascade is activated

by a Wnt ligand binding to a receptor. The receptor for Wnt mainly consists of two proteins, Frizzled and low-density lipoprotein receptor-related protein (LRP), only building a heterodimer in presence of a ligand. (Figure 12) (reviewed in *(145)*)

However, there are two different axes of the Wnt signaling cascade. The canonical Wnt signaling pathway was first described in murine breast cancer models in 1982 *(146)*. Later, two different non-canonical Wnt signaling pathways, the non-canonical polarity and the non-canonical Wnt/calcium pathway, were identified *(147)*. In general, the canonical Wnt pathway can be differentiated from the non-canonical pathways by the presence of the multifunctional protein β-catenin in the canonical signaling cascade. The non-canonical Wnt pathways however, are mostly β-catenin independent. (reviewed in *(145)*)

In the absence of activating trigger molecules, like the Wnt protein itself, the cytoplasmic β-catenin is phosphorylated by a multi-kinase complex. This complex consists of various proteins, including Axin, adenomatosis polyposis coli and GSK3β. *(148)* Accordingly, phosphorylated β-catenin gets prepared for ubiquitinylation, hence degradation in the proteasome *(149, 150)*. Therefore, no β-catenin is translocated into the nucleus, and can act as transcription factor. Additionally, the nuclear protein Groucho blocks the binding site for β-catenin on TCF/ Lymphoid Enhancer-Binding Factor (Lef) sites *(145, 151, 152*) (Figure 12)

When Wnt protein is present, it binds to the Frizzled/LRP dimer and the inhibitory protein Dishevelled blocks the kinase activity of GSK3β. Therefore, β-catenin does not get phosphorylated and accumulates in the cytoplasm until it is translocated into the nucleus. *(149, 150)* Nuclear β-catenin binds to TCF/Lef sites and promotes transcription of various genes including *c-Myc* and cyclin D1 *(153, 154)*. Accumulated β-catenin in the cytoplasm can also bind to membranous E-cadherin multimers, thereby regulating cell-cell interactions *(155)*. (Figure 12)

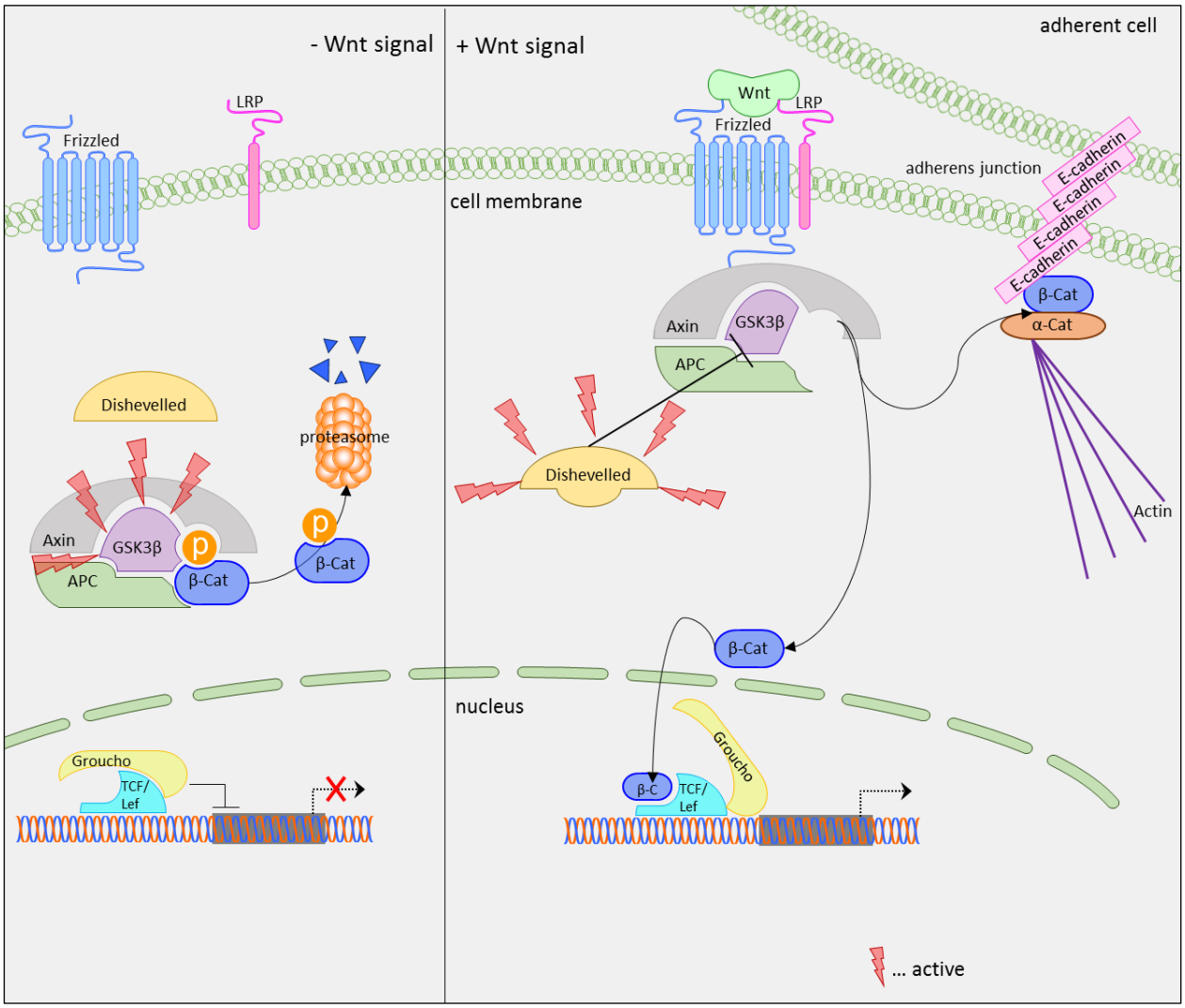

Figure 12. The Wnt signaling pathway. In absence of a triggering molecule, the Dishevelled-dependent kinase protein complex is activated and phosphorylates β-catenin in the cytoplasm. Therefore, β-catenin is tagged for ubiquitinylation and further proteasomal degradation. In the nucleus, Groucho occupies the binding site for β-catenin in the transcription factor complex, thus β-catenin target genes are not transcribed. In contrast, presence of a trigger leads to binding to the receptor, which in turn builds a Frizzled-LRP heterodimer. This promotes the inhibitory protein Dishevelled suppressing activation of the kinase protein complex. Therefore, unphosphorylated β-catenin translocates into the nucleus where it acts in a transcription factor complex with TCF/Lef. In parallel, unphosphorylated β-catenin can also bind to E-cadherin multimers at the cell membrane, whereas it acts in cell-cell interaction and cytoskeleton stabilization.

One central function of the Wnt signaling pathways is their regulation of neuronal development, especially regarding the neuronal stem cells (NSCs). Furthermore, aberrant activation of the Wnt signaling or mutations of Wnt signaling pathway members lead to malignant transformation and tumorigenesis *(156)*. Researchers also found that the Wnt signaling pathway plays a major role in GBM stem cells *(157-159)*. In GBM, activating Wnt signaling aberrations promote tumor growth and invasiveness via retaining stem cell functions like self-renewal ability *(160)*.

1.6.4 JAK/STAT signaling

The JAK/STAT signaling is a major regulatory pathway of biological functions including immune response, proliferation, differentiation, apoptosis and oncogenesis. *(161)*

The pathway can be stimulated by a broad set of ligands, reaching from growth factors and cytokines to foreign nucleic acids. One important receptor in this pathway is the interleukin 6 (IL-6) cytokine receptor consisting of two molecules gp130 and two interleukin 6 receptor alpha chains (IL6Rα). (reviewed in *(162)*) JAK are receptor-linked proteins with (auto-) phosphorylation activity and represent important adapter proteins, triggering the signaling from the receptor downstream. The JAK family is evolutionarily conserved and contains four members, JAK1, JAK2, JAK3 and tyrosine kinase 2 (TYK2) with partially homologous protein domains. *(163)* Activation of the different JAK family members is restricted to distinct interferon subsets. Such, TYK2 is restricted to IFNα/β, JAK1 is effected by IFNα/β and IFNγ, whereas JAK2 is exclusively limited to IFNγ. Nevertheless, also other soluble mediators or cytokines like interleukins use JAK as intracellular trigger molecules. *(163-165)* However, activated JAK phosphorylate molecules of the STAT family. The effector molecule STAT is evolutionarily conserved in all eukaryotes reaching from the single cell organism *Dictyostelium* to humans. *(165)* The STAT family assigns seven members encoded by the *STAT1, STAT2, STAT3, STAT4, STAT5A, STAT5B and STAT6* genes *(162, 166, 167).* Proteins of the STAT family have long been discussed for their impact in tumor promotion. Especially STAT3 increases tumor cell proliferation, survival and invasion *(168-170)*. Moreover, it inhibits the anti-tumor immunity and is involved in the generation of a procarcinogenic inflammatory microenvironment *(171)*. (Figure 13)

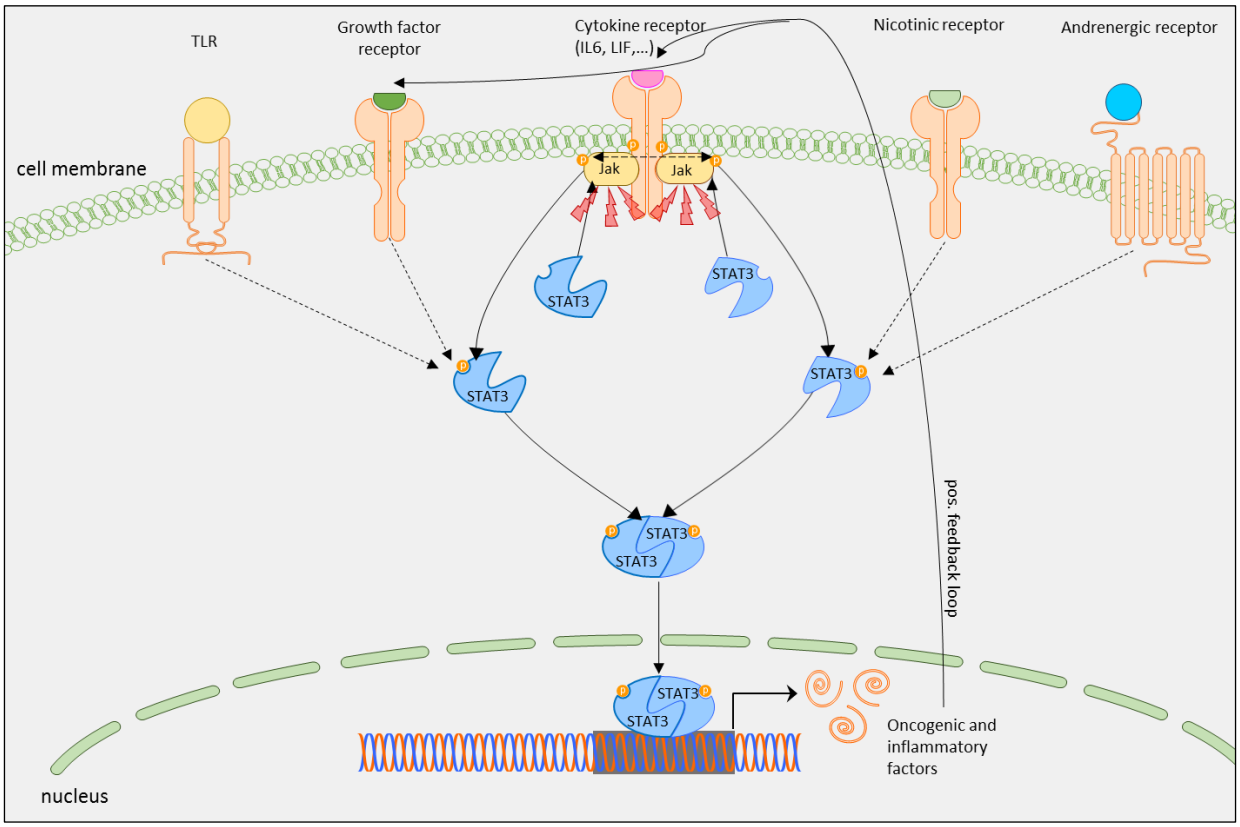

Figure 13. The JAK/STAT3 pathway. The pathway can be activated by various signals including IL-6. IL-6 specifically binds to the IL-6 receptor leading to a homo-dimerization and phosphorylation of its subunits. In turn, JAK molecules are recruited to the receptor and perform auto-phosphorylation in order to get active. The kinases phosphorylate STAT3 molecules, which form homodimers. These STAT3-STAT3 complex is able to translocate into the nucleus where it acts as transcription factor on various target genes involving IL-6 itself. Therefore, IL-6 binding leads to a positive feedback loop.

Activated STATs form homodimers or heterodimers with other STAT-family members through SH2-domain interaction *(172)*. With respect to STAT3, JAK1 represents the most important activator in order to form homodimers *(173)*. Each STAT molecule specifically controls the expression of a distinct cytokine gene subset. IL-6, for example, induces its own transcription via a positive regulatory feedback loop. IL-6 binds to the cytokine receptor, whereupon JAK kinases phosphorylate STAT3 *(82-84)*. In turn, STAT3 builds a homodimer and translocates into the nucleus. There it modulates the expression of IL6 encoding genes and other crucial mediators involved in acute phase immunity and cancer-promoting inflammation *(171)*. STAT3 target genes are mainly important in Th17-cells as well as anti-apoptotic, pro-proliferation, angiogenic and metastatic pathways. (reviewed in *(171)*)

1.7 Immune-regulatory signaling

1.7.1 Tumor-associated inflammation

The fact that inflammation and cancer are highly connected to each other was already postulated in the 19th century. (reviewed in *(174)*) The estimated amount of deaths caused by tumors associated with previous chronic-inflammation is estimated at 15-20% of all cancer deaths worldwide. *(175)* Such as, inflammations can be driven by microbial infections with *H.pylori,* inducing gastric cancer and mucosal lymphoma. Furthermore, infections with Hepatitis virus B or C promote the development of liver cancer and autoimmunological disorders like inflammatory bowel disease (IBD) induce colon cancer. *(7, 176)*

There are two molecular inflammatory pathways involved in cancerogenesis. The intrinsic pathway describes the development of inflammatory microenvironment by genetic alterations causing neoplastic transformation (oncogenes) *(6)* leading to activation of inflammatory pathways. The extrinsic pathway is distinguished from the intrinsic pathway by induction of an infection, resulting in a high abundance of inflammatory leukocytes that are responsible for increased cancer risk. *(177)*

Consequently, it can be concluded that suppression of inflammation by anti-inflammatory drugs can prevent cancer development in certain cases. Rothwell *et al.* demonstrated that patients with daily aspirin consumption had a significantly lower risk of death from cancer than those who did not consume the drug. As a result in this long-term study, the cancer-death risk was reduced to about 60% for gastrointestinal and to 30% for other solid tumors. *(178)* This leads to the conclusion that inflammatory events in the microenvironment promote cancer development and progression.

1.7.2 Tumor microenvironment

The tumor-surrounding tissue is characterized by a low pH and low oxygen values caused by the metabolic properties of cancer cells as well as by the specific vascularization in the tumor site. Besides viable cells, the tumor microenvironment is also composed of dying and already dead cells. These cells as well as resident innate immune cells release a variety of signals, recruiting specialized immune cells to the tumor site, which then cause an inflammatory reaction. *(7)* Attracted macrophages produce various wound-healing factors in order to repair the pretended damaged tumor tissue. Such repair mechanisms include more neovascularization, removal of apoptotic cells and cell debris, remodeling mechanisms and

immunosuppression *(7)*. All these processes are macrophage-mediated programs of tissue repair, but it is also likely that they support the tumor growth and subsequently cause progression of tumor proliferation and increase inflammation. *(179-181)*

Cancer-associated inflammation is characterized by specific inflammatory cells and mediators *(182)*. Leukocyte infiltration, especially infiltration of tumor associated macrophages (TAM) and the presence of cytokines like TNF-α, IL-1 and IL-6 or chemokines like Chemokine (C-C motif) ligand 2 (CCL2) and Chemokine (C-X-C motif) ligand 8 (CXCL8), are the main features of cancer-related inflammation. *(182)* TAM are a highly abundant cell population in solid tumors and release proangiogenic factors such as vascular endothelial growth factors (VEGF) *(183)*. Enhanced tissue remodeling and elevated angiogenesis represent two hallmarks of cancer, promoting tumor growth and progression. Due to the newly synthesized blood vessels in the tumor site, metastases to distant regions are enabled, subsequently promoting tumor progression. *(4)*

Lately it has been suggested that the high abundance of TAM or enrichment of TAM-associated gene patterns in the tumor microenvironment correlate with immunosuppression, neovascularization, invasiveness, metastases, poor prognosis and disease outcome and also limited response to therapy. *(184)* This leads to the suggestion that TAM have a certain tumor promoting function. Ostuni *et al*. suggest that *"these pathogenic activities derive from the tumor-induced repurposing of the same physiological properties that macrophages exert during tissue homeostasis." (185)*

Another hallmark of cancer important to mention in this context, is the release of factors promoting cell survival and vitality *(7)*. For example, macrophages release TNF-α, which activates various signaling pathways including the NFκB and STAT3 axes in target cells. Both pathways positively influence cell vitality and have an impact on cell differentiation. With regard to cancer-promoting inflammation, NFκB and STAT3 are probably the two most important signaling axes *(82-84)*. Moreover, the two pathways are strongly interconnected. NFκB targets a series of chemokine- and cytokine-encoding genes including IL6. IL6 is a main trigger molecule for the JAK/STAT axis. Furthermore, common NFκB and STAT3 target genes involve intercellular adhesion molecules (ICAM) and VEGF-A. Moreover, both pathways are triggered by receptor tyrosine kinases which induce activation of IKK and JAK kinases in the NFκB and STAT signaling, respectively. (reviewed in *(186)*) Especially the NFκB may be responsible for de-differentiation of already differentiated cells back to their stem cell lineage as for example in gastric cancer. Evidence for this is based on the knowledge of de-differentiation of intestinal

epithelial cells into stem-like cells with tumorigenic potential by NFκB-caused enhanced Wnt signaling. Furthermore, the DNA-binding protein β-catenin is modulated in a specific way and the de-differentiation can take place. *(187, 188)*

1.7.3 TAM have tumor-progressive potential

Antigen presenting cells (APC) like TAM can cause a suppression of the anticancer immune reaction, e.g. lead to progression of cancer due to their reduced potential to stimulate the immune response . They activate T-cells and release the proinflammatory cytokine IL12, leading to natural killer (NK) cell activation and further to T-cell differentiation into type I $CD4^+$ T-helper cells (Th1). Th1 cells are cytotoxic effector T-cells and secrete the acid-labile interferone γ (IFNγ), the macrophage activating factor also known as Type II IFN. *(189-192)* (Figure 14)

In addition to their reduced immunostimulatory potential, APC also produce directly functional immunosuppressive factors like IL10 or TGF-β and prostaglandin E_2 (PGE_2). IL10 reduces the IL12 production, thus stimulates the generation of Th2 cells out of naïve T-cells. Th2 cells secrete IL-4 and IL-13, ending in a positive feedback loop of further differentiation of naïve T-cells to Th2 effector cells (Figure 14). *(189-192)* Since IL10 has a suppressing effect on the antitumor immunity due to chemotherapy, high levels of the cytokine can limit the response to anticancer therapy *(183)*. PGE_2 leads to an elevation of the cyclic adenosine-monophosphate (cAMP) level, inhibits IL2 and IFNγ release of T-cells, and increases the IL6 release, thus limiting the inflammatory reaction. PGE_2 further recruits immunosuppressive T-regulatory cells (Treg) via secretion of CCL22. (Figure 14) *(189, 191-194)*

The tumorigenic function of TAM also relies on a suppression of T-cell function through arginase 1 (ARG1). ARG1 is a hydrolase and is involved in the metabolism of the semi-essential amino acid L-arginine. The tumor-associated factors IL4, IL10 and hypoxia in the tumor tissue lead to a higher amount of ARG1 which further causes a reduced amount of L-arginine, decreased T-cell activation and reduced immune response in the tumor site *(185, 195, 196)*. Furthermore, a reduced L-arginine level goes hand in hand with a decrease of nitric oxide synthase 2 (NOS2) and thus a lower nitric oxide (NO) amount. During normal inflammation, macrophages induce NOS2, which causes pathogen toxicity, but in tumors the NO suppresses the T-cell function. *(197-199)*

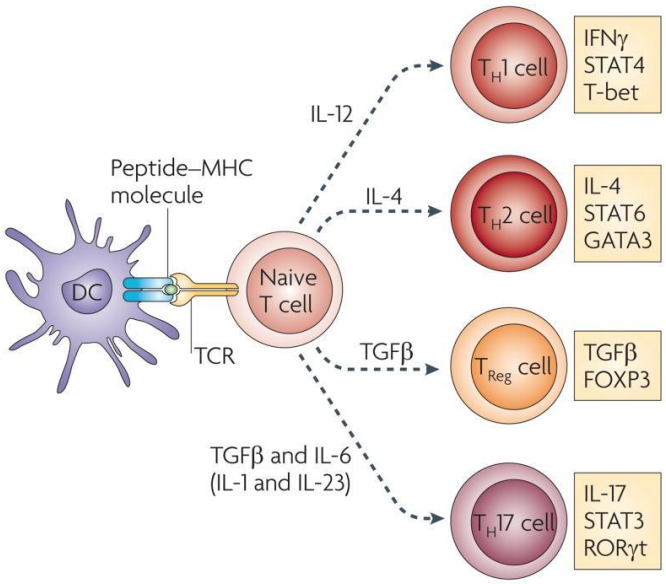

Figure 14. Naïve T-cell differentiation into effector T-cells. Naïve T-cells are characterized by receptor CD4 positivity. When an antigen is present, it is taken up from APC like DC and presented on their surface via an MHC-molecule. APC prime naïve T-cells via MHC-T-cell receptor (TCR) interaction. Depending on their cytokine environment, the T-cells can be polarized into different T-cell effector subsets, such as TH1, TH2, Treg and Th17. The differentiation is controlled by distinct sets of transcription factors. Presence of both, IL6 and TGFβ, triggers Th17 cell differentiation, characterized by expression of the transcription factors IL-17, STAT3 and RORγt. TGFβ alone promotes differentiation into Treg, expressing TGFβ and FOXP3. IL4 primes Th2 differentiation, activating IL4, STAT6 and GATA3 transcription factors. Th1 cells express IFNγ, STAT3 and T-bet and their differentiation is promoted by IL12. *(193)*

With respect to Treg cells, TGFβ leads to differentiation into this lineage. They themselves express TGFβ and Forkhead box P3 (FOXP3) leading to a positive regulatory feedback loop in the cells *(200)*. The biological function of Treg cells is mainly restricted to discriminate between self and non-self. Tregs constitute an immunosuppressive T-cell subset important in preventing pathological self-reactivity resulting in autoimmunological disorders. Besides Treg cells, the programmed death 1 (PD-1) receptor/ programmed death ligand 1 (PD-L1) pathway is instrumental in the maintenance of peripheral self-tolerance. Furthermore, Treg and PD-1/PD-L1 are interconnected, because PD-L1 regulates Treg cell development and function. *(201, 202)*

1.7.4 PD-1 and PD-L1

Activation of the adaptive immune system, particularly activation of naïve T-cells, is a major step in the defense against pathogens as well as cancer cells. Pathogens or pathogen-associated molecular patterns (PAMPs) are presented by MHC on APC. *(203)* The recognition of these

presented pathogens is the initial signal in T-cell stimulation. Therefore, the T-cell binds to the MHCII via a T-cell receptor (TCR) and its co-receptor CD4 (Figure 15). However, a variety of other co-stimulatory signals are essential to induce total T-cell activation and signal transduction (Figure 15). The co-stimulation is tightly controlled by a set of inhibitory and stimulatory regulators, referred to as immune checkpoints. *(203)* One co-stimulatory trigger is constituted by the interaction of the T-cell marker CD28 with APC molecules B7.1 (CD80) or B7.2 (CD86), facilitating forwarding of the defense signal into the nucleus of the T-cell. However, the positive regulatory molecule CD28 competes with the negative stimulatory protein cytotoxic T-lymphocyte-associated antigen 4 (CTLA-4) for binding to B7.1 (CD80) and B7.2 (CD86), leading to promotion or inhibition of T-cell activation, respectively (Figure 15). *(203)*

Another negative regulatory immune checkpoint mechanism is constituted by the interplay between receptor PD-1 and its ligand PD-L1. The T-cell-located receptor PD-1 binds to its APC-bound ligand PD-L1, consequently resulting in blockade of the T-cell activation (Figure 15). PD-1 is not permanently expressed on the cell surface, but needs stimulation via proinflammatory cytokines in order to get expressed. These proinflammatory molecules include IFNγ or IL4. *(204)* The ligand PD-L1 is encoded by the *CD274* gene on chromosome 9 consisting of seven exons. It is classified into the family of B7 transmembrane proteins, including also other immune checkpoint molecules like CD80 (B7.1) and CD86 (B7.2). *(205)* Physiologically, PD-L1 is expressed on the surface of APC, including microglia cells, macrophages and dendritic cells, and represents a negative regulator for T-cell activation. However, PD-L1 *per se* is not a sufficient immunosuppressor, but it rather needs the PD-1 receptor on the T-cell surface. (reviewed in *(203)*) PD-1 downstream target is SHP2, a protein tyrosine phosphatase and inhibitor of the PI3K pathway. Usually, the PI3K pathway activates AKT and other downstream targets involved in processes like, cell growth, proliferation, differentiation, motility, survival and intracellular trafficking. In general, PD-1 is activated via binding of its ligand PD-L1 leading to recruitment of SHP2. SHP2 dephosphorylates PI3K, leading to a blockade of the PI3K pathway, negatively influencing the cell fate. Furthermore, SHP2 recruitment results in dephosphorylation of one chain of the TCR, mediating decreased TCR signaling. (reviewed in *(206)*)

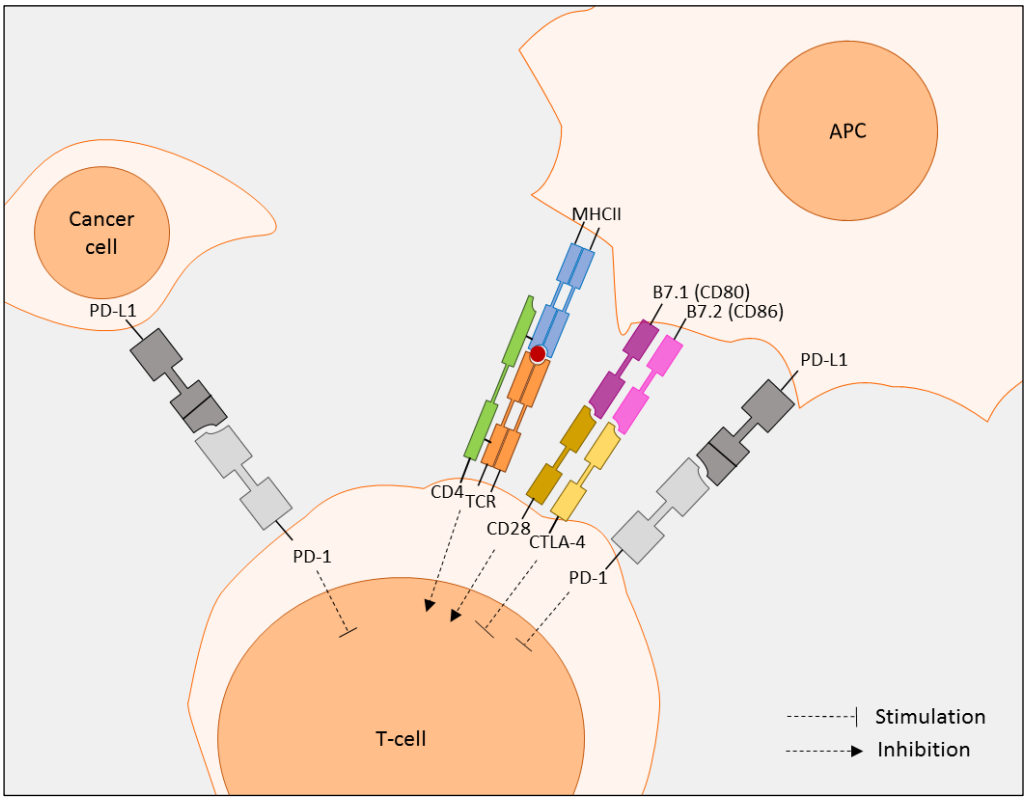

Figure 15. **T-cell activation.** T-cell activation is initiated by the recognition of a MHCII bound antigen on an APC by the TCR and the TCR co-receptor CD4. This first initiator signal is forwarded by a complex-set of co-stimulatory signal molecules regulating the T-cell activation. Thereby, the T-cell receptor CTLA-4 inhibits T-cell activation, thus competes with the stimulatory protein CD28 for binding to B7.1 (CD80) and B7.2 (CD86). Another negative regulatory signal is the interaction of PD-L1 on APC or tumor cells with PD-1 on the T-cell.

PD-L1 is present at the surface of APC, but it has also been found in various kinds of tumor cells as well as on the tumor-resident APC including tumor associated macrophages (TAM) (Figure 15). Generally, the PD-1/PD-L1 axis represents one mechanism of tumors to shut down the anti-tumor immune response. *(207, 208)*. Examples of PD-L1-positive tumors include malignant melanoma, thymic cancer, B-cell lymphoma, non-small cell lung cancer (NSCLC) and GBM (reviewed in *(209)*). PD-L1 positive tumors are more likely to escape endogenous immune response, thus facilitating the survival of tumor cells. Consistently, in many cases, PD-L1 positive solid tumors are characterized by higher malignancy and poorer overall survival. *(210)* Moreover, PD-L1 positivity is a strong predictive marker for PD-1/PD-L1 immune checkpoint therapy response *(211)*.

1.7.4.1 PD-1 and PD-L1 in GBM

The immune system in the brain is mainly composed of microglia cells, a special type of glial cells with multiple functions. The microglia accounts for about 15% of all cells in the brain and function in scavenging, phagocytosis and extracellular signaling. *(212, 213)* The brain and the spinal cord are protected from the rest of the body by endothelial cells building a physical border, referred to blood-brain barrier (BBB). Physiologically, the traffic into the CNS is tightly controlled by the highly specialized BBB. In healthy individuals, the immune cell traffic is very low, but under (tumorous) inflammatory conditions, the BBB gets leaky and smaller cells like certain specified immune cells can enter the CNS. *(214)*

The priming as well as recruitment of activated T-cells in GBM greatly differs from their equivalents in tumors not located in the brain. In general, antigens released from degenerating tumor cells are taken up by APC like microglia or macrophages. The APC migrate to nearby lymph nodes, for example cervical lymph nodes. There, the antigens are presented on MHC molecules at the surface of APC and subsequently naïve T-cells bind to the MHC with their TCR. *(203)*

Additionally, co-stimulatory molecules CD80/86 on the APC bind to CD28 or CTLA4 on the T-cell in order to regulate T-cell priming *(215)*. Activated T-cells are sent to the tumor site in order to attack and degrade the tumor cells *(202)*. The T-cells migrate via the blood stream and can overcome the leaky BBB until they reach the tumor in the brain *(216)*. However, some tumors developed a mechanism to overcome the T-cell mediated anti-tumor immunity by expressing the immunosuppressive molecule PD-L1 on their cell surfaces *(216)*. Physiologically, PD-L1 is expressed on APC like microglia cells and macrophages and binds to their receptor located on the T-cell, thereby blocking the T-cell in its action. Tumor cells expressing PD-L1 mimic APC in order to inhibit T-cell mediated immunity. This negative regulatory signal inhibits T-cell mediated tumor cell destruction, thus supporting the tumor to escape the adaptive immune system. *(203, 206, 214, 217)* Figure 16 summarizes the PD-1/PD-L1 system in GBM.

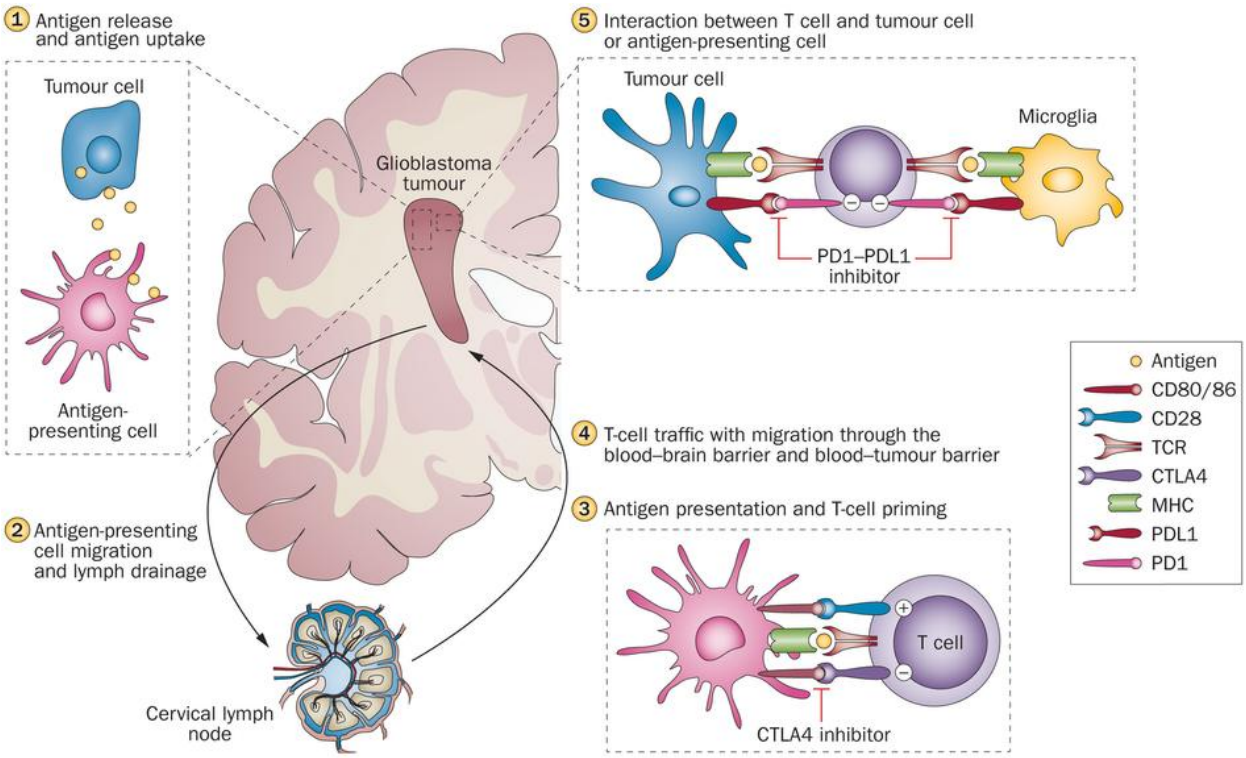

Figure 16. Anti-tumor immunity in GBM. Antigens released by degenerating tumor cells are taken up by APC **(1)**, which migrates to the next lymph node via lymph drainage **(2)**. In the lymph node, naïve T-cells are primed via the antigen-presenting APC **(3)**. Activated T-cells migrate back to the tumor site via the blood stream and overcome the leaky BBB **(4)**. T-cells are sent to the tumor site in order to degenerate the tumor cells, however, when the tumor expresses the negative regulatory molecule PD-L1, the T-cell mediated immunity is inhibited **(5)**. *(217)*

1.8 Therapeutic options

Targeting and healing cancer is the main goal in cancer research. Cancer is often referred to as “never healing wound” and successful treatment is hard to find, because malignant cells have the ability to adapt and develop resistance mechanisms. A feasible way to bypass such “escape mechanisms” of cancer cells is to treat not only malignant cells directly by conventional anti-cancer therapies, but also indirectly by treating the surrounding non-malignant tissue, altered by tumor-mediated signals. The extracellular matrix is essential for providing nutrients and optimal conditions for the tumor growth. Characteristic properties of tumor microenvironment are low oxygen level and low pH, resulting from both, proliferating and dying cells and release of waste products *(7)*.

Usually, cells of the tumor surrounding tissue do not have an altered genome and respond very well to therapy. This tumor surrounding microenvironment includes cells immune cells like TAM,

cancer associated fibroblasts and endothelial cells *(7)*, all of them representing potential targets for the fight against cancer.

1.8.1 Gold standard

Since 2005, maximal safe resection in combination with radiotherapy and adjuvant chemotherapeutic treatment with TMZ are used as first line triple gold standard for GBM therapy *(25, 218)*. Comparable to other chemotherapeutic drugs, unspecific side effects for TMZ include fatigue, hair loss, rash, loss of appetite, diarrhea, amenorrhoea, loss of fertility, liver changes and leukemia. The primary treatment goal for all grades of brain tumors is maximal surgical resection. Considering the infiltrating growth pattern of GBM, the entire tumor can hardly be removed. Thus, GBM resection is followed by external beam radiotherapy (60Gy in 30-35 fractions) and concomitant TMZ treatment (75mg/m2/day peroral on days 1-42, usually 1-1.5 hours before radiation). *(219-223)*. After irradiation, TMZ is administered at higher doses (150-200 mg/m2/day peroral on days 1-5 every 28d) *(224)*.

In general, the efficacy of TMZ varies between age groups and correlates with the *MGMT* promoter status *(30)*. Therefore, testing of the *MGMT* promoter status is an essential step in GBM classification and therapy selection. While patients younger than 70 years and patients with *MGMT* promoter methylation benefit from TMZ therapy, elderlies and/or *MGMT* promoter unmethylated patients are treated with rational therapy solely, since TMZ does not show a significant profit in case of overall survival in this subgroup. *(225)* Even radiotherapy is administered as short and hypo-fractioned course in elderly and *MGMT* promoter unmethylated patients. Figure 17 highlights treatment recommendations according to the different types of glioma, whereas GBM are classified to WHO group IV. *(225)*

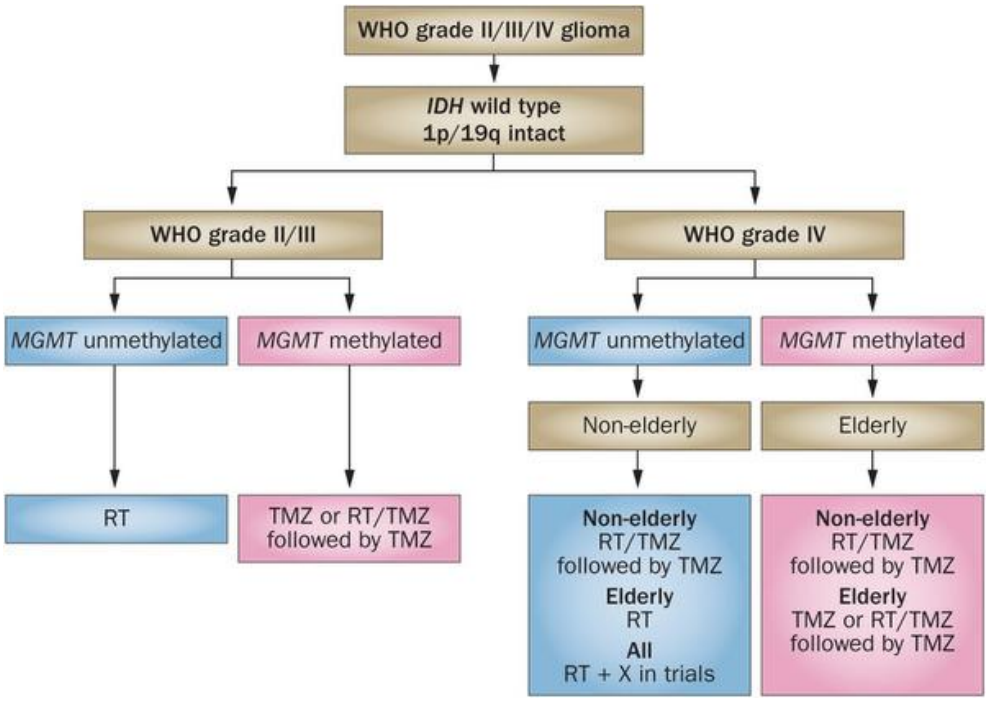

Figure 17. Treatment recommendations for patients with CNS tumors. GBM are assigned to WHO grade IV. Specific treatment options according to the *MGMT* promoter status as well as to the age group are depicted. *(225)*

Despite the gold standard treatment, the median overall survival after diagnosis is limited to 15-17 months *(226)*. Furthermore, GBM recurrence is observed in virtually all affected patients after 6.8 months post diagnosis and a variety of resistance mechanisms against the drug has been observed *(227-230)*.

For recurrent GBM, no generalized therapy is defined. In case of primary therapy failure or disease recurrence, experimental therapy approaches are applied in many cases. Accordingly, various hormones like progesterone were identified as synergistic agents in combination with TMZ *(231)*. TMZ treatment causes diverse side effects, indicating an unspecific mode of action. Thus, intense research is conducted in order to improve the standard GBM therapy and to develop targeted therapy options and novel immunotherapeutic approaches. *(230)*

1.8.2 Immunotherapy

Modern cancer therapy is no longer exclusively composed of chemotherapy, targeted therapy and irradiation. Based on recent findings identifying immune cells in the tumor site, a novel form of therapy has been developed. During the last few years the so called “onco-immunotherapy” is described as highly promising therapy in the specific treatment of tumor cells *(232)*. One advantage of immunotherapy is that it specifically targets the tumor cells without affecting the

healthy surrounding tissue. Immunotherapy comprises passive and active strategies, comparable to vaccinations *(232)*. Active immunotherapy reaches a long-lasting immune response against tumor cells and is discussed to be effective to prevent recurrences and metastases. In contrast, passive immunotherapy creates a short-term immunity against tumor cells. Moreover, passive immunotherapy is characterized by an immediate therapy response after application and mainly makes use of monoclonal antibodies and cytokine-mediated strategies. *(232)* Several vaccination studies have been performed, all trying to target the tumors specifically, however, the outcomes of the studies were contradictory. In order to reach optimal therapy efficacy, it is necessary to verify a tumor-specific antigen and to develop specific antagonizing antibodies or primed T-cells. *(233-238)*

Theoretically, tumor-specific antigens are recognized by APC, which migrate to a lymph node in order to prime naïve T-cells for the antigen. Activated T-cells are recruited to the tumor site and try to attack the cancer cells. However, tumors developed several protection mechanisms against this immunity, for example expression of the T-cell inhibitory molecule PD-L1 (see chapter 1.7.1). PD-L1 represents an immune checkpoint in various malignancies. *(217, 230, 238)* Such PD-L1 is overexpressed in 70-80% of GBM cases, especially in GBM cells and GBM-associated macrophages *(239)*, therefore serving as a potential therapeutic target for GBM treatment *(240)*. The respective immune checkpoint inhibitors are mostly based on monoclonal antibodies targeting various inhibitory regulators mediating a T-cell blockade. Nivolumab and Pembrolizumab represent two checkpoint inhibitors FDA-approved for application in e.g. malignant melanoma and NSCLC. The monoclonal antibodies specifically target the immunosuppressive molecule PD-1 in humans. *(241)* Ipilimumab is another representative of immune checkpoint inhibitors approved for malignant melanoma, targeting CTLA4, thus enhancing central cytotoxic T-cell activation. *(242)* Both, GBM and malignant melanoma originate from the neuroectodermic lineage, thus share certain similarities in their expression profiles and response to therapy *(243)*. Currently, Nivolumab is investigated in a phase III trial as monotherapy, but also in combination with ipilimumab versus bevacizumab, a recombinant humanized anti-VEGF antibody, for the treatment of recurrent GBM (NCT02017717).

Trabectedin, for instance, is a DNA-damaging drug which has recently been discovered killing TAM rather than tumor cells, even in drug-resistant soft tissue carcinomas transplanted into immunocompetent mice. Based on the interplay between immune cells, stroma cells of the microenvironment as well as tumor cells, manipulation of TAM is considered as promising strategy for further treatment of cancer. *(180, 185)* Inhibition of colony stimulating factor 1

(CSF1) or its receptor (CSF-1R) limits tumor growth and is also essential for survival of macrophages in tumors. Figure 18A highlights the interplay between tumor cells, TAM and adaptive immune cells, without treatment. TAM produce proangiogenetic factors for elevated tumor survival and also suppress the generation of adaptive immune cells. *(185)* After treatment with TAM-inhibitors or anti-CSF-1R antibody (RG7155), the adaptive immune cells can develop and execute their antitumor function Figure 18B. When treated with CSF-1R brain-permeable peptide inhibitors, a re-education of TAM takes place rather than killing them. So, the drug blocks the tumor-promoting function of TAM and further enhances their immunostimulatory properties (Figure 18C). *(185)*

Currently, manipulation of TAM alone is not sufficient to induce a therapeutic effect, however, combinational therapy together with chemotherapy shows efficacy. There are already substances for the inhibition of CSF-1R, leading to a depletion of TAM and subsequently increasing the efficacy of paclitaxel in breast cancer patients. *(191)* Not only inhibitors, but also the monoclonal antibody RG7155 against human CSF-1R is effective in treatment of diffuse-type giant cell tumors. *(244)* The brain-permeable peptide inhibitor BLZ945 against CSF-1R works through a downregulation of protumorigenic genes like *Arg1* and *mannose receptor 1 (Mrc1)*. *(245)* (Figure 18)

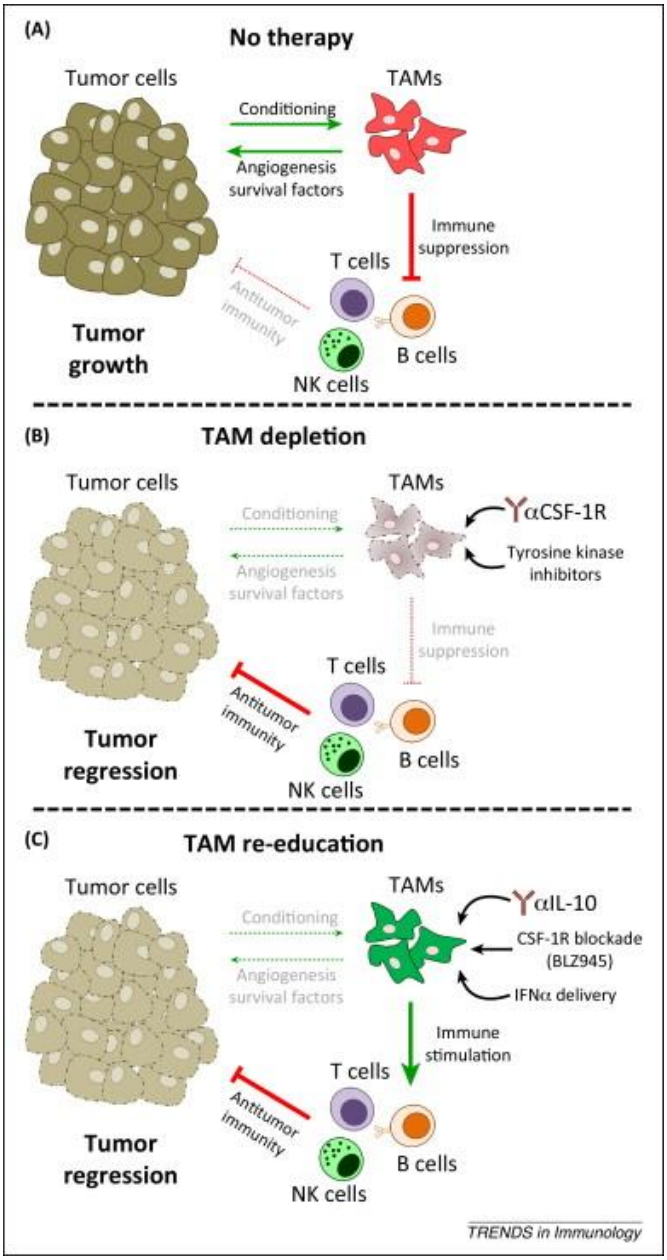

Figure 18. **Therapeutic targeting of TAM. (a)** Interplay between TAM and tumor cells without treatment. **(b)** TAM depletion after treatment with CSF-1R monoclonal antibody RG7155. **(c)** TAM re-education after treatment with brain-permeable CSF-1R inhibitor BLZ945. *(185)*

Nevertheless it has to be kept in mind that also non-tumor macrophages can be affected by immunotherapy, thus it needs further improvement to treat human tumors in a very effective and specific way.

1.8.3 Tyrosine kinase inhibitors

Currently, a large set of tyrosine kinase inhibitors has been investigated as mono- or combinational therapy for GBM *(112)*. Concerning EGFR, erlotinib and gefitinib were applied in two separate phase II trials for patients with recurrent GBM *(246-248)*. Erlotinib did not show any benefit for the patients as monotherapy *(246, 247)*. Interestingly, patients suffering side effects from gefitinib like diarrhea and rash displayed a better overall survival, but EGFR expression status (EGFR WT or EGFRvIII) did not show any impact on the overall survival *(248)*. Furthermore, inhibitors of the platelet derived growth factor receptor (PDGFR) and the VEGFR are investigated for use in recurrent GBM (NCT01229644).

In addition, diverse multitarget tyrosine kinase inhibitors are under preclinical investigations. In the literature, they are characterized as antagonists for a whole set of different kinases. To name some examples, while lapanitib and vandetanib reversibly inhibit kinases in the EGFR pathway, Bay846 represents an irreversible EGFR pathway kinase inhibitor. Accordingly, lapatinib did not show any effect on outcome in a phase I/II study in recurrent GBM. *(249)*

1.8.4 Experimental therapy

Due to the severe side effects and with respect to the high recurrence rate after application of the triple gold standard therapy, new non-invasive therapy options have to be developed for GBM treatment. Promising results were shown by an experimental photodynamic therapeutic approach in brain tumors *(250)*. The idea of photodynamic therapy is based on the fact that nearly 90% of the GBM relapses are located in a 2cm area surrounding the primary tumor bed, which may be formed by local residual cancer cells *(251, 252)*. Thereby, photodynamic therapy is under investigation in addition to standard therapy or as second line treatment. Photodynamic therapy, also referred to as photo-chemotherapy, combines a photosensitizing substance, excited by use of a laser and therefore elicits phototoxic effects on the tumor cells, thus inducing cell death. Vanaclocha *et al.* characterized the side effects of this therapy modality as “mild and manageable”, reaching from brain edema, which can be controlled with corticosteroid treatment, to hemiparesia (recovering in 3 of 4 patients by use of dexamethasone and mannitol), hydrocephalus, ptosis, scalp burn, cutaneous toxicities and erythema *(250)*.

Besides photodynamic therapy, Nogueira *et al*. identified the NFκB pathway as novel experimental approach in GBM treatment. They could send GBM cells into senescence when they used NFκB inhibitors *in vitro* as well as in mouse models. *(253, 254)* However, the induced

senescence was only transient, which might be due to reactivation of cancer cells by survival promoting triggers. Thus, bringing tumor cells into senescence does not represent a cure, but more likely a reversible cell cycle arrest of these cells.

1.9 Aims of this study

According to recent findings of Spiegl-Kreinecker *et al.,* GBM harboring an activating *TERT* promoter MUT are characterized by higher tumor aggressiveness as compared to WT GBM. However, underlying mechanisms explaining this fact have not been identified yet. *TERT* promoter mutations go hand in hand with reactivation of telomerase, leading to elongation of the telomeres and increased cellular longevity, hence reduced self-limiting potential of tumor cells. Telomerase activity in somatic cells is mostly restricted to malignant transformation processes. With respect to *TERT* reactivation in cancer, various non-canonical functions of telomerase came into focus. Accordingly, the NFκB as well as the JAK/STAT signaling pathways were outlined. Both constitute important regulatory pathways concerning cell differentiation, proliferation, oncogenesis and immune-modulation. Another important factor influencing cancer aggressiveness and therapy response is the tumor-associated immune recognition and activation. The tumor-associated immunity is tightly controlled by a variety of immune-checkpoints. Especially the PD-1/PD-L1 system has recently been discussed in this respect. The immune-checkpoint modulator PD-L1 is expressed in 70-80% of all GBM cases, representing a repressor of T-cell activation and adaptive immunity in this tumors.

In short, the aim of the study was to identify the molecular mechanisms underlying the enhanced aggressiveness in *TERT* promoter MUT GBM samples as compared to WT cells. We investigated the associations between the *TERT* promoter mutation status and NFκB and JAK/STAT pathways as well as PD-L1 expression levels in nine GBM cell lines. According to the literature, we had hypothesized more pronounced NFκB and JAK/STAT pathway activities as well as PD-L1 positivity in GBM harboring a *TERT* promoter mutation as compared to WT cases.

2 Materials and Methods

2.1 Cell culture, cell lines and media

The panel of cell lines used for this project is listed in Table 1. All cell models were kept in cell culture flasks under humidified conditions containing 5% CO_2 at 37°C (normal cell culture conditions). Each growth medium was supplemented with 10% fetal bovine serum (FBS, Sigma-Aldrich, Missouri, USA) (Table 1). Antibiotics or any other anti-pathogenic substances were never used during the study.

Table 1. Panel of cell lines used for this project.

Cell line	Entity	*TERT* promoter status	SNP[~]	Growth medium	Source
BTL53	GBM	WT	TT	RPMI* 1640 (Sigma-Aldrich)	Sabine Spiegl-Kreinecker; Neuromed Campus of the Kepler University Hospital in Linz
BTL1333	GBM	WT	CT	RPMI* 1640 (Sigma-Aldrich)	Sabine Spiegl-Kreinecker; Neuromed Campus of the Kepler University Hospital in Linz
Gli66	GBM	WT	CT	RPMI* 1640 (Sigma-Aldrich)	Department of Neurosurgery, General Hospital of Vienna; established in the ICR[+]
Gli72	GBM	WT	TT	RPMI* 1640 (Sigma-Aldrich)	Department of Neurosurgery, General Hospital of Vienna; established in the ICR[+]
U373	GBM	C228T	TT	MNP[‡] (Sigma-Aldrich)	ATCC (The Global Bioresource Center)
U87MG	GBM	C228T	TT	DMEM[Þ] (Sigma-Aldrich)	ATCC (The Global Bioresource Center)
T98G	GBM	C250T	TT	MNP[‡] (Sigma-Aldrich)	ATCC (The Global Bioresource Center)
HUMI	GBM	C228T	CC	RPMI* 1640 (Sigma-Aldrich)	Sabine Spiegl-Kreinecker; Neuromed Campus of the Kepler University Hospital in Linz

AMCH	GS[†]	C250T	TT	RPMI* 1640 (Sigma-Aldrich)	Sabine Spiegl-Kreinecker; Neuromed Campus of the Kepler University Hospital in Linz

[‡]DMEM Dulbecco's Modified Eagle's Medium
[†]GS Gliosarcoma
[+]ICR Institute for Cancer Research, Vienna
[‡]MNP Modified Eagle's Medium supplemented with 0.2% Na-pyruvate and 1% non-essential amino acids
*RPMI Roswell Park Memorial Institute
[~]SNP Single nucleotide polymorphism rs2853669
CC homozygous carrier of SNP rs2853669
CT heterozygous carrier of SNP rs2853669
TT noncarrier of SNP rs2853669.

In order to freeze the cells for storage, the cell pellet was dissolved slowly in the appropriate medium containing 7.5% dimethyl sulfoxide (DMSO). In brief, the cells were trypsinized and afterwards centrifuged at 240g for five minutes at room temperature. The cell pellet was resuspended very slowly in the appropriate medium supplemented with 7.5% DMSO. Subsequently, the aliquots were frozen at -80°C for one day until they were transferred to liquid nitrogen for long-term storage. *Vice versa* to freezing, the cells were thawed very quickly in warm water and then transferred into a cell culture flask with warm medium immediately.

Table 2 summarizes the appropriate cell numbers for the applied experiments. The amounts of cells seeded per experiment were chosen according to the particular proliferation times of the cell models as well as to the experiment-specific demands.

Table 2. Number of seeded cells per mL adapted to assay specificities.

Cell line	MTT[+] assay	Colony formation assay	Luciferase reporter assay	Flow cytometry	qRT-PCR[~]	Spheroid assay
BTL53	$3x10^4$	1000	$3.5x10^5$	$3x10^5$	$3x10^5$	$1x10^4$
Gli72	$3x10^4$	1000	$3x10^5$	$3x10^5$	$2x10^5$	$1x10^4$
BTL1333	$3x10^4$	1000	$3.5x10^5$	$3x10^5$	$3x10^5$	$1x10^4$
Gli66	$3x10^4$		$3.5x10^5$			$1x10^4$
T98G	$2x10^4$	500	$3x10^5$	$2x10^5$	$2x10^5$	$1x10^4$

U373	$2x10^4$	500	$3x10^5$	$2x10^5$	$2x10^5$	$1x10^4$
HUMI	$2x10^4$	500		$2x10^5$		$1x10^4$
U87MG	$2x10^4$	500		$2.5x10^5$	$2x10^5$	$1x10^4$
AMCH	$2x10^4$	500		$2.5x10^5$	$2x10^5$	$1x10^4$

[+]MTT 3-(4,5-Dimethylthiazol-2-yl)-2,5-diphenyltetrazolium bromide assay

[~]qRT-PCR quantitative reverse transcriptase polymerase chain reaction

2.2 Drugs

All drugs that were used in this study are summarized in Table 3.

Table 3. Drugs that were used during this project.

Drug	Target	Chemical structure	Solvent	Source
QNZ (EVP4593)	SOC[†]	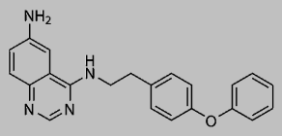	DMSO[₱]	Sigma-Aldrich
Bay-11-7082	IkBα	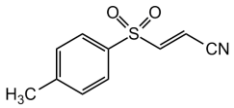	DMSO[₱]	Sigma-Aldrich
STATTIC	STAT-3	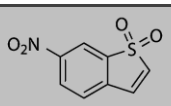	DMSO[₱]	Sigma-Aldrich
WP1066	STAT-3	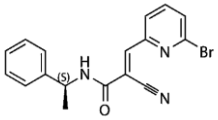	DMSO[₱]	Calbiochem, San Diego, California, USA

[†]SOC Store-operated calcium

[₱]DMSO Dimethyl sulfoxide

QNZ (EVP4593) is an NFκB pathway inhibitor by blocking the neuronal store-operated calcium (SOC) entry into the cell. Hence, it works upstream of NFκB and indirectly inhibits the transcription factor activation *(255)*. Furthermore, it inhibits IL6 and the TNF-α production, thus it possesses anti-inflammatory efficacy. The experimental agent QNZ is a derivate of quinazoline and was primarily developed for treating Huntington's disease. *(256-258)*

Bay-11-7082 is another inhibitor of the NFκB pathway specifically impeding the cytokine-induced phosphorylation of the kinase IkBα. Phosphorylation of the kinase, induces degradation of the molecule, thereby NFκB is released from the inhibitory protein IkBα and can be translocated into the nucleus. Unphosphorylated IkBα is inactive, thus NFκB is retained in the complex with IkBα and no signal is transduced into the nucleus. *(124, 259-261)*

STATTIC is a non-peptidic small molecule inhibiting the function of the SH2 domain of STAT3. Thus, it hinders the activation and (homo-) dimerization of STAT3 regardless of the STAT3 phosphorylation status. Subsequently, it indirectly inhibits nuclear translocation of the transcription factor STAT3 *(262, 263)*.

WP1066 is a small molecule multi-target drug, a derivative of the natural compound caffeic acid. Primarily, it inhibits STAT3, but it has further been reported to possess proapoptotic and antiproliferative activity in human GBM cell lines U87MG and U373, thus it has potent intrinsic antiglioma activity. WP1066 is a powerful immune modulator in GBM patients. It can reverse the common immune tolerance in GBM by upregulating co-stimulatory molecules CD80 and CD86 on peripheral macrophages and tumor-infiltrating microglia, which are important signaling molecules in T-cell activation. *(264-269)*

2.3 Buffers and solution mixes

Recipes for all buffers and solutions used during this study are listed in Table 4.

Table 4. Summary of all used buffers and solutions.

Buffer/ solution/ mix	Volumes/ weights	Source
PBS	**10x**	
Na_2HPO_4 x 2 H2O	95g	Merck, Darmstadt, Germany
NaH_2PO_4 x H2O	32g	Merck
NaCl	44g	Merck
ddH2O	→ 1L	
TBS	**10x**	
Tris	120g	Merck
NaCl	90g	Merck
ddH2O	→ 1L and bring to pH 7.6	
TBST	**1x**	

TBS (10x)	100mL	
ddH2O	900mL	
Tween20	1mL	Bio-Rad, Hercules, California, USA
FACS-PBS		
Na_2PO_4 x 2 H2O	11.5g (78.1mM)	Merck
KH_2PO_4	2g (14.7mM)	Merck
KCl	2g (26.8mM)	Merck
NaCl	80g (1.37M)	Merck
ddH2O	→ 1L	
Lysis buffer for protein isolation		
Lysis buffer 500µL	50mM Tris/HCl (pH 7.6) 300mM NaCl 0.5% Triton X-100	Sigma-Aldrich
PMSF (protease inhibitor)	5µL	Roche, Rotkreuz, Switzerland
cOmplete (protease inhibitor)	12.5µL	Roche
PhosSTOP (phosphatase inhibitor)	25µL	Roche
Separation gel (10% Acrylamid)	**Per gel**	
H2O	3.65mL	
Acrylamid	1.875mL	Bio-Rad
Tris/HCl, 1.5M, pH8.8	1.875mL	Merck/Sigma
20% SDS in ddH2O	75µL	Sigma-Aldrich
10% APS	25µL	Sigma-Aldrich
TEMED	5µL	Biochemica, Billingham, UK
Collecting gel (4.5% Acrylamid)	**Per gel**	
H2O	1.56mL	
Acrylamid	0.281mL	Bio-Rad
Tris/HCl, 0.5M, pH6.8	0.625mL	Merck/Sigma-Aldrich
20% SDS in ddH2O	25µL	Sigma-Aldrich
10% APS	12.5µL	Sigma-Aldrich

TEMED	2.5µL	Biochemica
Running buffer	**10x**	
Tris	30g	Merck
Glycine	144g	Merck
SDS	10g	Sigma-Aldrich
ddH2O	→ 1L	
Bjerrum MeOH		
Tris	5.82g	Merck
Glycine	2.93g	Merck
MeOH	200mL	Merck
ddH2O	→ 1L	
Bjerrum SDS		
Tris	5.82g	Merck
Glycine	2.93g	Merck
SDS	0.375 g	Sigma-Aldrich
ddH2O	→ 1L	
Sample loading buffer	**4x**	
10% Glycine	4mL	Merck
2-Mercaptoethanol	2mL	Merck
SDS	0.92g	Sigma-Aldrich
1M Tris/HCl (pH 6.8)	2.5mL	Merck/Sigma-Aldrich
ddH2O	→ 10mL	
Ponceau S staining solution		
Ponceau S	1g (0.1%(w/v))	Sigma-Aldrich
Acetic acid	50ml (5%(v/v))	Merck
ddH2O	→ 1L	
Luminol solution		
p-Coumaric acid	125µL	Sigma-Aldrich
Luminol	250µL	Sigma-Aldrich
1M Tris/HCl (pH 8.8)	5mL	Merck/Sigma-Aldrich
ddH2O	→ 50mL	

Reverse transcription master mix	Per sample	
5x transcription buffer	4µL	Thermo Fisher Scientific, Waltham, Massachusetts, USA
Random hexamer primers	1µL	GE Healthcare, Little Chalfont, UK
dNTPs (10mM each)	1µL	life technologies, Carlsbad, California
DTT	2µL	life technologies
RevertAid MMLV reverse transcriptase (37°C)	1µL	Thermo Fisher Scientific
qPCR Master Mix	**Per well**	
GoTaq qPCR Master Mix	5µL	Promega, Madison, Wisconsin, USA
Forward primer	0.1µL	Eurofins Genomics, Luxemburg
Reverse primer	0.1µL	Eurofins Genomics
Crystal violet staining	**Stock**	
Crystal violet	1g	Sigma-Aldrich
Ethanol	10mL	Merck
Working solution	→ Stock 1:1000 in PBS	

APS	Ammonium persulfate
dNTP	Deoxy-nucleoside triphosphate
DTT	Dithiothreitol
FACS-PBS	Fluorescence-activated-cell-sorting – Phosphate-buffered-saline
MeOH	Methanol
PMSF	Phenyl-methane-sulphonyl-fluoride
PBS	Phosphate-buffered saline
SDS	Sodium dodecyl sulfate
TBST	Tris-buffered saline with 0.1% Tween20
TEMED	Tetramethylendiamin

2.4 Growth behavior characterization assays

2.4.1 Cytotoxicity assay (MTT)

The cytotoxicity assay is a widely used method in cell culture to determine cell viability, therefore it is also referred to as viability assay. The results of it can further be used to calculate the half maximal inhibitory concentration (IC50) of drugs or toxic substances, thus it determines the sensibility of a cell line to a certain treatment. In this study we used EZ4U cytotoxicity assays (Biomedica, Vienna, Austria), which are non-radioactive enzymatic cell proliferation assays. The method is based on the ability of living cells to reduce slightly colored or uncolored tetrazolium salts into intensely colored formazan derivatives (3-(4,5-Dimethylthiazol-2-yl)-2,5-diphenyltetrazolium bromide (MTT)) (Figure 19). This color signal can be measured with a spectrophotometer, at 450nm filter and 620nm as a reference. Since the reaction takes place in viable mitochondria, this reductive process can only be performed by living cells. Hence, a higher amount of living cells correlates directly with more MTT and more intense color.

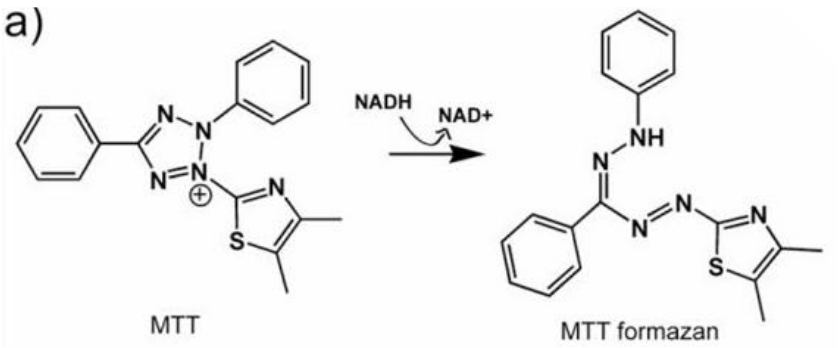

Figure 19. Reduction of MTT to formazan. MTT is reduced to formazan by the mitochondrial reductase and the reduction equivalents NADH and NAD+ *(270)*.

Procedure

On the first day, cells were seeded in 100mL per well into 96-well microtiter plates (Table 2). The cells were incubated overnight under normal cell culture conditions in order to recover and attach to the surface. On the second day, the cells were treated with serially increasing drug concentrations. We usually incubated the cells for 7two hours under normal cell culture conditions. On the fifth day after seeding, the cell viability was determined with the EZ4U kit following the manufacturer's guidelines (Biomedica, Vienna, Austria). The incubation time of the EZ4U developer solution on the cells varied between one and four hours (normal cell culture conditions), depending on the amount of cells and their metabolic activity. The enzymatic

reaction was measured spectrophotometrically at 450 and 620nm (ASYS Expert Plus, Biochrom Ltd, Cambridge, UK).

2.4.2 Colony formation assay

Colony formation assays are commonly used to investigate the growth behavior of cells and their ability to form clones from a single cell, optionally drug treatment can be included. For performing this assay, the cells must be seeded at a very low density, thus cell death due to isolation from other cells, can be evaluated.

Procedure

Cells were seeded in 24-well plates in appropriate cell number (compare Table 2) and kept under normal cell culture conditions for recovery. After 24 hours, the cells were optionally treated with the drug of interest in varying concentrations and incubated for seven days. Afterwards, the old media was sucked off and remaining media was washed away with phosphate buffered saline (PBS, recipe see Table 4). Subsequently, the cells were fixed with ice-cold (-20°C) methanol (MeOH) for at least 20 minutes at 4°C. The MeOH was washed away with PBS and crystal violet (recipe see Table 4) was added. The cells were incubated on a shaker until they took up the violet color. The remaining crystal violet was rinsed with normal tap water and the plates were dried. Photographs of the wells were taken (Nikon Digital Camera D3200, Minato, Tokyo, Japan).

Quantification of the cell growth can be conducted differentially: On the one hand the plates can be scanned on the Typhoon scanner (Typhoon TRIO Variable Mode Imager, GE Healthcare Life Sciences) since crystal violet is fluorescent when excited by a red laser (633nm). This method measures the area in the well covered by the cells. In this case, a well without cells was included in the experimental setting to normalize the background staining of crystal violet. On the other hand, 2% SDS can be used to dissolve the crystal violet stain from the cells. The eluent was pipetted onto a 96-well plate in triplets and the fluorescence was measured on the Tecan spectrophotometer (Tecan Infinite M200 Pro, Männedorf, Switzerland) at 560nm.

2.4.3 Sphere formation assay

In order to investigate the neuronal growth pattern of cells with respect to their ability to form spheres, sphere formation assays were performed. 5000 cells per well were seeded in doublets in 24-well-plates and kept for one week in NB^+ medium (recipe below). Spheroid growth was documented on microphotographs taken with the AxioCam ICc 5 (Zeiss, Oberkochen, Germany) after four and seven days upon seeding. One week after seeding, the spheres were distributed and set back to standard cell culture plates in their appropriate differentiation media. After one week, cell growth was re-evaluated and cells were fixed and stained with crystal violet as described in section 2.4.2. Quantification and measurement of the cellular growth was performed via elution of the crystal violet from the cells by use of 2%SDS as described previously (section 2.4.2).

NB+ medium

48mL	Neurobasal medium (1x) (life technologies)
1mL	B27 (life technologies)
0.5mL	L-Glutamine (Sigma-Aldrich)
0.5 mL	N2 Supplement A (life technologies)
100µL	EGF (Sigma-Aldrich)
10µL	basal fibroblast growth factor (bFGF) (life technologies)

2.5 Flow cytometry

Flow cytometry technology is a method to analyze the cells according to their morphological properties. It is a laser-based method and can be used in various approaches including cell counting, cell sorting according to their morphology, cell cycle distribution, separation of cells based on cell surface markers or on internal cell similarities. The method has a throughput rate of 10,000 cells per second passing the laser in single cells. When the laser beam hits the cell, the light is scattered depending on the cell's granularity, size and/or antibody binding and detected via differently positioned photomultiplier tubes. Even without any staining the cells can be characterized by their granularity and size according to their side and forward scatters, respectively. Therefore, granularity and size are the two standard markers in flow cytometry. To analyze more specific cell characteristics like a certain surface marker or another protein of interest, cells must be stained with appropriate antibodies marked with fluorescent dyes.

2.5.1 Cell cycle analysis with propidium iodide (PI) staining

One approach of flow cytometry is the separation of cells into subsets according to their characteristic markers; this separation is also referred to as fluorescence-activated-cell-sorting (FACS). One prominent dye used for cell cycle analysis is propidium iodide (PI). PI is a DNA intercalating agent that allows verification of the amount of DNA per cell. This method is especially interesting for drug testing with respect to its impact on the cell cycle distribution, hence G0-G1, S, G2-M phases and apoptotic cells (Figure 20).

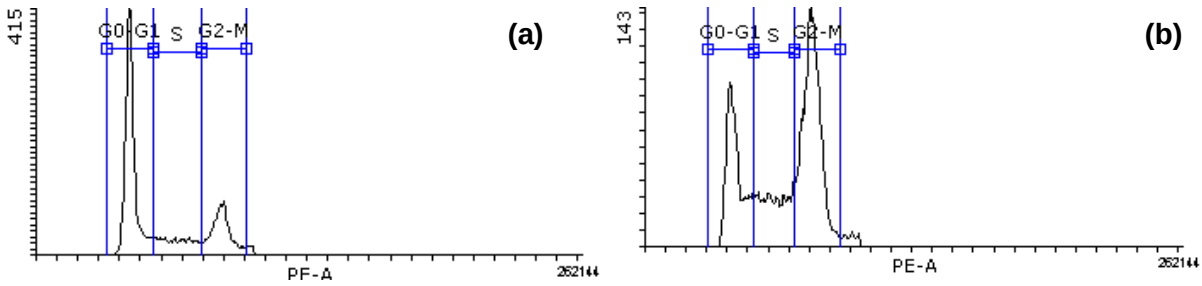

Figure 20. Cell cycle analysis via FACS-PI. FACS-PI provides information about the distribution of the cell cycle phases of the cells after optional treatment with a certain drug. While the y-axis defines the number of counted events (cells), the x-axis describes the light channel. **(a)** Representative FACS-PI histogram of an untreated sample. The majority of cells is enriched in the G0-G1 phase. **(b)** Exemplary FACS-PI histogram of cells treated with a drug. The histogram changes in comparison to the control samples **(a)**, the cells arrest in G2-M phase.

Procedure

For FACS-PI analysis, cells were seeded in 6-well plates and incubated under normal cell culture conditions to recover overnight (Table 2). On the next day, cells were optionally treated with certain drug concentrations. After the incubation time, the cells were prepared for measurement. Therefore the old media was collected and the cells were detached from the bottom of the well by trypsin. The cell suspension was centrifuged (240g, eight minutes) and the supernatant was removed until only 500µL covered the pellet, containing both, the apoptotic and viable cell fraction. The pellet was washed with PBS once and subsequently resuspended in NaCl (0.9%), before the cells were fixed with ice-cold 70% ethanol in a dropwise manner. The fixation step was performed at -20°C for at least one hour. After the incubation time, the cells were collected (240g, three minutes, 4°C) and resuspended in 1mL FACS-PBS (Table 4). Before adding the PI (Sigma-Aldrich), RNA residuals were digested by RNase A (0.79 Kunitz units/mL, 30 minutes at 37°C). Subsequently, the samples were filtered into FACS tubes and the PI dye was added (1mg/mL) and incubated for 30 minutes at 4°C (light sensitive). Finally,

fluorescence was measured by flow cytometry (FACS Calibur – Becton Dickinson, Palo Alto, CA) and quantified using Cell Quest Pro software.

2.6 Protein isolation and analysis methods

2.6.1 Total protein isolation

To harvest the proteins and prepare the protein extracts, the cells were scratched into their medium and centrifuged at 240g for five minutes. After a washing step with PBS, the pellet was dissolved in 30-50mL lysis buffer (Table 4) and incubated for at least 30 minutes on ice. For better lysation, the tubes were mixed by pipetting every ten minutes. After the incubation on ice, the samples were treated with ultrasound for three to five minutes and subsequently centrifuged at full speed (18,000g) for 15 minutes at 4°C. The protein-containing supernatant was transferred into a new tube (separate 2.5µL for protein determination) and stored at -80°C for further usage.

2.6.2 Cytoplasm and nucleus fractioning

The separation of proteins located in the cytoplasm from those in the nucleus was performed with the “NE-PER™ Nuclear and Cytoplasmic Extraction Reagents Kit” (Thermo Fisher Scientific) according to manufacturer’s recommendations.

2.6.3 Total protein determination

Concentrations of protein lysates were determined using “Pierce™ BCA Protein Assay Kit” (Thermo Fisher Scientific). The procedure was performed according to manufacturer’s recommendations. To perform a standard curve, a series of dilutions of known albumin (Thermo Fisher Scientific) concentrations was pipetted onto each plate.

2.6.4 Western blot analysis

Western blot analysis is a semi-quantitative method for analyzing the presence of certain proteins in a sample. In general, Western blot technique is composed of two main steps: First, equal concentrations of the isolated proteins are separated according to their atomic mass via two-gel poly-acrylamid-gel-electrophoresis (PAGE) (Table 4). In a second step, the proteins are transferred from the electrophoresis gel onto a membrane via Western blotting. The blotting procedure is an electrophoretic method using electric voltage in order to force the negatively

charged proteins to migrate from the gel to the membrane where they are bound due to hydrophobic interactions. The protein transfer is evaluated by total protein staining with Ponceau solution. Before incubation with the specific primary antibody, endogenous epitopes on the membrane are blocked by addition of 0.5% bovine serum albumin (BSA) and 1% non-fat milk powder. The primary antibody is detected via specific binding of a horse radish peroxidase labeled secondary antibody. The signal is detected via a chemiluminescent reaction triggered by an added substrate and is visualized on an x-ray film. Figure 21 schematically illustrates the Western blot procedure.

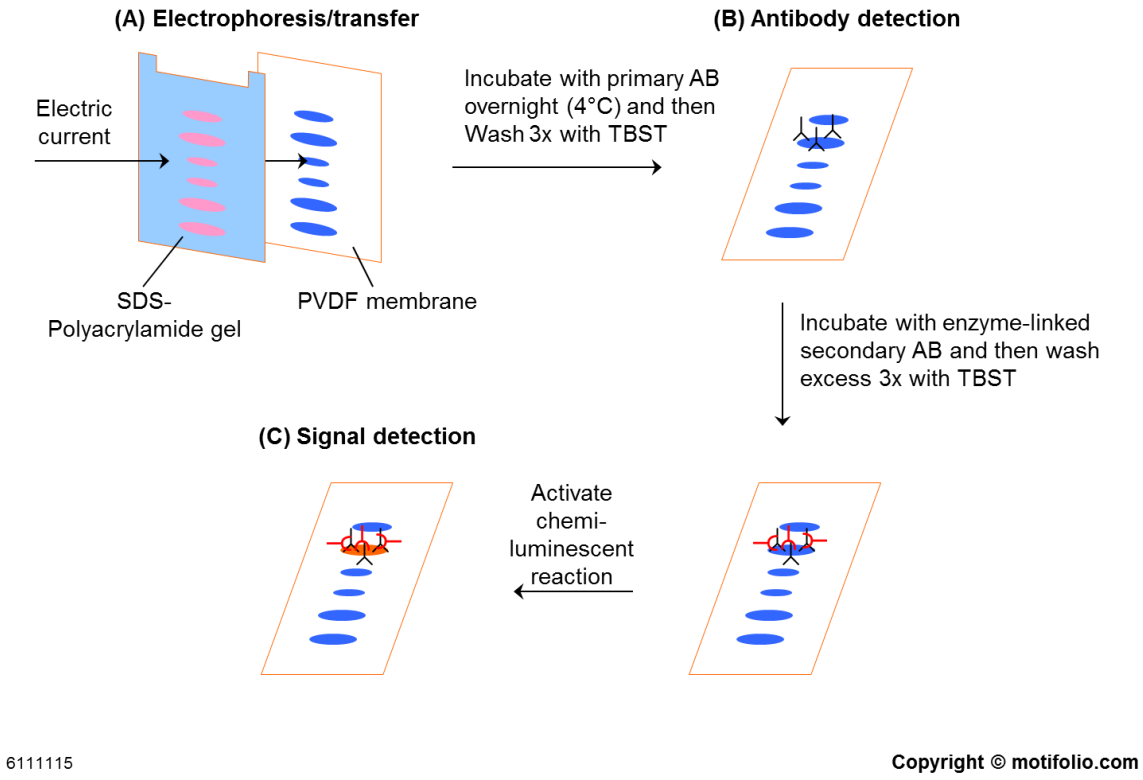

Figure 21. Schematic overview of the Western blot procedure. (A) First, proteins are separated according to their molecular weight by electrophoretic separation via a SDS-PA gel and afterwards the proteins are blotted onto a PVDF membrane. **(B)** The target antibodies on the membrane are detected via specific monoclonal antibodies, which themselves are targeted by use of an enzyme-linked secondary antibody binding to the Fc region of the primary antibody. **(C)** Addition of substrate for the antibody-linked enzyme triggers an active chemiluminescent reaction for visualizing the antibody binding. *(271)*

Procedure

10 or 15µg of protein were used for separation via Western blot. Therefore, the protein stocks were diluted in lysis buffer and 4x sample loading buffer. PAGE was performed in running buffer (Table 4) at 90V (Power-Pac HC, Bio-Rad). Afterwards, the separated proteins were transferred

to a polyvinylidenfluorid (PVDF) membrane via semidry Western blotting. In detail, the PVDF membrane was activated with MeOH and subsequently washed in Bjerrum MeOH (Table 4). The blotting sandwich was built in the following order and blotting procedure was performed in a semidry manner (0.08mA for one blot or 0.16mA for 2 gels for 45-60 minutes) (Trans-Blot Turbo Transfer System, Bio-Rad):

1) Filter (with Bjerrum buffer with MeOH)
2) Activated membrane (activate with MeOH)
3) Electrophoresis gel
4) Filter (with Bjerrum buffer with SDS)

After blotting, the membrane was washed with A.bidest. for ten seconds and incubated in Ponceau solution (Table 4) for ten minutes in order to evaluate the protein separation and blotting success. After several washing steps in A.bidest and Tris-buffered saline with Tween20 (TBST, recipe see Table 4), the membrane was incubated in milk solution (TBST with 1% powdered milk and 0.5% BSA) for one hour in order to block endogenous epitopes. Then the primary antibody solution (diluted 1:1000 in TBST with 3% BSA; antibodies are listed in Table 4) was added and incubated overnight at 4°C. On the next day, the primary antibody was removed and the blot was washed three times with TBST for ten minutes each, before the secondary antibody (1:10,000 in TBST with 1% BSA; antibodies are listed in Table 4) was added and incubated for one hour at RT. After three further washing steps with TBST, luminol (recipe see Table 4) was activated with H_2O_2 (Sigma-Aldrich; per blot: 2mL luminol + 0.6µL H_2O_2) and finally the signal was developed in the dark chamber on an x-ray film (GE Healthcare). Table 5 summarizes all used primary and secondary antibodies.

Table 5. List of all used antibodies.

Primary antibodies (1:1000 in TBST with 3%BSA)	**Source**	**Company**
β-Actin	Mouse	Sigma-Aldrich
AKT	Rabbit	Cell signaling (Cambridge, UK)
P-AKT (Ser473)	Rabbit	Cell signaling
β-Catenin	Rabbit	Cell signaling
EGFR	Rabbit	Cell signaling

ERK	Rabbit	Cell signaling
P-ERK (Tyr202/Ser204)	Rabbit	Cell signaling
ETS1	Rabbit	Cell signaling
IκBα	Mouse	Cell signaling
P-IκBα (Ser32)	Mouse	Cell signaling
Lamin A/C	Mouse	Cell signaling
NFκB (p65)	Rabbit	Cell signaling
P-NFκB (p65) (Ser536)	Rabbit	Cell signaling
PD-L1	Rabbit	Cell signaling
PTEN	Rabbit	Cell signaling
S6	Rabbit	Cell signaling
P-S6 (Ser240/244)	Rabbit	Cell signaling
STAT3	Rabbit	Cell signaling
P-STAT3 (Tyr705)	Rabbit	Cell signaling
TERT	Rabbit	Santa Cruz (Dallas, Texas, USA)
α-Tubulin	Mouse	Cell signaling
Secondary antibodies (1:10,000 in TBST with 1%BSA)	**Source**	**Company**
α-mouse antibody	Rabbit	Cell signaling
α-rabbit antibody	Goat	Cell signaling

2.6.5 Telomerase repeat amplification protocol (TRAP assay)

The telomerase activity was investigated using the TRAPEZE® Telomerase Detection Kit from Chemicon (Millipore, Billerica, MA, USA). *(272)* based on the method described by Kim *et al. (273)*. This polymerase chain reaction (PCR)-based assay is performed in two steps. In the first step, the telomerase adds a number of telomeric repeats (GGTTAG) to the 3´end of a telomerase substrate (TS) oligonucleotide. In the second step, the extended products are

amplified by PCR using the TS and reverse (RP) primers, generating a ladder of six base products starting at 50bp. Following PCR, the amplification products are separated by gel electrophoresis (Figure 22) *(274)*. All analyses were performed together with the Theoretische Neurochirurgie at the Neuromed Campus of the Kepler University Hospital in Linz.

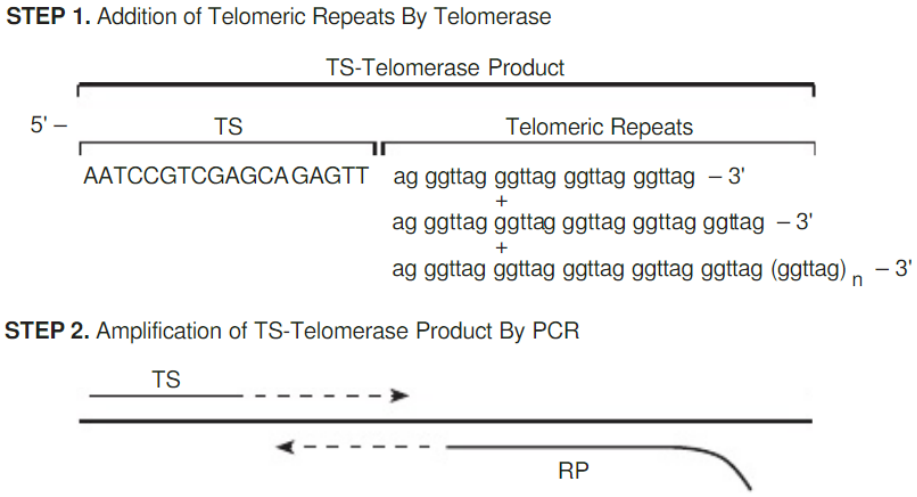

Figure 22. The telomeric repeat amplification protocol (TRAP assay). For quantification and characterization of the telomerase activity, the TRAP assay uses an artificial TS primer representing a template for the cellular telomerase to elongate its G-rich repeats by adding dNTPs **(STEP 1)**. The resulting double-strand is denatured in a second step and finally amplified in a PCR reaction before separation on via gel electrophoresis **(STEP 2)**. *(272)*

Procedure

Cells were lysed in 200µL 1xCHAPS Lysis Buffer supplemented with 100units/mL RNase Inhibitor and kept on ice for 30 minutes before centrifugation (12,000g, 20 minutes, 4°C). The supernatant was stored at -80°C. After protein determination (see chapter 2.6.3.), the further procedure was performed according to manufacturer's recommendations (Millipore, Billerica, MA, USA) *(272)*. An internal 36bp standard was added to each sample in order to exclude contamination with proteases. Furthermore, a negative control containing CHAPS lysis buffer instead of the sample was included in the experimental setting. The defined oligo template thrombospondin type 1 repeat 8 (TSR8) (0.1 atto-mole) served as telomerase quantification control for each set of assays. Additionally, for the telomerase control every sample was heat-inactivated (85°C, ten minutes) to exclude contamination. PCR products were separated by PAGE (12% gel) and the gels were stained with ethidium bromide. Visualization was conducted under UV illumination (ChemiDoc; Bio-Rad).

Product ladder bands were quantified by Quantity One Quantification software (Bio-Rad) and calculated relatively to the DNA ladder of 0.1 atto-mol Telomerase Quantitation Control Template TSR8 following the manufacturer's instructions. All results were confirmed in at least two independent experiments.

For quantification, the following parameters have to be measured: a) signals of the gel lanes corresponding to the DNA ladder from all samples including non-heat-treated (x) and heat-inactivated samples (x_0), b) negative control (CHAPS buffer) (r_0) and TSR8 quantification control (r) and c) internal standard in non-heat-treated (c) and TSR8 quantification control (c_R). Finally, the total product generated (TPG) units were calculated according to the following formula:

$$\text{TPG units} = \frac{(x - x_0) / C}{(r - r_0) / C_R} \times 100 \text{ (if 0.1 atto-mol of TSR8 was used)}$$

According to the manufacturer's protocol, *each unit of TPG corresponds to the number of TS primers (in 1 x 10^{-3} amole or 600 molecules) extended with at least 4 telomeric repeats by telomerase in the extract in a 30 minute incubation at 30°C. The assay has a linear range of 1 to 300 TPG, which is equivalent to telomerase activity from approximately 30 to 10,000 control cells. Results shown in Figure 23 demonstrate application of this quantitation methodology. (272)*

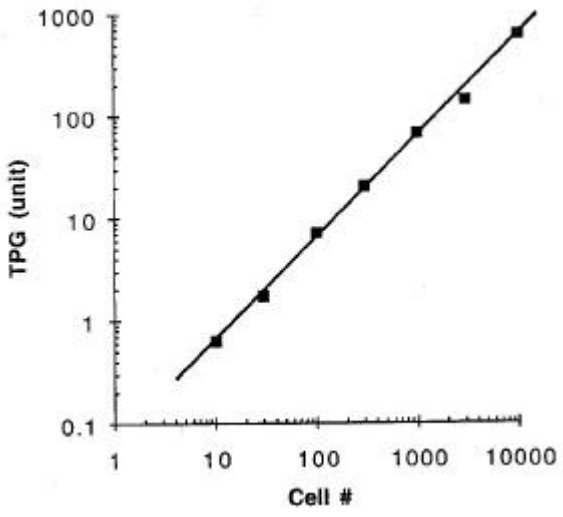

Figure 23. Quantification curve for TRAP assay. The assay ranges from 1 to 300 TPG units in a linear manner. This corresponds to the telomerase activity of about 30 to 10,000 control cells, respectively. One TPG unit is defined as the number of TS primers elongated with at least four telomeric repeats after the specified incubation time. *(272)*

2.7 Luciferase reporter assay

In order to elucidate the transcriptional activity and functionality of the WT as well as the MUT *TERT* promoter variants, luciferase reporter assays were performed. Therefore, different expression plasmids were designed, each with an inserted functional promoter sequence and a reporter sequence. The functional sequence encodes either for the WT *TERT* promoter or *TERT* promoter variants, while the reporter sequence encodes for the firefly luciferase and is activated via a prior signal.

Previously, it has been postulated that there are two main point mutations in the *TERT* promoter, together accounting for more than 90% of all *TERT* promoter alterations in GBM *(34, 100)*. Both mutations are C to T transitions, however, one is located -124bp (C228T) and the other -146bp (C250T) upstream from the ATG start codon in the *TERT* promoter. Furthermore, the SNP rs2853669 has been reported to be important in GBM pathology, especially with respect to the patients' prognoses. *(38)* Therefore, each plasmid was additionally designed with this inserted SNP (rs2853669) in the *TERT* promoter. Each of the TERT promoter constructs was kindly provided by Prof. Kumar/ DKFZ Heidelberg (published by Rachakonda *et al. (275)*).

In addition, a negative and a positive control plasmid were included in the experimental setting in order to exclude false positive and negative results, respectively. The negative promoter-less control was used to normalize the background- or auto-luminescence. The positive control harbors a highly active cytomegalovirus (CMV) promoter. Furthermore, a plasmid for determination of the transfection efficiency was included and served as the internal control. This plasmid harbors a reporter encoding for *Renilla* luciferase (Promega), which can be differentiated from the firefly luciferase. All used vectors and the appropriate vector maps are summarized in Table 6 and Figure 49, respectively.

Table 6. Vector constructs for luciferase reporter assay.

Vector	Promoter	Reporter
WT	*TERT* WT	Firefly luciferase
WT SNP	*TERT* WT + SNP rs2853669	Firefly luciferase
C228T	*TERT* C228T	Firefly luciferase
C228T SNP	*TERT* C228T+ SNP rs2853669	Firefly luciferase
C250T	*TERT* C250T	Firefly luciferase

C250T SNP	*TERT* C250T+ SNP rs2853669	Firefly luciferase
Internal Ctrl	TK[†]	*Renilla* luciferase
neg. Ctrl	Promoter-less	Firefly luciferase
pos. Ctrl	CMV[‡]	Firefly luciferase

[†]TK Thymidine kinase promoter

[‡]CMV Cytomegalovirus promoter

Procedure

The assay needs roughly 80-90% cell confluence on the day of transfection. Therefore, cells were seeded in their appropriate medium in 6-well plates (Table 2) and incubated overnight under normal cell culture conditions in order to recover. On the next day, the transfection was performed using Lipofectamine 2000 (Invitrogen, Carlsbad, California, USA) for reaching better permeability of the cellular membrane. The used plasmids *(275)* are summarized in Table 6. For transfection, 1µg of each reporter plasmid as well as 100ng *Renilla* construct were diluted in 250µL serum-free media. In parallel, 6µL of the Lipofectamine 2000 (Invitrogen) per well were mixed in serum free medium. Each tube was first incubated separately for five minutes and afterwards Lipofectamine 2000 was added to the reporter plasmids, mixed and kept at 37°C for 20 minutes. In the meantime, old medium was sucked off from the 6-well plates and exchanged by 1.5mL appropriate fresh medium. Finally, 500µL transfection mix was added to each well and the transfection reaction was incubated for eight hours under normal cell culture conditions.

After the incubation time, the media was exchanged and cells were optionally treated with various drugs for 24 hours. In order to harvest the proteins, cells were washed with PBS (4°C) once. Then 140µL of a 0.25M Tris/HCl buffer (pH7.5, 0.5% TritonX100) was added to each well and cells were scratched into the buffer and transferred into 1.5mL tubes. The tubes were kept on ice for at least half an hour, with further mixing by pipetting every ten minutes. After mechanical destruction of the cell membranes by ultrasound for three to five minutes, the lysate was centrifuged for 15 minutes (18,000g, 4°C) and the supernatant was transferred into 500µL tubes, which as stored at -80°C until measurement.

The luciferase activity was analyzed using the “Dual-Glo® Luciferase Assay System” (Promega) and the signal was measured spectrophotometrically (Tecan Infinite M200 Pro). The reaction mix was prepared according to manufacturer’s recommendation: In brief, each sample was

pipetted in doublets onto a white 96-well OptiWell plate (2x60µL) and the same volume of "Dual-Glo® Luciferase Buffer" (Promega) was added and incubated for ten minutes in the dark before measuring (luminescence, 3000ms). After measurement of the first signal, the "Dual-Glo® Stop&Glo" (Promega) buffer was added in order to eliminate the prior firefly signal and to promote activation of *Renilla* luminescence by an enzymatic reaction. After three minutes incubation time in the dark, the *Renilla* signal (internal control) was measured with the same photometric settings. In order to normalize to the transfection efficiency, the firefly/*Renilla* ratio was calculated for each well. Finally, the means of the doublets were calculated and normalized to the negative control in order to exclude auto-luminescence or unspecific background signal.

2.8 RNA isolation and analysis methods

2.8.1 RNA isolation

Total cellular RNA was extracted from the cells using the acid guanidinium thiocyanate-phenol-chloroform extraction. It constitutes a liquid-liquid extraction technique characterized by its highly pure RNA products as well as by the isolation of RNAs, even short RNA species. The RNA was extracted by use of Trizol reagent (Life Technologies, Carlsbad, CA), which also denatures proteins including RNases. After centrifugation, the mixture was separated into an upper aqueous phase, an interphase and a lower organic phase. The RNA-containing upper phase was carefully extracted from the other phases. Subsequently, the RNA was precipitated from the Trizol solution by adding chloroform (Sigma-Aldrich). After centrifugation, the RNA pellet was washed with 70% ethanol twice, and the dried RNA pellet was finally dissolved in RNase-free PCR water and stored at -80°C until further investigation. All centrifugation steps were performed at 12,000g for ten minutes at 4°C. *(276)*

The RNA concentration and quality were assessed by the nanodrop® spectrophotometer (NanoDrop ND-1000, Thermo Fisher Scientific). In cases of insufficient RNA quality (260/280 ratio <1.8; 260/230 ratio <2.0) the RNA was purified by precipitation according to the following solution:

x µL RNA + 4x µL $EtOH_{abs.}$ + 0.1x µL NaAc (3M; 5.2 pH)

$EtOH_{abs}$	absolute ethanol
NaAc	Sodium acetate

The precipitated RNA was centrifuged at the above mentioned settings and washed with ice-cold 70% ethanol. Afterwards RNA was diluted in RNase-free PCR water again.

2.8.2 Reverse transcription

For every experiment, 1000ng of RNA were diluted in RNase-free PCR water and transcribed into complementary DNA (cDNA). First, remaining double-stranded DNA was denatured by heating up to 70°C. After ten minutes, the samples were immediately transferred onto ice, before 9µL of the reverse transcription master mix were added (recipe see Table 4) and incubated at 37°C for 90 minutes. The cDNA product was diluted with RNase-free PCR water (1:25) and stored at -20°C.

2.8.3 Quantitative reverse transcription PCR (qRT-PCR)

qPCR or real-time PCR, is a widely used technique to analyze the mRNA expression in a quantitative way. It is based on the principle of PCR, but additionally monitors the PCR reaction steadily in real-time. The isolated RNA is converted into a cDNA by reverse transcriptase and subsequently amplified via a qPCR. Therefore, the method is referred to as qRT-PCR. In order to detect the PCR products, different fluorescent DNA probes can be added to the reaction. The two most common probes are SYBR Green and TaqMan probes.

In this study, we used SYBR Green probes as PCR detection system. When SYBR Green binds to dsDNA it emits light upon excitation, however, it does not only bind to dsDNA of the PCR product but also to primer dimers. Thus, unspecific binding and therefore overestimation is a common problem. Hence, the use of SYBR Green probes must be strictly validated in order to minimize overestimation caused by unspecific binding of the probes.

TaqMan probes are small oligonucleotides with a quencher unit at the 3’ end and a fluorophore unit at the 5’ end. Due to the close proximity of the two units, the quencher inhibits the fluorescence of the fluorophore. First, the probe hybridizes to the target site of the cDNA by complementary base-pairing. When the DNA polymerase starts the elongation, the probe is sequentially split apart from the cDNA. During this step, the fluorophore unit is separated from the probe and the quencher cannot block the fluorescent signal. This signal can be measured and is directly proportional to the number of the probe cleavage cycles.

Procedure

For each qPCR sample, 5µL of cDNA (1:25) were mixed with 5µL of qPCR master mix (Table 4). Each sample was pipetted in triplets onto a 96-well microtiter plate (MicroAmp Fast Optical 96-Well Reaction Plate (0.1mL), Applied Biosystems by life technologies). mRNA levels were

quantified and normalized either to *β-Actin* or to *ribosomal protein L41 (RPL41),* both serving as housekeeping genes. In order to exclude water or master mix contamination with sample mRNA, a negative control containing RNase-free water instead of cDNA was used. The qPCR analyses were performed on the "ABI qPCR 7500 Fast real-time" automate (Applied Biosystems, Foster City, California, USA) and analyzed by use of the appropriate 7500 Software 2.3 (Applied Biosystems). The results were processed according to the following formula *(277)*:

$$2^{-\Delta CT} = 2^{-(CT\ target\ -\ CT\ housekeeping)}$$

Table 7. List of used primers (Eurofins Genomics).

Target gene	Forward primer	Reverse primer
β-Actin	5´-GGATGCAGAAGGAGATCACTG-3´	5´-CGATCCACACGGAGTACTTG -3´
CD274 (PD-L1)	5'-AAGGCCGAAGTCATCTG-3'	5'-TGGTGGTGGTGGTCTTAC-3'
TERT	5´-CGGAGGAGTGTCTGGAGCAA-3´	5´-GGATGAAGCGGAGTCTGGA-3´
NFκB1	5'-ACTCTGGCGCAGAAATTAGG-3'	5'-TGACTGTACCCCCAGAGACC-3'
RPL41	5'-CAAGTGGAGGAAGAAGCGA-3'	5'-TTACTTGGACCTCTGCCTC-3'
STAT3	5'-GGAGGAGTTGCAGCAAAAAG-3'	5'-TGTGTTTGTGCCCAGAATGT-3'

2.9 Immunohistochemistry (IHC)

Immunohistochemistry was performed in order to confirm previous *in vitro* findings on patient-derived samples. GBM tumor specimens were kindly provided by the Theoretische Neurochirurgie at the Neuromed Campus of the Kepler University Hospital in Linz.

Paraffin embedded samples of one *TERT* promoter WT and one MUT GBM were sliced (3µm) and mounted on slides (Superfrost, Thermo Scientific). For immunohistochemistry, the samples were heated for ten minutes at 65°C, deparaffinized in ethyl-n-butyl ether (EBE) and rehydrated in alcohols with decreasing concentrations, ending up with ddH2O. To evaluate tumor cell morphology of tumor localization, slides were stained with haematoxylin and eosin (HE) (Merck).

2.9.1 Immunostaining for P-STAT3

Samples were boiled in Tris/ ethylenediaminetetraacetic acid (EDTA) buffer (PBS, pH 9.0, DAKO, Agilent technologies, Santa Clara, California, USA) in an autoclave for ten minutes. Following two washing steps in PBS, endogenous peroxidase was blocked with 0.3% H_2O_2 (Sigma Aldrich) in PBS (recipe see Table 4) for ten minutes at room temperature. Samples were rinsed three times with PBS containing 0.1% Tween20 (PBST) and afterwards incubated with Avidin (0.001% in PBS, Sigma Aldrich) as well as with Biotin block (0.02% in PBS, Sigma Aldrich) for ten minutes each. Ultra V Block (UltraVision LP Detection System, Thermo Fisher Scientific) was applied for five minutes at room temperature. Subsequently, slides were incubated with the primary antibody against P-STAT3 (anti-human, anti-mouse, #9145, Cell Signaling) overnight at 4°C. The antibody was diluted 1:100 with the antibody diluent (#8112, Cell signaling), supplemented with 1% goat serum (#5425, Cell signaling). The next day, slides were rinsed three times with PBST, following an incubation with the secondary antibody for 30 minutes (1:150 in PBST, anti-rabbit HRP antibody, Santa Cruz). Afterwards, the signal was developed using DAB Substrate Chromogen System (Dako, Agilent technologies) according to manufacturer's guidelines. Finally, samples were counterstained with Haematoxylin Gill III (Merck), dehydrated and covered with coverslips by use of Entellan (Merck).

2.9.2 Immunostaining for PD-L1

After deparaffinization and rehydration, samples were boiled in a 10mM citrate buffer (TBS, pH 6.0) for six minutes. Following two washing steps in TBS with 0.1% Tween20 (TBST), slides were treated with Ultra V Block (UltraVision LP Detection System, Thermo Fisher Scientific) for five minutes at room temperature. Subsequently, the primary antibody against PD-L1 (1:100 in antibody diluent, Cell signaling; supplemented with 1% goat serum, Cell signaling) was applied and incubated for one hour at room temperature. After two rinsing steps in TBST, Primary Antibody Enhancer (UltraVision LP) was applied for ten minutes at room temperature. Following, slides were incubated with HRP Polymer (UltraVision LP) for 15 minutes at room temperature. Afterwards, the signal was developed using DAB Substrate Chromogen System (Dako, Agilent technologies) according to manufacturer's guidelines. Finally, samples were counterstained with Haematoxylin Gill III (Merck), dehydrated and covered with coverslips by use of Entellan (Merck).

2.10 Statistical analyses

Statistical analyses were performed by using Microsoft Excel as well *as* the calculation software GraphPad Prism 5.0. Significance levels are marked with stars: *** $p<0.001$, ** $p<0.01$, * $p<0.05$.

3 Results

The *TERT* promoter status was already previously described as important factor in the patients´ prognosis. In literature, presence of a *TERT* promoter mutation predicts a worse course of disease in GBM *(9, 38, 40, 278)*. This prognostic value may be influenced by a common SNP rs2853669 in the *TERT* promoter *(38)*. A collaborating group furthermore hypothesized that tumors harboring such an activating *TERT* promoter mutation may be more aggressive as compared to WT GBM *(38)*.

In the current study we first focused on clarifying the hypothesis implying more pronounced tumor aggressiveness in GBM possessing *TERT* promoter MUT background *(9, 38, 40, 100, 278)*. All cell lines (n=9) were characterized according to their special morphological features and growth behaviors. Furthermore, the TERT mRNA and protein expression levels of all cell lines were investigated and related to the *TERT* promoter status. The *TERT* promoter and telomerase activities were compared between the different *TERT* promoter and SNP variants. Especially with respect to recently discovered non-canonical functions of telomerase *(75, 78, 79, 81, 86, 87)*, we analyzed the canonical NFκB cascade as well as the JAK/STAT3 axis as a close NFκB-induced pathway. Finally, we investigated the impact of immune-regulatory protein PD-L1 on the *TERT* promoter status with respect to the tumor aggressiveness in GBM.

3.1 The association between *TERT* promoter status and GBM cell morphology and growth pattern

Detailed information about the GBM cell models and their appropriate cell culture conditions are outlined in section 2.1 (Table 1). Regarding the growth patterns and duplication times, the *TERT* promoter WT cell lines tended to proliferate considerably slower as compared to the *TERT* promoter MUT models. Moreover, the morphology of all cell models differed according to the respective *TERT* promoter status; characteristically, the *TERT* promoter MUT sublines tended to represent an epithelioid shape, while the WT cells harbored a fibroblastoid phenotype. Figure 24 summarizes microphotographs of all investigated GBM cell lines separated according to their *TERT* promoter status.

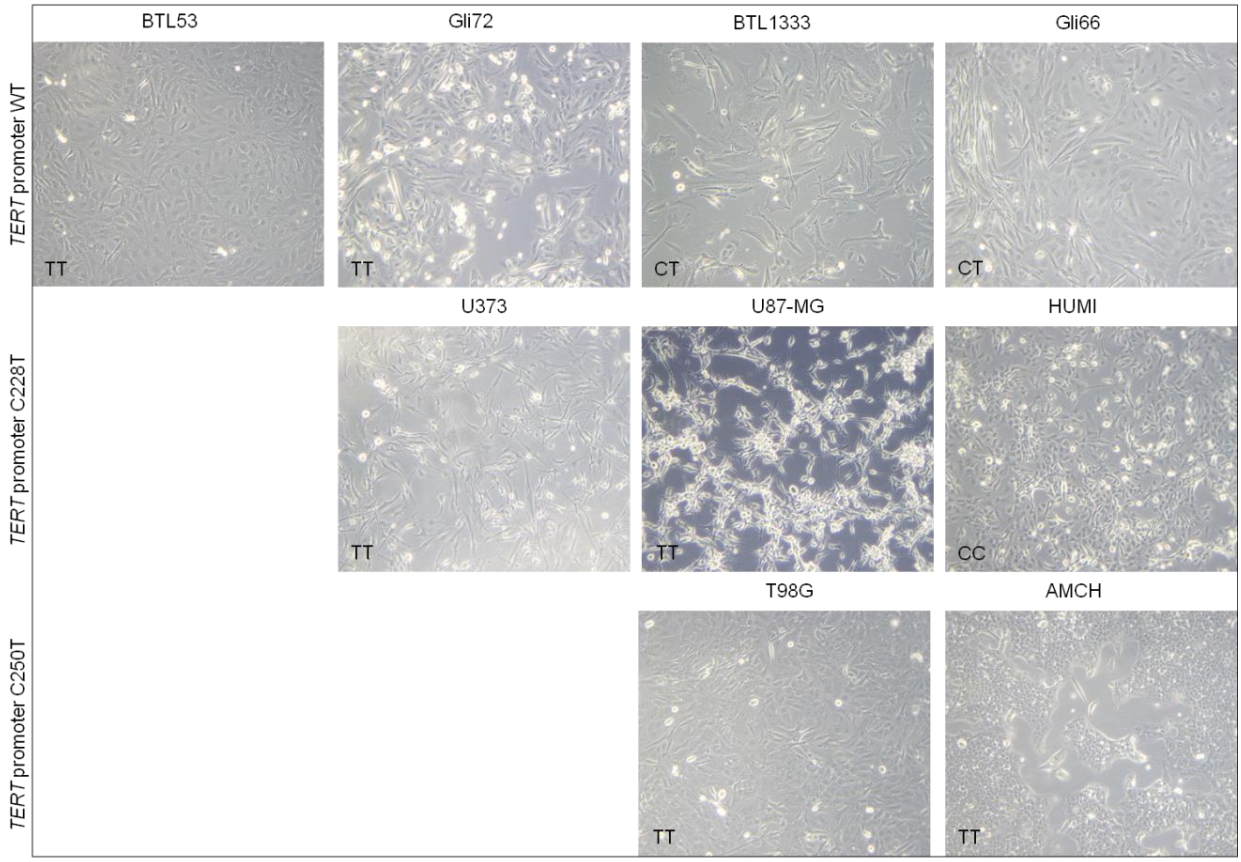

Figure 24. Cell morphology of *TERT* promoter WT and MUT GBM models. Various GBM cell lines were kept in their appropriate medium under normal cell culture conditions. Representative microscopic photographs of *TERT* promoter WT cell lines (upper panel), of C228T *TERT* promoter MUT (middle panel) and C250T *TERT* promoter MUT cell models (lower panel) are depicted. Cells were analyzed using the Primovert microscope (Zeiss) equipped with the Plan-ACHROMAT 4x/0.10Ph0 objective (Zeiss). Microphotographs were taken with the AxioCam ICc5 microscope camera (Zeiss) controlled via the ZEN 2 software (Zeiss). CC=homozygous for SNP rs2853669, CT=heterozygous for SNP rs2853669, TT=noncarrier of SNP rs2853669.

Strikingly, the two *TERT* promoter C228T MUT cell lines U87MG and HUMI tended to merge to multi-cellular clusters in standard cell culture plates. Moreover, these two cell lines only basely attached to the surface of the cell culture flask and could easily be detached with short-term trypsin/EDTA treatment. Both of these cell models did not always form a confluent monolayer, but rather grew into the third dimension. (Figure 24)

3.2 The *TERT* promoter status affects the tumor aggressiveness

Besides the two-dimensional morphology, all cell models were analyzed with regard to their stemness-capacity, hence their ability to grow as neurospheres under stem cell culture conditions. Therefore, 5000 cells were seeded in NB+ medium into low-attachment

24-well-plates and incubated for four and seven days under normal cell culture conditions. Sphere formation assays revealed that all of the investigated cell lines were able to form three-dimensional neurospheres, however, the size and the time needed to establish spheres varied distinctly. BTL53 and Gli72, both harboring a *TERT* promoter WT and an additional TT SNP, formed big spheres after seven days. Contrarily, BTL1333 and Gli66, characterized by a WT *TERT* promoter with CT SNP, formed smaller spheres after seven days. The C228T MUT cell line U373 already formed big spheres after four days, extending in size after seven days. Surprisingly, U87MG and HUMI, the two cell lines with a preference to grow into the third dimension in standard cell culture plates, only had limited sphere formation potential after four days in low-attachment plates. However, both, U87MG and HUMI proliferated strongly in the low-attachment plates. T98G and AMCH, both characterized by C250T *TERT* promoter mutation and a TT SNP, presented a comparable growth behavior to U87MG and HUMI in stem cell medium. In short, all of the GBM cells had the ability to form neurospheres after incubation in low-attachment plates under stem cell conditions for seven days. Figure 25a summarizes the sphere formation capacity of all investigated GBM cell lines after four and seven days of incubation.

After an incubation time of seven days in low-attachment plates, the spheres were centrifuged and transferred into normal 24-well cell culture plates for re-differentiation in their appropriate growth media. Seven days later, the cells were fixed and stained as described in section 2.4.2. In Figure 24b photographs of the fixed GBM cells are depicted. The eluated color intensity was quantified spectrophotometrically as outlined in section 2.4.2. Figure 24c summarizes cell-specific values that were pooled according to the *TERT* promoter status of the investigated cell models. The capacity of re-differentiation was significantly more pronounced in the *TERT* promoter MUT cells as compared to the WT cells.

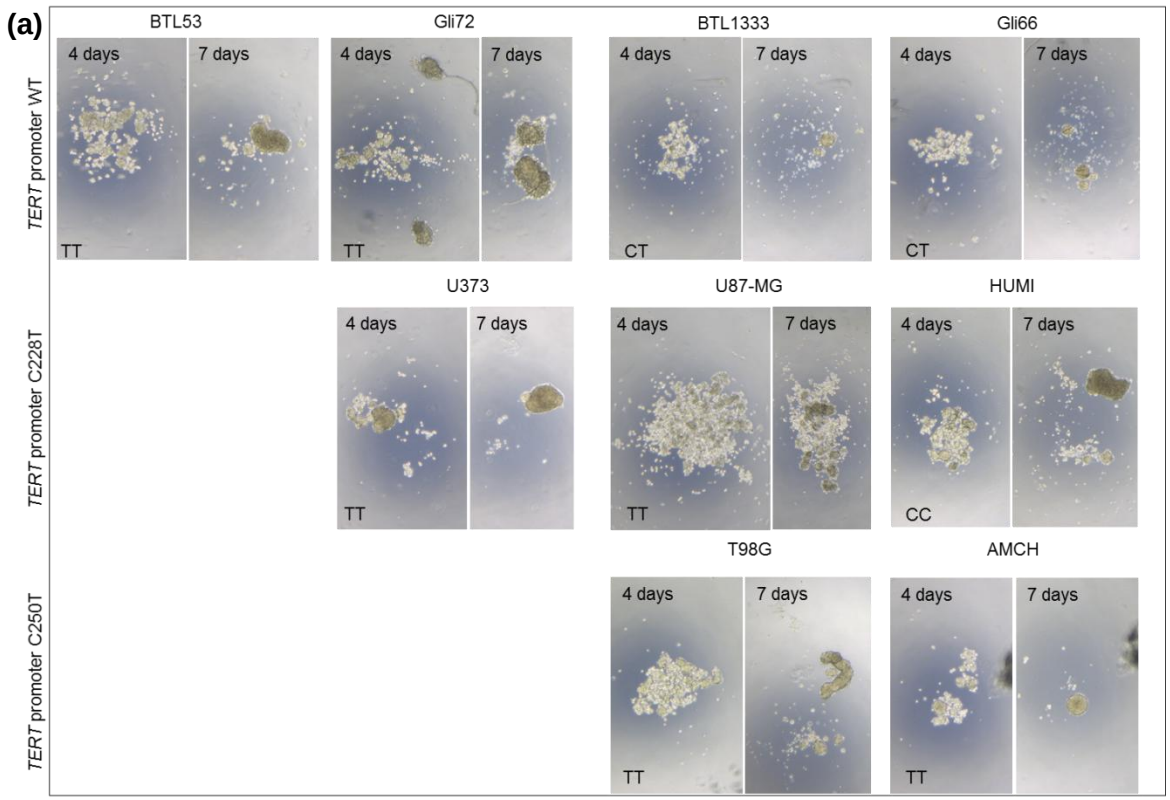
(a)
BTL53
Gli72
BTL1333
Gli66
4 days
7 days
TT
CT
CC
U373
U87-MG
HUMI
T98G
AMCH
TERT promoter WT
TERT promoter C228T
TERT promoter C250T

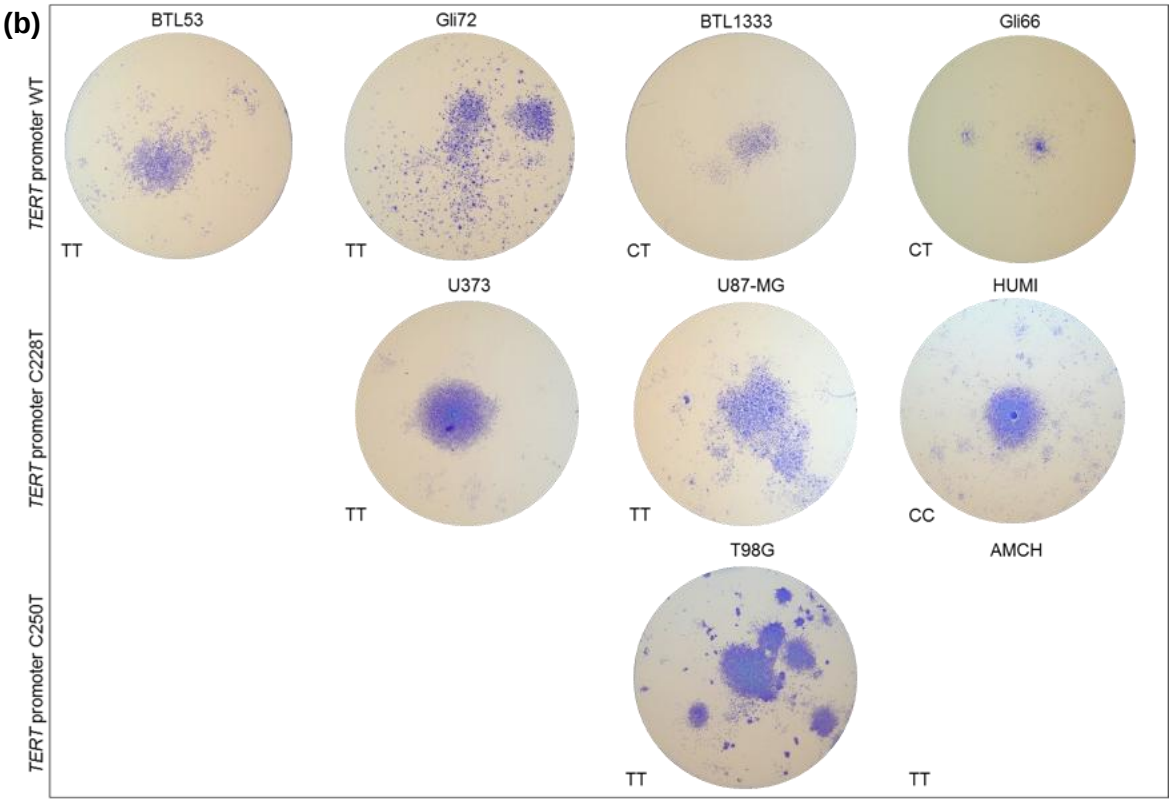
(b)
BTL53
Gli72
BTL1333
Gli66
TT
CT
CC
U373
U87-MG
HUMI
T98G
AMCH
TERT promoter WT
TERT promoter C228T
TERT promoter C250T

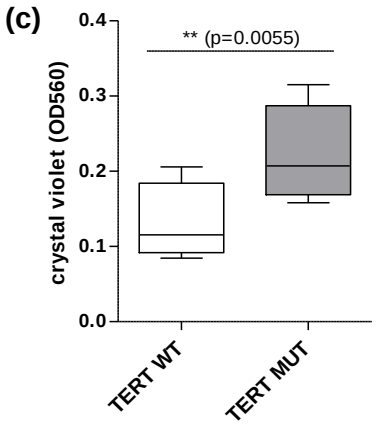

Figure 25. Sphere formation ability of *TERT* promoter WT and MUT GBM cell lines and their potential to re-differentiate. (a) 5000 cells of each model were seeded in NB+ medium in low-attachment plates. Microphotographs were taken at the indicated time points. Representative microscopic photographs of *TERT* promoter WT cell lines (upper panel), of C228T *TERT* promoter MUT (middle panel) and C250T *TERT* promoter MUT cell models (lower panel) are depicted. Cells were analyzed with Primovert microscope (Zeiss) equipped with the Plan-ACHROMAT 4x/0.10Ph0 objective (Zeiss). Microphotographs were taken with the AxioCam ICc5 microscope camera (Zeiss) equipped with the ZEN 2 software (Zeiss). CC=homozygous for SNP rs2853669, CT=heterozygous for SNP rs2853669, TT=noncarrier of SNP rs2853669. **(b)** After the incubation in NB+ medium for seven days, the cells were transferred into standard cell culture plates and cultured in their appropriate medium for seven days. Cells were fixed with MeOH and stained with crystal violet. Photographs were taken (Nikon Digital Camera D3200). **(c)** The crystal violet was eluted from the cells with 2% SDS and absorbance was measured (560nm, Tecan Infinite M200 Pro). The spheres of AMCH were lost during centrifugation prior to the re-differentiation assay. The bar graphs represent the pooled values of the indicated *TERT* promoter status (mean±SD). Significance values were analyzed by t-test (p=0.0055) and are marked with stars: *** p<0.001, ** p<0.01, * p<0.05.

3.3 The *TERT* promoter status influences the endogenous TERT expression

The two most common *TERT* promoter variants in GBM are C228T and C250T point mutations *(100)*. Both are believed to promote *TERT* promoter activity, thus inducing TERT expression on mRNA and protein levels *(80, 101, 279)*. In our GBM models, the *TERT* expression patterns were analyzed on mRNA (Figure 26b left) and protein (Figure 26a left) levels in correspondence to the *TERT* promoter mutation status. Cell lines harboring such an activating point mutation in the *TERT* promoter expressed significantly more TERT than the WT cells (t-test, p=0.0074) (Figure 26a right). This result was also confirmed on mRNA levels by use of qRT-PCR (t-test, p=0.0001) (Figure 26b right).

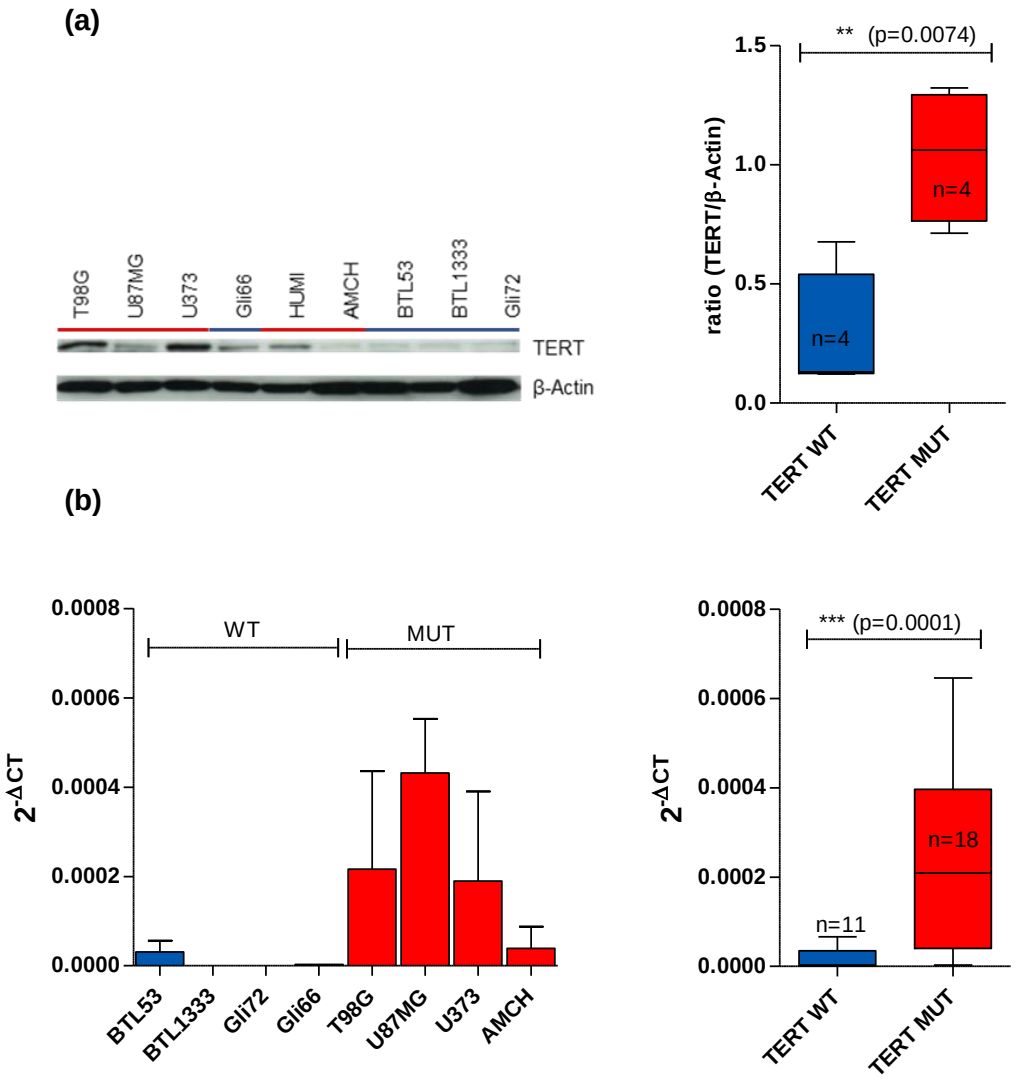

Figure 26. Determination TERT mRNA and protein expression in various GBM cell lines. (a) Analysis of TERT expression levels via Western blots in the indicated cell lines (left). Expression levels were quantified using ImageJ software and normalized to β-Actin serving as loading control (t-test, p=0.0074, right). **(b)** *TERT* mRNA expression levels were tested in the indicated cell lines with qRT-PCR (left). Expression values were normalized to the housekeeping gene β-Actin (ΔCT) and converted to a linear form using $2^{-\Delta CT}$ (t-test, p=0.0001, right). Each box plot represents the mean±SD of WT and MUT cell lines.

The GS cell model AMCH was identified as outlier in the MUT models (Grubbs test p>0.05) and therefore excluded in the t-test analyses **(a and b right)**. *TERT* promoter WT lines are marked with blue, and *TERT* promoter MUT cell lines are highlighted in red. Significance values are marked with stars: *** p<0.001, ** p<0.01, * p<0.05

3.4 Endogenous *TERT* promoter status in association with the *TERT* promoter and telomerase activity

In human malignant melanoma, *TERT* promoter mutations have previously been correlated with increased promoter activity *(80, 101, 102)*. In the present study, we tested the *TERT* promoter activity of our GBM samples with respect to the promoter status using luciferase reporter assays. Therefore, the activity of the WT *TERT* promoter constructs was compared to constructs harboring two most common point mutations, C228T and C250T. Moreover, the impact of the common SNP rs2853669 on the *TERT* promoter activity was evaluated for each of the above mentioned promoter sequences. The setting of the luciferase reporter assay included an internal transfection control (*Renilla*). Furthermore, a promoter-less plasmid served as negative control set as 1. The impact of the different *TERT* promoter variants on the promoter activities was tested via one-way ANOVA analysis (Bonferroni's multiple comparison test; *** $p<0.001$, ** $p<0.01$, * $p<0.05$). Vector maps of all used plasmids are depicted in the Appendix (Figure 49).

The activities of the *TERT* promoter variants were highly variable within the transfected cell lines. Nevertheless, the basal *TERT* promoter activities of the WT and WT SNP sequences were comparable to the negative controls. Moreover, activity of C228T MUT *TERT* promoter tended to be elevated compared to the WT variant. Presence of the C250T sequence had only a minor impact on the *TERT* promoter activity. (Figure 27a).

In Figure 27b, the *TERT* promoter activities are depicted for each transfected cell line. Accordingly, T98G and Gli66 had a three- to five-times higher *TERT* promoter activity than all other tested cell models. The promoter activity profiles of the endogenously *TERT* promoter mutant T98G and Gli66 cells were very similar in intensity and distribution (Figure 27b). Activities of C228T SNP and C250T SNP promoter constructs were significantly higher than the WT SNP promoter activity. In these cell models, presence of the SNP tremendously increased the *TERT* promoter activity in both MUT sequences. (Figure 27b)
Significant differences in the *TERT* promoter activities were also found in BTL1333 *TERT* promoter WT cells. The activities of both, the C228T and C250T MUT promoters with SNP, were significantly higher as compared to the WT SNP sequence. Additionally, the activity of the C250T promoter MUT sequence with SNP was considerably higher than the activities of the C250T and the WT SNP sequences. (Figure 27b)

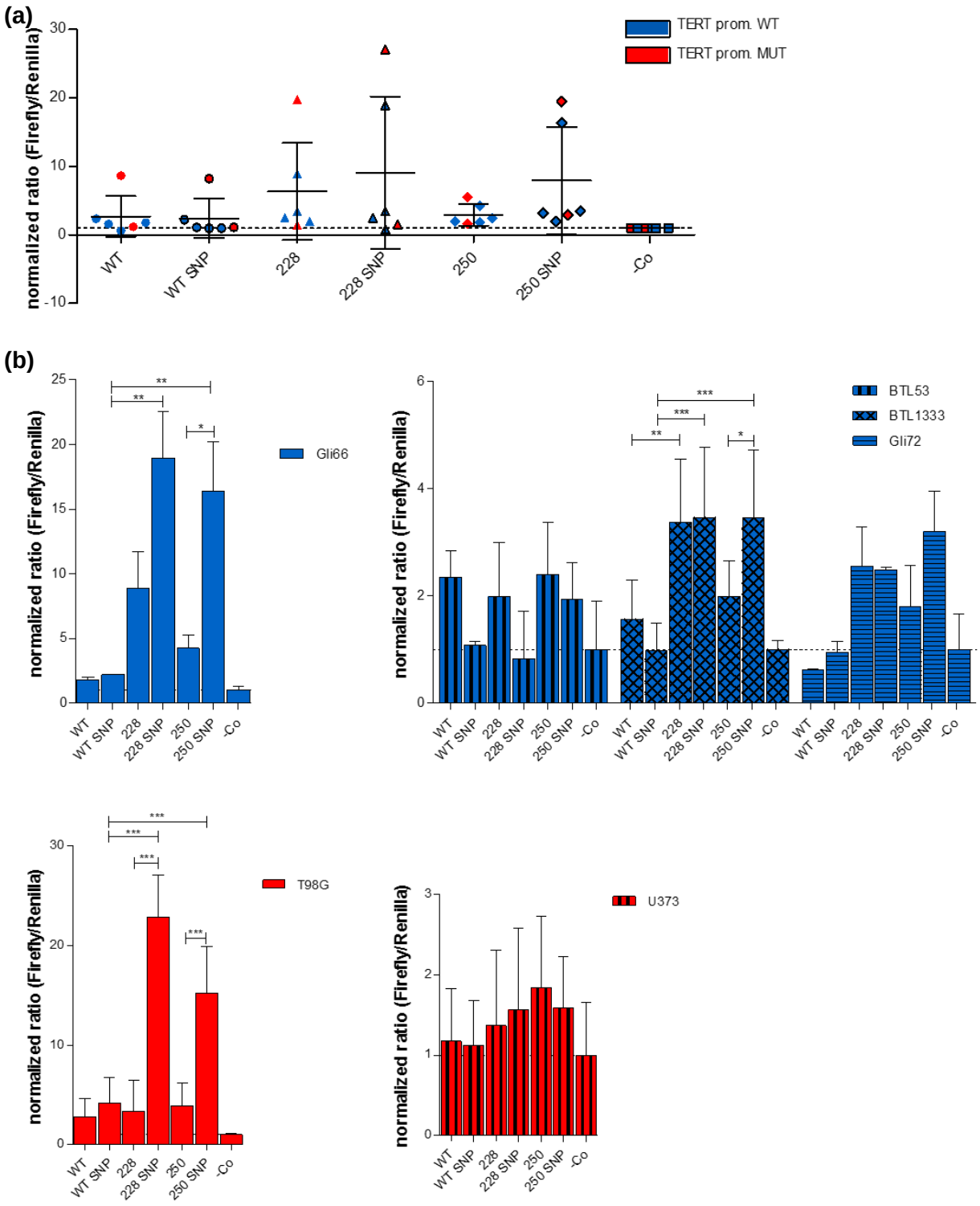

Figure 27. The *TERT* promoter activities of different *TERT* promoter variants are highly variable according to the transfected cell lines. (a and b) WT GBM (Gli66, Gli72, BTL53, BTL1333) and MUT models (T98G, U373) were transfected with the following *TERT* promoter constructs: WT, WT sequence with the variant allele of the rs2853669 SNP (WT SNP), C228T (228), C228T with the SNP (228 SNP) as well as C250T sequence alone (250) and C250T with the SNP (250 SNP). **(a)** The luciferase

signals of all transfected cell lines are pooled and separated according to the indicated *TERT* promoter variants. The symbols illustrate means of biological replicates. **(b)** The activity values of the indicated *TERT* promoter variants are depicted for every WT (upper panel) as well as of the MUT (lower panel) cell line. One-way ANOVA analysis (Bonferroni's multiple comparison test) revealed significant differences in certain plasmid pairs.
Values are depicted as ratios Firefly/*Renilla* and were additionally normalized to the negative control (-Co; promoter-less pGL3 vector), set as 1 (dotted line). WT cell lines are shown in blue, MUT cell lines are highlighted in red. Significance values are marked with stars: *** $p<0.001$, ** $p<0.01$, * $p<0.05$.

In literature, TERT-positive GBM are characterized by higher telomerase activity and shorter telomeres as compared to TERT-negative tumors *(38, 101, 102, 105, 280)*. In the current study, we tested the telomerase activity of two *TERT* promoter WT (BTL53, BTL1333) and to MUT (T98G, U373) GBM using TRAP assay. Accordingly, we found notably higher telomerase activities in those samples harboring a mutated promoter as compared to the WT tumor cells (Figure 43).

3.5 The connection between *TERT* promoter status and PD-L1 expression

PD-L1 was already previously described to be highly expressed in GBM *(239)*. Some studies imply that PD-L1-expressing GBM tumors predict a worse prognosis as compared to those lacking tumor-associated PD-L1 *(281-284)*. However, a specific pattern explaining which particular GBM samples are more likely to overexpress PD-L1 has not been identified yet. Presence of a *TERT* promoter mutation is also characterized as negative prognostic factor in GBM *(9, 38, 40, 100, 278)*. In this study, we wanted to analyze the importance of the immune-regulator PD-L1 on the tumor aggressiveness with respect to the *TERT* promoter status.

A panel of four *TERT* promoter WT (Gli66, BTL53, BTL1333, Gli72) and five MUT GBM cell lines (T98G, U87MG, U373, HUMI, AMCH) were investigated with respect to their PD-L1 expression levels (Figure 28a, left). Interestingly, we found significantly higher PD-L1 protein expression in the *TERT* promoter WT samples as compared to the MUT ones (t-test, $p=0.021$) (Figure 28a, right). Furthermore, the gene expression of *PD-L1 (CD274)* was analyzed using qRT-PCR (Figure 28b left). Results confirmed considerably higher *PD-L1 (CD274)* mRNA levels in the *TERT* promoter WT sublines as compared to the MUT GBM (t-test, 0.0219) (Figure 28b right).

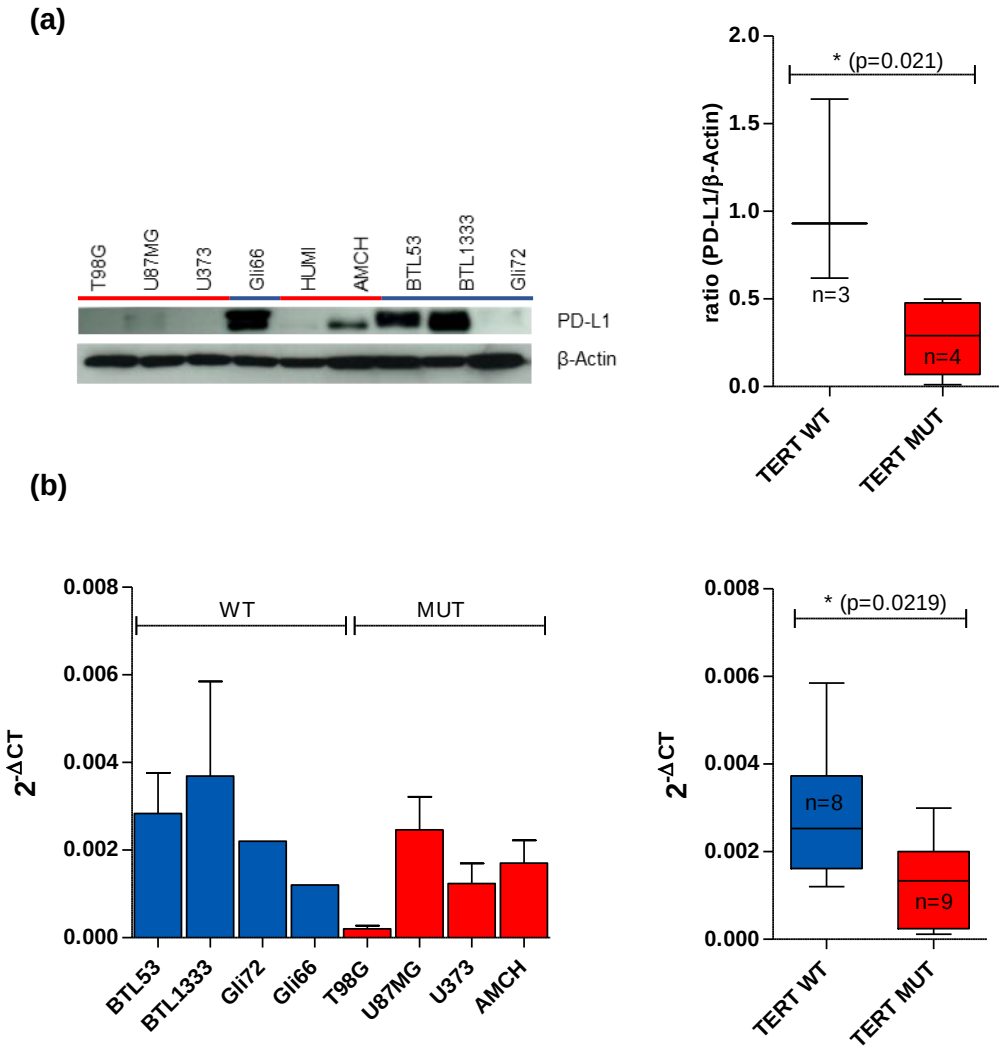

Figure 28. ***TERT* promoter status is associated with PD-L1 expression. (a)** Total protein extracts were isolated from four *TERT* promoter WT (Gli66, BTL53, BTL1333, Gli72) and five MUT cell lines (T98G, U87MG, U373, HUMI, AMCH). PD-L1 protein levels were analyzed by Western blot analysis (left). The results were quantified using ImageJ software and normalized to the loading control β-Actin (t-test, p=0.021; right). The GS model AMCH as well as Gli72 were detected as outliers (Grubbs test p<0.05) and not included in the quantification (right). **(b)** *PD-L1* mRNA expression was tested in certain cell lines with qRT-PCR (means of biological replicates ±SD, left). Expression values were normalized to the housekeeping gene β-Actin (ΔCT) and were converted to a linear form using $2^{-\Delta CT}$. Results of *TERT* promoter WT and MUT cell lines were separately pooled (t-test, 0.0219.; right). *TERT* promoter WT lines are marked with blue, and *TERT* promoter MUT cell lines are shown in red. Significance values are marked with stars: *** p<0.001, ** p<0.01, * p<0.05

3.6 The interplay between the NFκB pathway and TERT in GBM cells

The NFκB pathway is a complex multi-step signaling cascade, which is tightly controlled by panoply of proteins. Such as, NFκB activation and phosphorylation is triggered by different upstream signaling proteins. Unphosphorylated IκBα holds the NFκB dimer in the cytoplasm, however, phosphorylation of IκBα by the IKK complex leads to degradation of the molecule in the proteasome and release the NFκB dimer for phosphorylation and translocation into the nucleus. *(139-141)*

It is further known that telomerase possesses so-called non-canonical functions regulating NFκB signaling. Li *et al.* described that the non-canonical NFκB pathway is required for TERT reactivation in *TERT* promoter MUT cells *(79)*. Based on this knowledge, we analyzed a feasible interconnection between of the *TERT* promoter mutation status and the NFκB pathway in our GBM cell lines.

3.6.1 Basal expression levels of NFκB pathway molecules

Total protein extracts of the GBM cells were isolated and Western blot analysis was performed using different antibodies against driver proteins in the NFκB signaling pathway. Accordingly, activated NFκB (p65) was higher expressed in *TERT* promoter WT as compared to the MUT GBM cells. *Vice versa*, IκBα in its phosphorylated and unphosphorylated forms tended to be present at higher amounts in *TERT* promoter MUT cell lines (Figure 29).

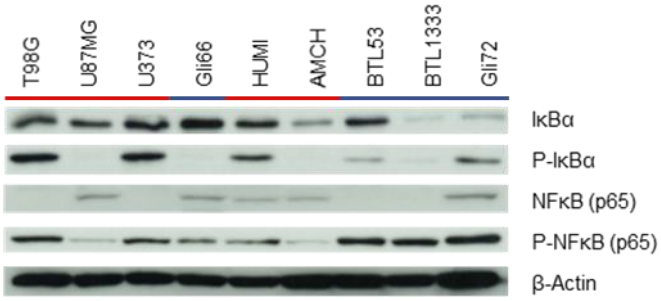

Figure 29. Basal protein expression of the NFκB pathway members in *TERT* promoter WT and MUT GBM cell lines. Total and phosphorylated protein levels of NFκB and IκB were analyzed by Western blots in the indicated cell lines. The blue bars mark WT and the red ones MUT cell lines. β-Actin served as loading control.

3.6.2 Cytotoxicity of NFκB inhibitors and their impact on clone formation capacity

In order to analyze the dependency of our GBM cell lines on the NFκB pathway, the signaling axis was inhibited by use of two small molecule inhibitors, QNZ and Bay-11-082, both acting upstream of the transcription factor NFκB. While QNZ inhibits NFκB transcription factor activity *(255)*, Bay-11-7082 irreversibly blocks phosphorylation of IκBα *(124, 259-261)*.

Viability assays and clone formation assays were conducted and the cells were incubated with the drugs for three and seven days, respectively. Viability assays with QNZ revealed that *TERT* promoter WT cell lines are more resistant to the drug than the MUT samples (Figure 30a). These results were confirmed by long-term treatment with QNZ (5µM) as investigated in clone formation assays (Figure 30c/d). In contrast, treatment with the second NFκB inhibitor Bay-11-7082 did not reveal any differences in response rates between *TERT* promoter WT and MUT cell models as seen in viability assays (Figure 30b). Interestingly, clone formation assays revealed a significantly higher sensitivity of the *TERT* promoter WT samples as compared to the MUT ones upon treatment with 1µM of Bay-11-7082. However, upon treatment with 5µM of this drug the *TERT* promoter MUT samples were significantly more sensitive than the WT cells (Figure 30e/f).

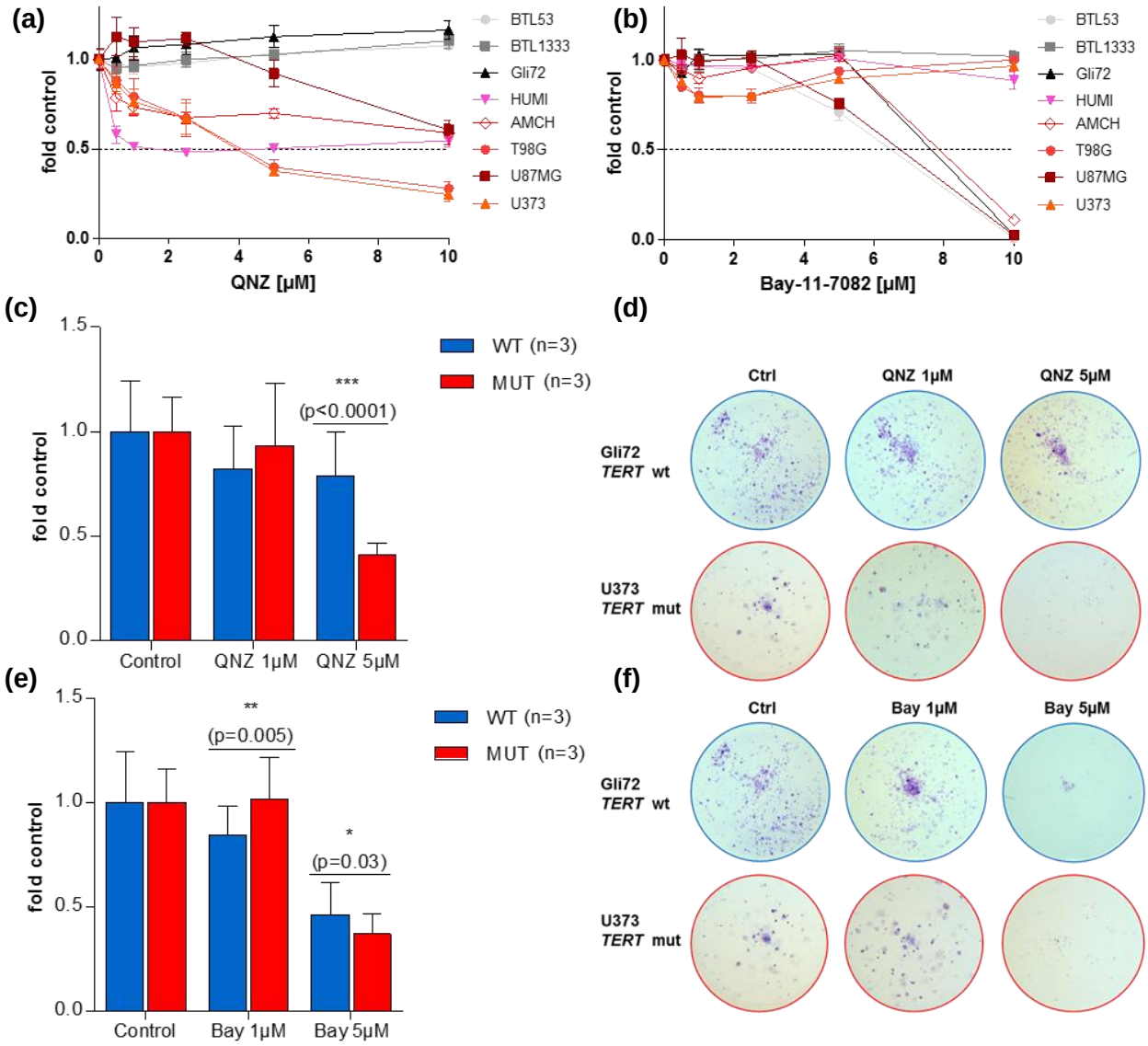

Figure 30. The impact of the *TERT* promoter status on the response to NFκB inhibitors. Following 72 hours QNZ **(a)** or Bay-11-7082 **(b)** treatment, dose-response curves were established in WT (grey-scale) as well as in MUT (reddish colors) cell lines**. (c and e)** Values of colony formation assays upon long-term QNZ **(c)** and Bay-11-7082 **(e)** treatment are summarized for each *TERT* promoter status (WT, MUT) and illustrated as histograms (mean±SD; t-test). The crystal violet was eluted from the cells with 2% SDS and absorbance was measured (560nm, Tecan Infinite M200 Pro). Results were normalized to the corresponding untreated controls, and set as 1.
(d and f) Representative pictures of fixed and crystal violet-stained cells (WT: Gli72, blue circles; MUT: U373, red circles) are depicted for QNZ **(d)** as well as for Bay-11-7082 treatment **(f)**. Photographs were taken with a Nikon Digital Camera D3200. Significance values are marked with stars: *** p<0.001, ** p<0.01, * p<0.05

3.6.3 Impact of QNZ on the cell cycle progression of GBM cells

One feasible mode of action of QNZ was analyzed via flow cytometry using PI DNA staining, investigating the cell cycle distribution in our GBM cells upon drug treatment. Three *TERT* promoter WT and five MUT cell lines were incubated with 5µM QNZ for 24 hours. Figure 31 outlines the respective cell cycle distribution according to the endogenous *TERT* promoter status. In particular, around 70% of the cells were found in the G0/G1 phase and about 20% of the cells were distributed into the G2/M and S phases to equal parts. Overall, QNZ treatment did not change the cell cycle distribution in the tested cell lines. Cell cycle distribution patterns for every single cell line are depicted in section 3.10.2 (Figure 48a).

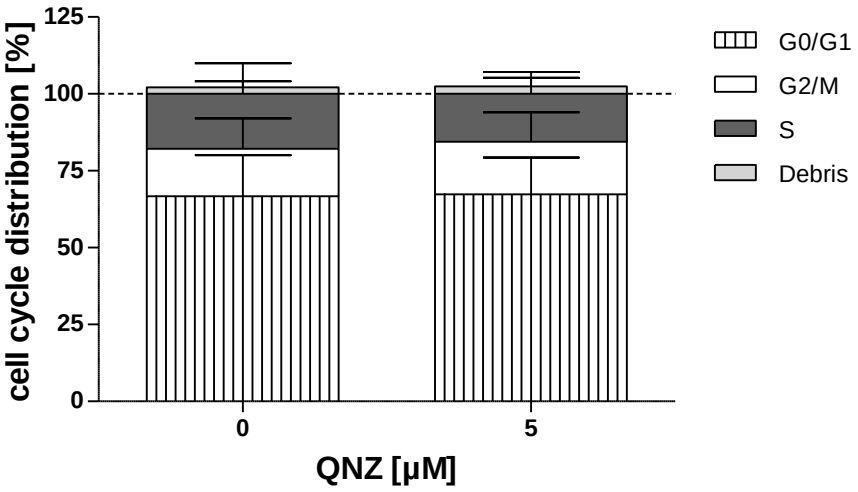

Figure 31. Cell cycle analysis after QNZ treatment. Three *TERT* promoter WT GBM and five MUT cell lines were incubated with 5µM QNZ for 24 hours. Cells were fixed, DNA was stained with PI and the cell cycle distribution was analyzed by flow cytometry. Cell cycle distribution results of the cell lines were pooled together and are depicted as stacked box plots (mean±SD).

3.6.4 NFκB pathway inhibition drives STAT3 downregulation

In the current study, two *TERT* promoter WT (BTL53, BTL1333) and three MUT cell lines (HUMI, U373, T98G) were treated with 5µM of the NFκB inhibitor QNZ for 48 hours. Microphotographs of the untreated controls (ctrl) as well as of the QNZ treated cells were taken (Figure 32a). Subsequently the proteins were isolated and fractioned using the "NE-PER™ Nuclear and Cytoplasmic Extraction Reagents Kit" and Western blot analysis was performed (Figure 32b). The purity of nuclear protein extract was examined with an antibody against the nuclear protein Lamin A/C. However, QNZ did not have any considerable impact on the PD-L1

expression in these cell lines. Interestingly, phosphorylation of NFκB (P-NFκB) was distinctly inhibited by QNZ in the cytoplasm as well as in the nucleus of HUMI, BTL53 and BTL1333. In contrast, in U373 and T98G cells, P-NFκB was not changed upon QNZ treatment. (Figure 32b)

The directed interaction network between the NFκB and the JAK/STAT3 axes via IL6 is generally accepted *(82-84)*. Thus, we were interested whether NFκB inhibition influences the STAT3 signaling. Indeed, phosphorylation of STAT3 (P-STAT3) followed comparable inhibition pattern as P-NFκB upon QNZ treatment. (Figure 32b)

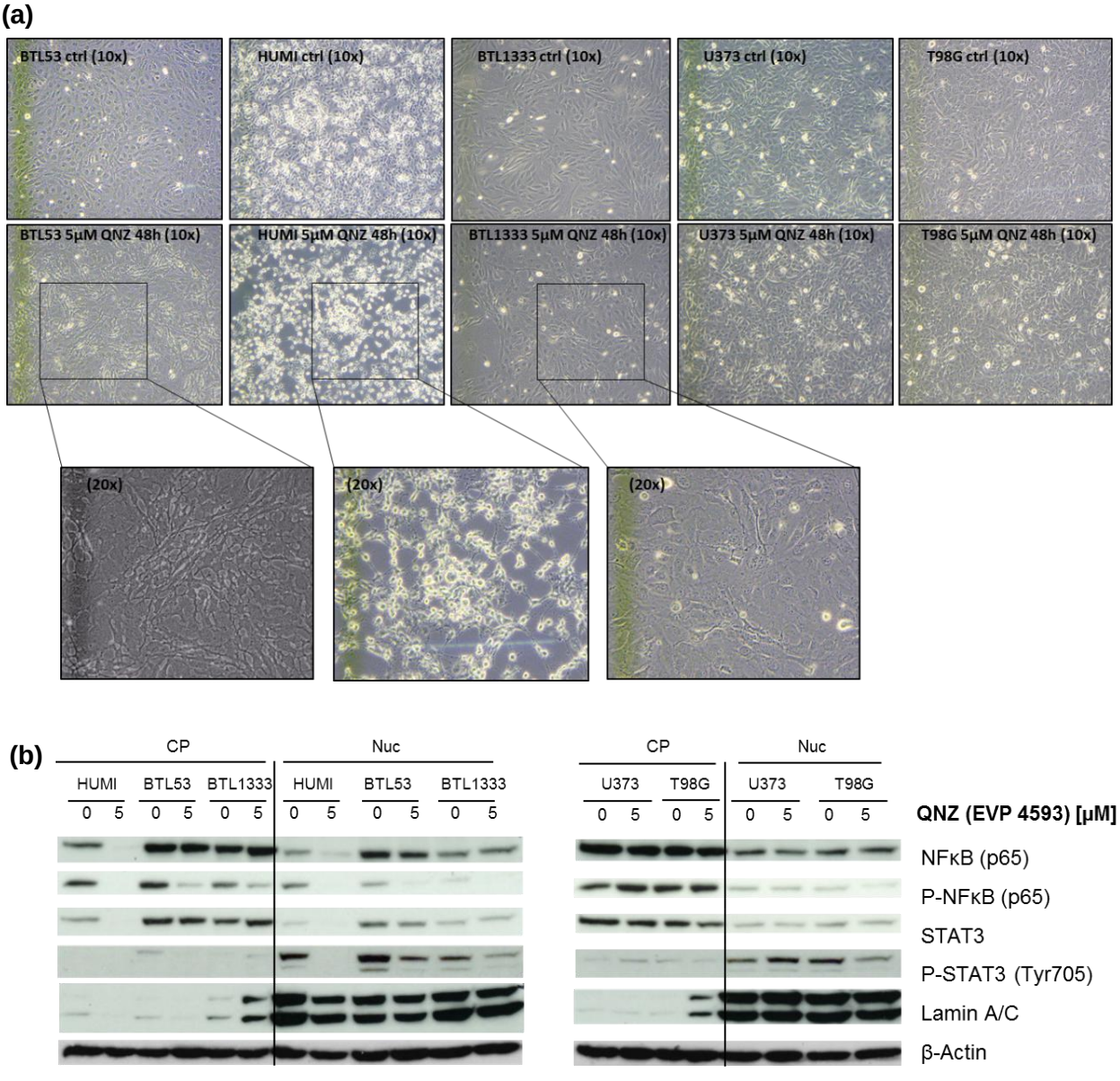

Figure 32. The impact of QNZ on the protein expression and cellular localization of proteins. (a) Two *TERT* promoter WT (BTL53, BTL1333) and three MUT (HUMI, U373,

T98G) were treated with 5µM QNZ for eight hours. Cells were analyzed using the Primovert microscope (Zeiss) equipped with the Plan-ACHROMAT 10x/0.25Ph1 objective (Zeiss) and 20x/0.30Ph1. Microphotographs were taken with the AxioCam ICc5 microscope camera (Zeiss) controlled via the ZEN 2 software (Zeiss). **(b)** Cytoplasmic and nuclear protein extracts were isolated. Total and phosphorylated protein levels of NFκB and STAT3 were analyzed by Western blots as indicated. The purity of nuclear protein extract was examined with an antibody against the nuclear protein Lamin A/C. β-Actin served as loading control.

3.6.5 Impact of QNZ on *NFκB1, STAT3, PD-L1* and *TERT* mRNA expression

Two *TERT* promoter WT (BTL53, BTL1333) and four MUT models (U373, T98G, U87MG, AMCH) were treated with 5µM QNZ for 48 hours and the RNA was isolated with Trizol. qRT-PCR was performed with primers targeting *TERT, STAT3, NFκB1* and *PD-L1 (CD274)* gene expression*.* All samples were normalized to *β-Actin* serving as housekeeping gene. Results were compared to the untreated control cells (dotted line), set as 1. qRT-PCR revealed that the QNZ treatment tended to increase the *TERT* expression in the cell lines BTL53, T98G, U87MG and AMCH, while in U373 cells *TERT* mRNA levels were decreased upon *NFκB* inhibition (Figure 33a). As already previously observed (Figure 26b), BTL1333 did not express measurable *TERT* mRNA levels (Figure 33a). qRT-PCR revealed that the mRNA expression of *NFκB1* decreased compared to the untreated control in the cell lines BTL1333 and T98G (Figure 33b). However, the *NFκB1* mRNA levels were only slightly reduced in U87MG, remained unchanged in AMCH and were even increased in BTL53 after QNZ treatment (Figure 33b). Interestingly, besides *NFκB1*, the expression of *STAT3* was decreased in all tested GBM cell lines (Figure 33c). *PD-L1* mRNA expression was tremendously increased in BTL53 and slightly in T98G upon NFκB inhibition with QNZ (Figure 33d), however it stayed unchanged in U87MG and even decreased in BTL1333 and AMCH (Figure 33d).

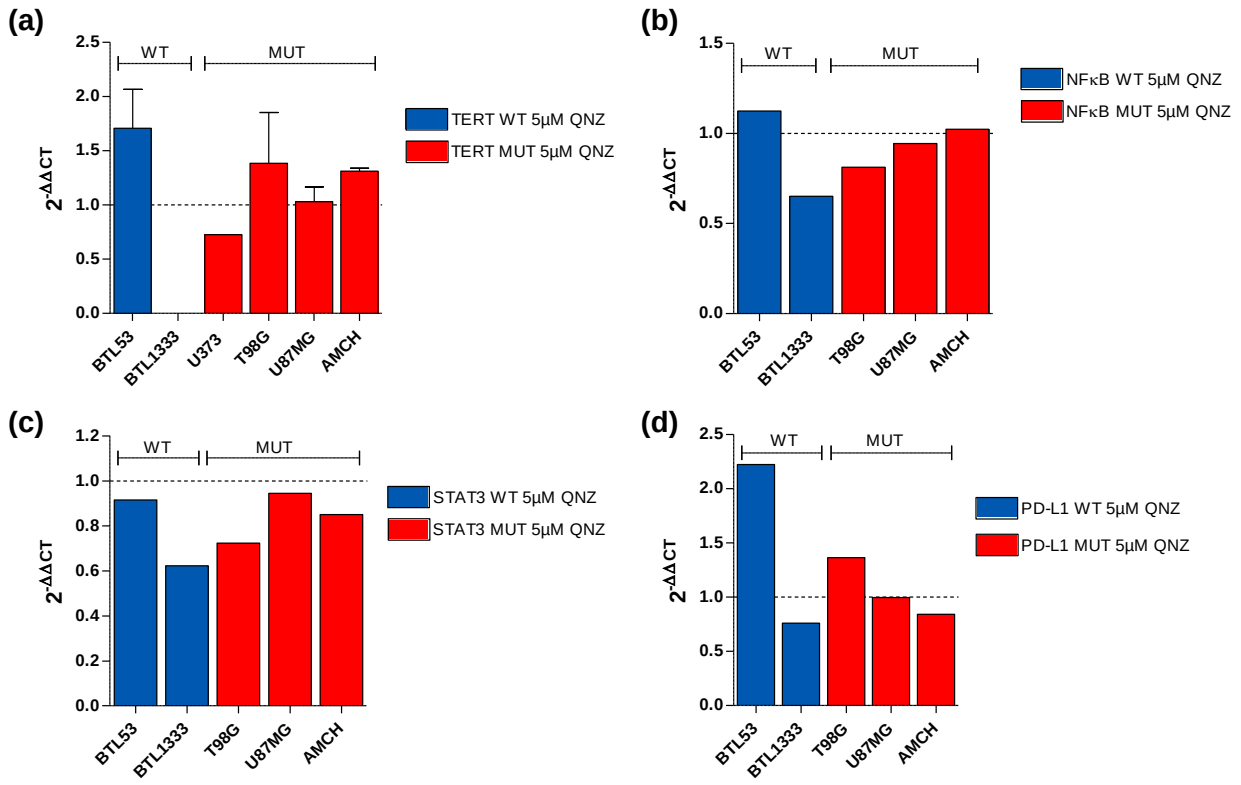

Figure 33. mRNA expression levels of different target genes upon treatment with QNZ. Two *TERT* promoter WT cell lines (BTL53, BTL1333) and four MUT models (U373, T98G, U87MG, AMCH) were treated with 5µM QNZ for eight hours. *TERT* **(a)**, *NFκB1* **(b)**, *STAT3* **(c)** and *PD-L1 (CD274)* **(d)** mRNA expression levels were tested with qRT-PCR. Expression values were normalized to the housekeeping gene β-Actin as well as to the untreated control (ΔΔCT), set as 1 (dotted line), and were converted to a linear form using $2^{-\Delta\Delta CT}$.
TERT promoter WT lines are marked with blue, and *TERT* promoter MUT cell lines are highlighted in red. Significance values are marked with stars: *** p<0.001, ** p<0.01, * p<0.05

3.6.6 The impact of QNZ on the *TERT* promoter activity

The impact of QNZ on *TERT* promoter activity was analyzed by luciferase reporter assays. Two *TERT* promoter WT cell lines, BTL53 and BTL1333, one C228T MUT cell line, U373, as well as one C250T MUT model, T98G, were transfected with plasmids containing either a WT or a MUT promoter sequence (C228T or C250T) in an rs2853669 SNP carrier or non-carrier background. The transfected cells were treated with 5µM QNZ for 24 hours. The results were expressed as the ratio firefly/*Renilla*, serving as internal transfection control in each sample. Furthermore, every value was normalized to the promoter-less negative, auto-luminescence control, set as 1. In the WT cell line BTL53 *TERT* promoter activities decreased in the majority of tested promoter variants upon QNZ treatment (Figure 34a). On the contrary, in BTL1333 also harboring a WT TERT promoter sequence, QNZ rather induced an increase of luciferase signals, especially

after transfection with the C228T and C228T SNP reporter constructs (Figure 34b). Similar effects were observed when analyzing the *TERT* promoter activities in the MUT cell lines U373 (Figure 34c) and T98G (Figure 34d). Again, in the C228T, SNP carrier background QNZ treatment resulted in the highest promoter activity levels. (Figure 34b-d)

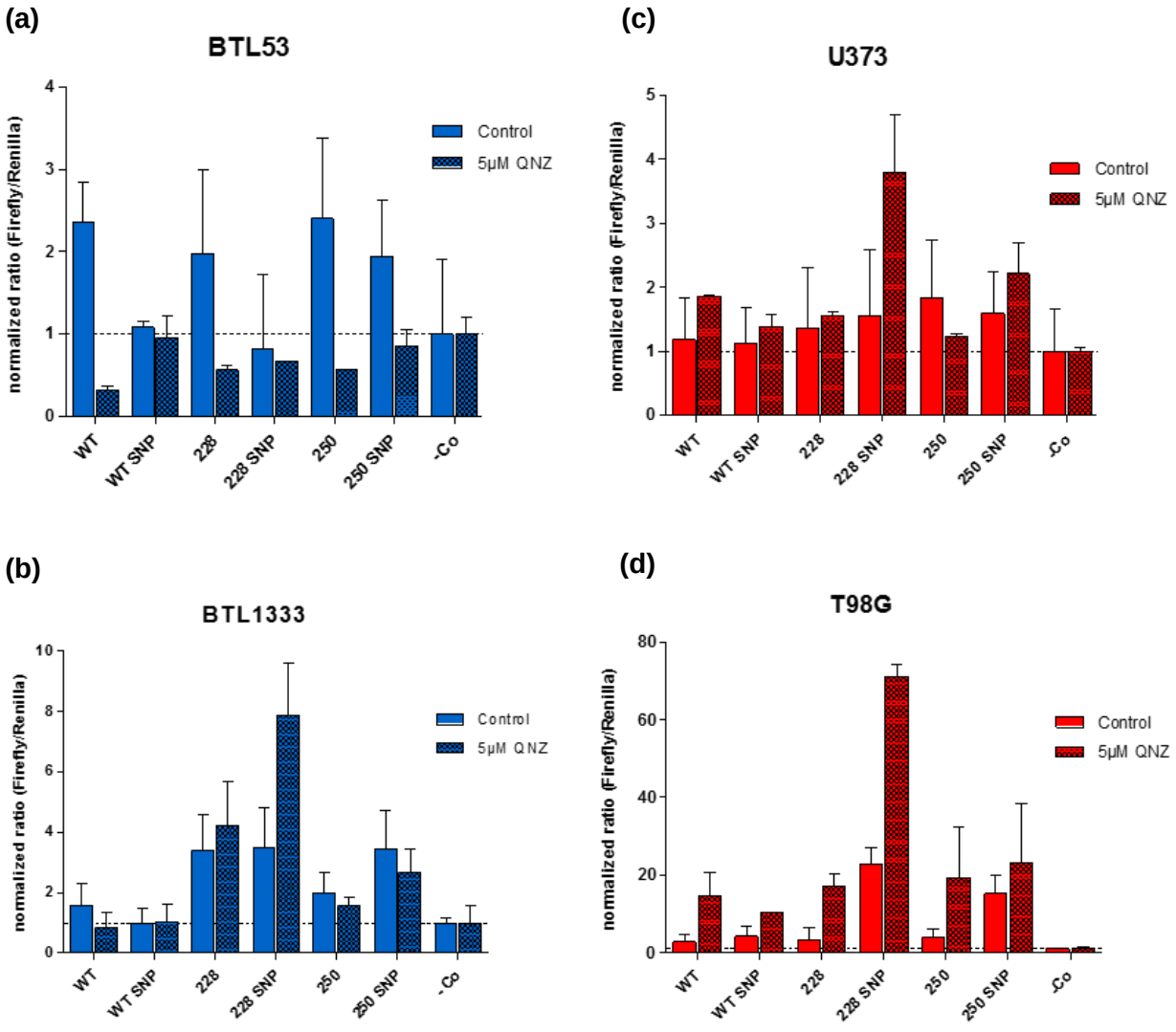

Figure 34. Impact of QNZ treatment on *TERT* promoter activities using different *TERT* promoter luciferase constructs. WT GBM cells, BTL53 **(a)** and BTL1333 **(b)**, as well as the MUT models U373 **(c)** and T98G **(d)** were transfected with the following reporter constructs: WT, WT sequence with the variant allele of the rs2853669 SNP (WT SNP), the C228T (228), and the C228T with the SNP (228 SNP) as well as the C250T sequence alone (250) and with the variant allele (250 SNP). After transfection, cells were treated with 5µM QNZ for 24h. Values are expressed as ratios of Firefly to *Renilla* and related to the promoter-less pGL3 vector (-Co), set as 1 (dotted line). *TERT* promoter WT lines are marked with blue, and *TERT* promoter MUT cell lines are highlighted in red.

3.7 The effect of IL6 on PD-L1, NFκB, STAT3

The cytokine IL6 plays a major role in the regulation of inflammatory reactions in the human body. Furthermore, IL6 is known to activate the JAK/STAT3 signaling pathway in several cancer types. *(171)* Thus we were interested whether differences in STAT3 activation between *TERT* promoter WT and MUT GBM cell lines exist. Furthermore, researchers identified an interconnection between STAT3 pathway and PD-L1. Hence, STAT3 promotes *PD-L1 (CD274)* expression via binding to its promoter acting as a transcription factor *(285, 286)*. Accordingly, cells were treated with the cytokine IL6 (PeproTech, Rocky Hill, New Jersey, USA) for different time points in order to mimic the primary inflammatory response. Prior to the addition of 50ng/mL IL6, the cells were starved using serum-free (sf) R medium for 24h.

PD-L1 was only expressed in the *TERT* promoter WT cell line, confirming previous results. Accordingly, PD-L1 was increased and reached a peak after 15 minutes upon stimulation with IL-6. Afterwards, PD-L1 expression decreased again, ending up at two hours IL6 stimulation at levels even lower than the untreated controls.
Yang *et al.* postulated an interconnection between the JAK/STAT3 and the NFκB pathways *(287)*. Regarding total and phosphorylated NFκB expression, in the WT cell model both proteins appeared after 15 minutes IL6 treatment and were then stably expressed for up to two hours cytokine application. On the contrary, in the MUT cell line T98G stimulation with IL6 induced phosphorylation of NFκB after ten minutes and reached the peak at two hours. (Figure 35)
STAT3 activation indicated by phosphorylation was already observed after five minutes IL6 treatment and reached the highest levels at 10 and 15min in the *TERT* promoter WT (BTL1333) as well as in the MUT cell line (T98G). Interestingly, in the WT cell line weak STAT3 phosphorylation was still detected upon one hour IL6 stimulation, while this signal was totally abolished in the MUT cell model. (Figure 35)

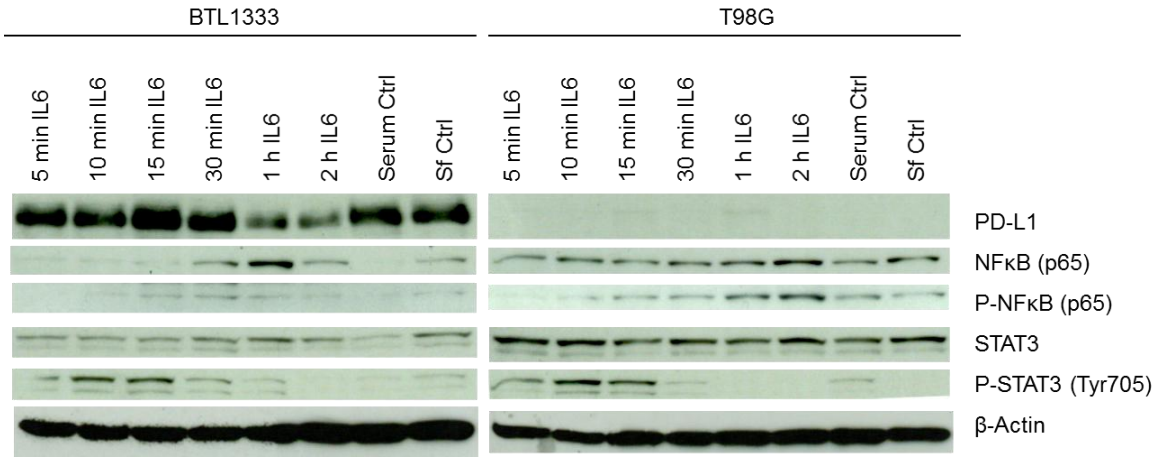

Figure 35. Impact of IL6 treatment on PD-L1 expression as well as on the NFκB and STAT3 signaling in different *TERT* promoter mutation backgrounds. Total and phosphorylated protein levels of PD-L1, NFκB and STAT3 were analyzed by Western blots in BLT1333 (WT) and T98G (MUT) as indicated. Cells were kept under starving conditions in serum-free R medium (sf control) and treated for several time points with 50ng/mL IL6. Appropriate 10% serum-containing media were used to mimic the basal protein expression levels (serum Ctrl). Lamin A/C was used to determine the purity of the nuclear fraction. β-Actin was used as loading control.

3.8 The interplay between the STAT3 pathway and TERT in GBM cells

As already described before, the JAK/STAT3 pathway represents one of the most important target pathways upon IL6 induction via resulting from the NFκB pathway *(82-84)*. Furthermore, STAT3 has been previously reported to interact with NFκB and acting as transcription factors on various genes *(84, 288-291)*. With regard to TERT, in STAT3 interacts with the *TERT* promoter regulating its transcription in human breast cancer *(85)*. Thus, we were interested in a feasible regulatory function of STAT3 on the *TERT* promoter in GBM, also with regard to a potential interaction with NFκB.

3.8.1 Basal expression levels of STAT3 pathway molecules

Total protein extracts of four *TERT* promoter WT (Gli66, BTL53, BTL1333, Gli72) and five MUT cell lines (T98G, U87MG, U373, HUMI, AMCH) cells were isolated and Western blot analysis was performed using total and phosphorylated STAT3 antibodies. Accordingly, highest STAT3 levels were detected in three *TERT* promoter WT cell lines (BTL53, BTL1333, Gli72) and in two MUT samples (U373, T98G). Furthermore, activated STAT3 was highly present in all four *TERT* promoter WT cell lines as well as in the MUT GS cell line AMCH and minor in the MUT GBM subline U373. Figure 36 illustrates basal protein expression levels of STAT3 and activated STAT3 in the depicted *TERT* promoter WT and MUT GBM models.

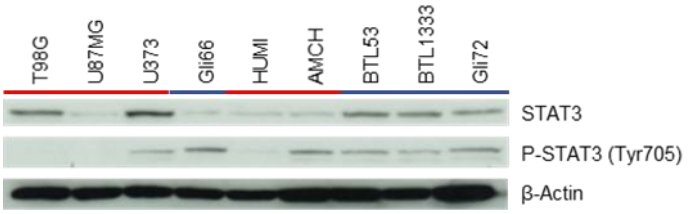

Figure 36. Basal protein expression of total and phosphorylated STAT3 in *TERT* promoter WT and MUT GBM cell lines. Total protein extracts were isolated from certain GBM cell lines as indicated and Western blot analysis was performed. The blue bars mark WT and the red ones MUT cell lines. β-Actin served as loading control.

3.8.2 Cytotoxicity of STAT3 inhibitors and their impact on clone formation capacity

In order to investigate the dependency of our GBM models on the STAT3 pathway, the cascade was inhibited by use of two drugs. The inhibitors WP1066 and STATTIC were tested in order to block the STAT3 signaling pathway. The non-peptidic small molecule inhibitor STATTIC targets the SH2 domain of STAT3, thus blocking STAT3 homo-dimerization *(262, 263)*. Besides proapoptotic and antiproliferative features, the caffeic acid derivate WP1066 also directly inhibits STAT3 *(264-269)*.

Viability assays revealed that the *TERT* promoter WT cell lines tended to be more resistant to WP1066 (IC50 values >10µM) than the MUT samples (Figure 37a). On the contrary, treatment with STATTIC did not follow a clear response pattern. While the MUT cell lines U373 and T98G were not very sensitive to the inhibitor (IC50 values > 5µM), all other tested cell lines exhibited IC50 values between 2 and 4 µM irrespectively of the *TERT* promoter mutation background (Figure 37b). In a second experimental setting, clone formation capacity upon STAT3 inhibition was analyzed. Again every tested WT cell line was significantly more resistant to WP1066 treatment (5µM) as compared to MUT cell models. (Figure 37c/d). Low concentrations of STATTIC did not show clear differences in clonogenicity between *TERT* promoter WT and MUT GBM cells (Figure 37e/f). However, quantification of clone formation assays upon 2.5µM STATTIC treatment revealed a significantly higher sensitivity in the *TERT* promoter MUT as compared to WT GBM cells (Figure 37e/f).

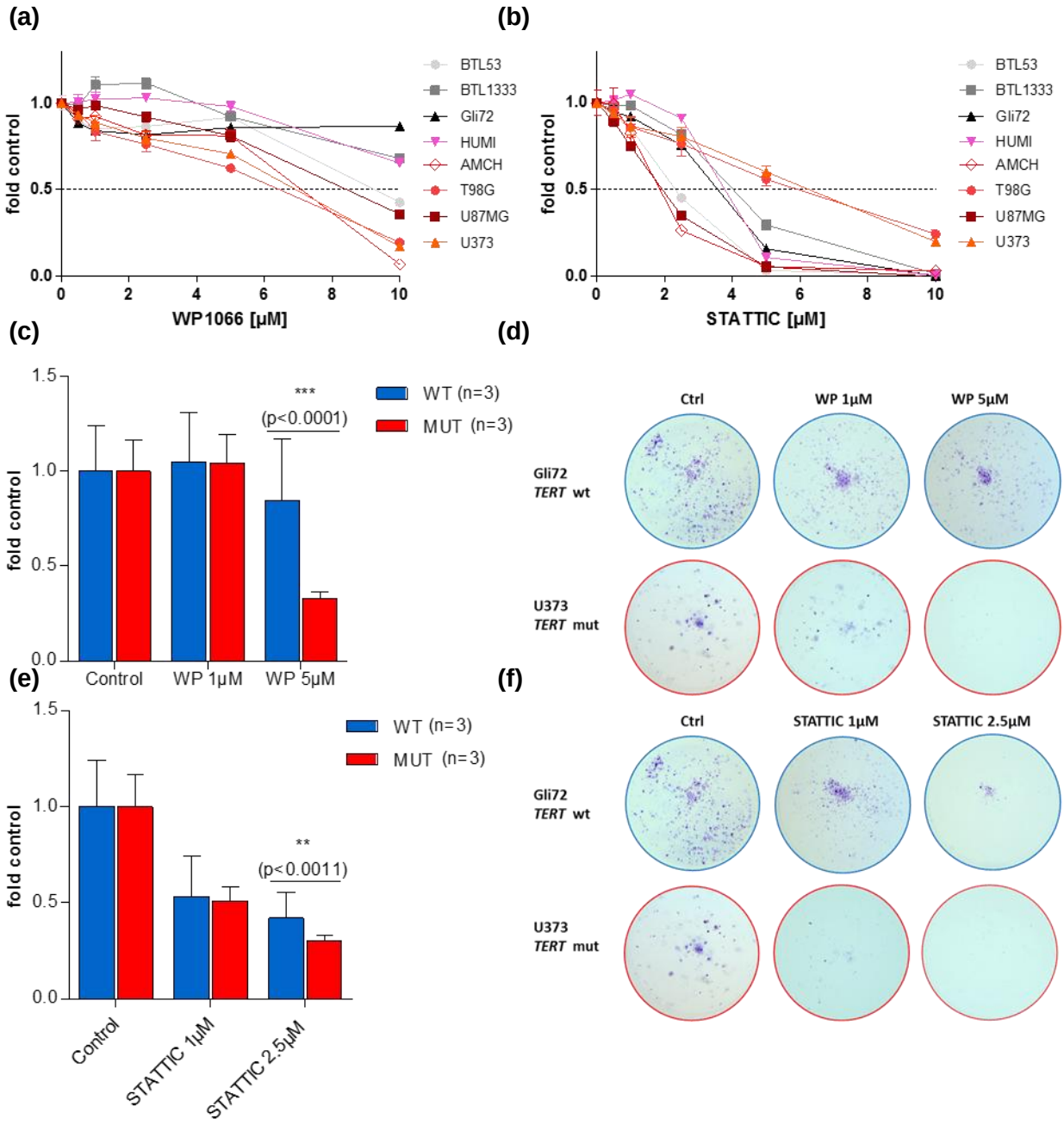

Figure 37. The impact of the *TERT* promoter status on the response to STAT3 inhibitors. Following 72 hours WP1066 **(a)** and STATTIC **(b)** treatment, dose-response curves were established in WT (grey-scale) as well as in MUT (reddish colors) cell lines. **(c and e)** Values of colony formation assays upon long-term WP1066 **(c)** and STATTIC **(e)** treatment are summarized for each *TERT* promoter status (WT, MUT) and illustrated as histograms (mean and SD; t-test). The crystal violet was eluted from the cells with 2% SDS and absorbance was measured (560nm, Tecan Infinite M200 Pro). Results were normalized to the corresponding untreated controls, and set as 1.
(d and f) Representative pictures of fixed and crystal violet-stained cells (WT: Gli72, blue circles; MUT: U373, red circles) are depicted for WP1066 **(d)** as well as for STATTIC treatment **(f)**. Photographs were taken with a Nikon Digital Camera D3200. Significance values are marked with stars: *** p<0.001, ** p<0.01, * p<0.05

3.8.3 Impact of WP1066 on the cell cycle progression of GBM cells

Previous studies dealing with other tumor entities already focused on the mode of action of the STAT3 inhibitor WP1066, revealing a distinctly different cell cycle distribution upon treatment *(292, 293)*. The impact of WP1066 on the cell cycle distribution of our GBM cells was tested in two *TERT* promoter WT and two MUT cell lines. The cells were incubated with 10µM WP1066 for 24 hours and microphotographs were taken (Figure 38a). Subsequently, cell cycle analysis was performed by flow cytometry using PI DNA staining. *TERT* promoter WT and MUT sublines were equally affected by the drug, thus, the results were pooled. Interestingly, WP1066 induced a considerable S-phase arrest in the tested GBM cell models; the abundance of cells in the S-phase was significantly higher in the WP1066 treated samples as compared to the untreated GBM cells (t-test, p=0.0283) (Figure 38b). Furthermore, we observed that WP1066 treatment let to an accumulation of cells in the G2/M phase, however, a statistical relevance was not detected. Cell cycle distribution patterns for every single cell line are depicted in section 3.10.2 (Figure 48b).

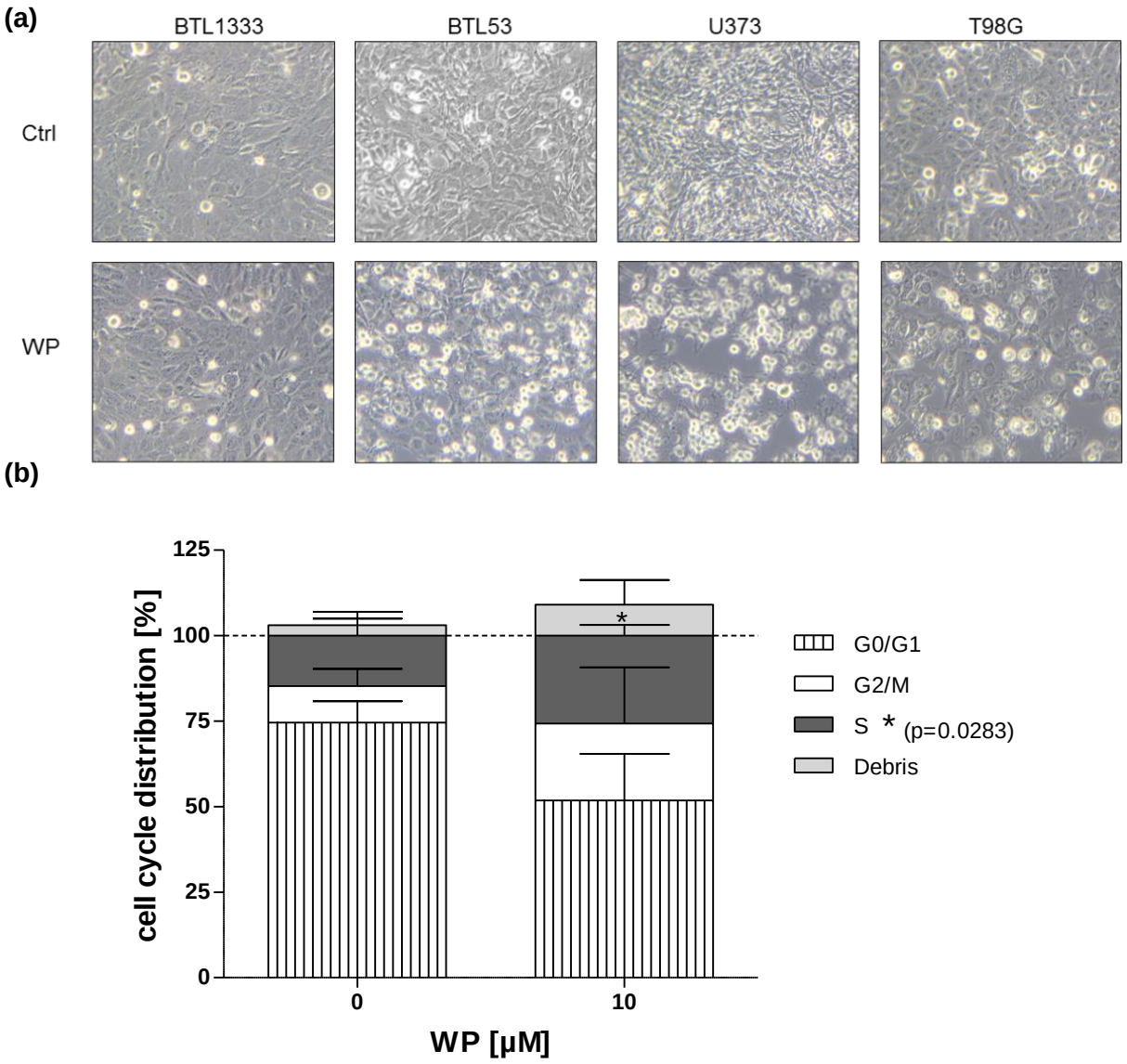

Figure 38. Cell cycle analysis after WP1066 treatment. Two WT (BTL53, BTL1333) and two MUT (U373, T98G) *TERT* promoter GBM cell lines were incubated with 10µM WP1066 for 24 hours. **(a)** Cells were analyzed using the Primovert microscope (Zeiss) equipped with the Plan-ACHROMAT 10x/0.25Ph1 objective (Zeiss). Microphotographs were taken with the AxioCam ICc5 microscope camera (Zeiss) controlled via the ZEN 2 software (Zeiss). **(b)** Cells were fixed, DNA was stained with PI and the cell cycle distribution was analyzed by flow cytometry. Cell cycle distribution results of the cell lines were pooled together and are depicted as stacked box plots (mean±SD) (S-Phase: t-test, p=0.0283). Significance values are marked with stars: *** p<0.001, ** p<0.01, * p<0.05.

3.8.4 STAT3 inhibition drives downregulation of the NFκB pathway

Yang *et al.* identified a novel interaction between the STAT3 and the NFκB pathways *(287)*. Therein, they describe that unphosphorylated STAT3 can interact with NFκB molecules, forming a transcriptionally active complex *(287)*. Previous studies furthermore claimed that PD-L1 may be one transcriptional target of STAT3 *(285, 286)*, thus we were interested in the impact of STAT3 inhibition on PD-L1 expression. In the present study, we blocked the STAT3 pathway by use of WP1066 and analyzed the expression profiles of STAT3 but also of PD-L1 as well as NFκB pathway members. The effect of WP1066 on the protein expression levels of two *TERT* promoter WT cell lines (BTL53 and BTL133), as well as on one C228T promoter MUT (U373) and one C250T MUT (T98G) cell line were tested via Western blot analysis. (Figure 39)

PD-L1 was only observed in the *TERT* promoter WT cell lines, confirming previous results. Strikingly, PD-L1 protein levels pretended to increase as a response to high concentrations (10µM) of WP1066 treatment in the *TERT* promoter WT cell lines. Interestingly, the NFκB signaling pathway also seemed to be targeted by WP1066. The P-STAT3 levels drastically decreased after treatment with 10µM WP1066 in the *TERT* promoter MUT cell lines. However, the WT cell lines seemed to be less affected by the drug. (Figure 39).

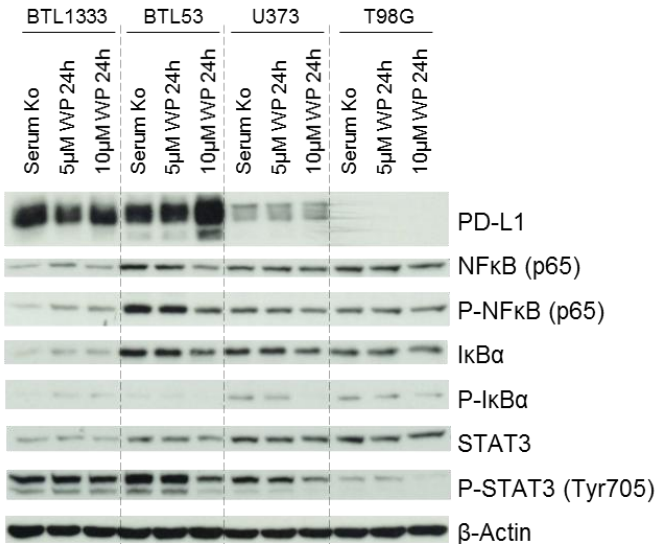

Figure 39. WP1066 and its impact on off-target proteins. BTL1333, BTL53 (both *TERT* promoter WT), U373 (C228T MUT) and T98G (C250T MUT) were treated with 5µM or 10µM WP1066 for 24 hours and proteins were isolated. Total and phosphorylated protein expression levels of PD-L1, STAT3, NFκB and IκB and were analyzed via Western blot analysis. β-Actin served as loading control.

A follow-up experiment was conducted in order to analyze possible differences in the effectiveness of WP1066 after stimulating the cells with IL6. Therefore, a *TERT* promoter WT GBM (BTL1333) as well as a MUT cell line (T98G) was kept under starving conditions in sf R medium for 16 hours (sf control) before they were treated with 10µM WP1066. After 2 hours, the drug was replaced and the cells were stimulated with 50 ng/mL IL6 for five, 15, 30 and 60 minutes. Furthermore, cells were kept in their appropriate growth media serving as serum control. α-Tubulin served as protein loading control. (Figure 40)

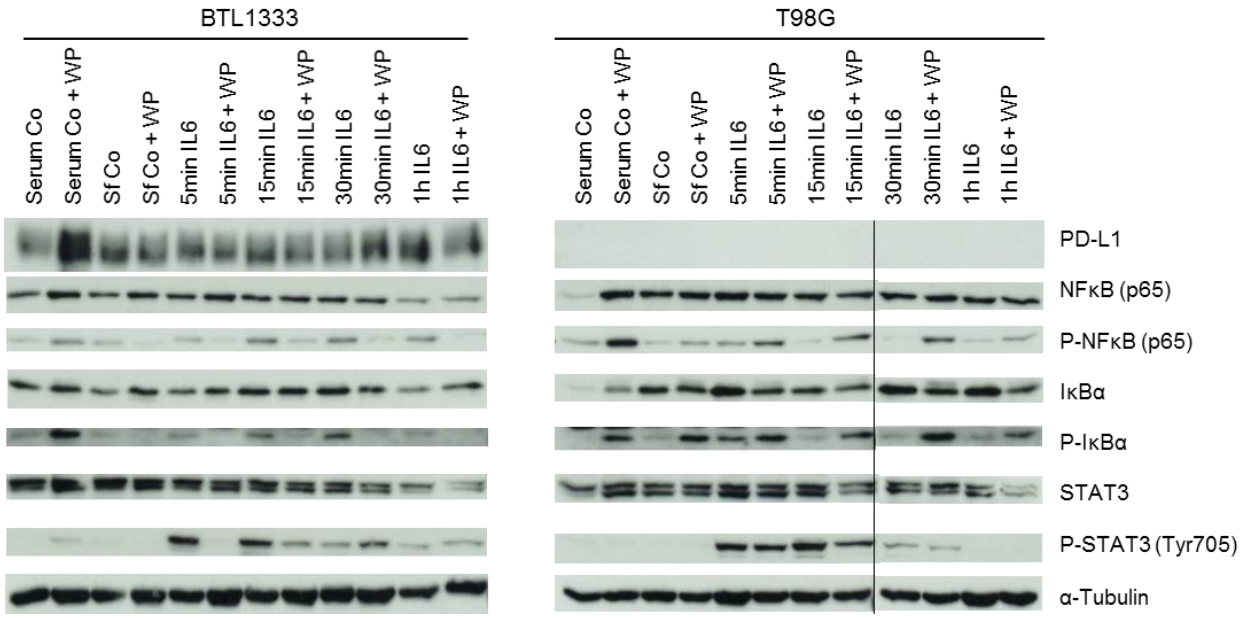

Figure 40. The impact of WP1066 after stimulation with IL6 on *TERT* promoter WT (BTL1333) and MUT (T98G) cells. Two cell lines were starved in serum-free medium (sf) overnight and afterwards treated with 10µM WP1066 for two hours. Subsequently, the cells were stimulated with 50ng/mL IL6 in sf R medium for 5, 15, 30min and one hour. A serum control with and without IL6 evaluated the impact of serum deprivation. α-Tubulin served as protein loading control.

Interestingly, starving the cells in sf medium had considerable effects in the *TERT* promoter MUT cell line T98G, however, the WT GBM BTL1333 was unaffected. Accordingly, NFκB (p65) and IκB were highly upregulated in response to serum deprivation. PD-L1 was again only expressed in the *TERT* promoter WT cell line, but absent in the MUT subline. Treatment of cells in 10% serum with WP1066 strikingly increased the PD-L1 expression. A similar effect was seen when cells were treated simultaneously with WP1066 and with IL6 for 30 minuntes. Interestingly, stimulation of BTL1333 with IL6 for one hour increased the PD-L1 expression, which could be reversed by the STAT3 inhibitor. (Figure 40)

Total NFκB (p65) was highly upregulated after treatment with WP1066 in the serum controls of both tested cell lines, however, the effect in T98G was considerably stronger. Furthermore, NFκB levels of BTL1333, but not of T98G, drastically decreased after one hour IL6. Strikingly, P-NFκB as well as P-IκBα levels increased in the serum controls of both cell lines in response to WP1066. However, the phosphorylation of these proteins was inhibited in response to WP1066 under sf conditions as well as in combination with IL6 in the WT cell model. On the contrary, in the MUT cell line T98G, treatment with WP1066 together with IL6 stimulation led to an upregulation of P-NFκB and P-IκBα at every time point investigated. (Figure 40)

STAT3 was considerably inhibited in response to WP1066 after one hour stimulation with IL6 in both cell lines, however, only minor effects were seen at the other time points. Phosphorylation of STAT3 (P-STAT3) was strongly induced upon five and 15 minutes IL6 stimulation in both cell lines. While in the WT cell model this phosphorylation levels were distinctly reduced upon additional WP1066 treatment, in MUT cells the effects were only minor pronounced. Interestingly, 30 minutes IL6 stimulation together with WP1066 treatment led to an increase of P-STAT3 solely in BTL1333 WT GBM cells. (Figure 40)

3.8.5 The impact of WP1066 on the expression of *STAT3, NFκB, PD-L1* and *TERT*

The *TERT* promoter WT cell line BTL53 as well as the MUT models T98G and U373 were treated with 10µM WP1066 for 3h or 5µM WP1066 for 24h and the RNA was isolated with Trizol. qRT-PCR was performed with primers targeting *TERT, STAT3, NFκB1* and *PD-L1 (CD274)* gene expression. All samples were normalized to *β-Actin* serving as housekeeping gene. Results were compared to the untreated control cells (dotted line), set as 1. qRT-PCR revealed that short-time and high concentrations of WP1066 decreased the *TERT* expression in the cell lines BTL53 (Figure 41a). Contrarily, *TERT* levels were tremendously increased after long-time and lower concentration WP treatment in BTL53 and U373 (Figure 41a). In BTL53, *STAT3* expression decreased upon short-time and high concentration of WP1066 and slightly increased after longer incubation of lower concentrations of WP1066 (Figure 41b). On the contrary, in U373 the *STAT3* levels distinctly increased after 3h WP1066 treatment and returned to the base line after 24h (Figure 41b). While mRNA expression levels of *NFκB1* were elevated upon 3h of WP1066 and unchanged after 24h treatment in BTL53, the opposite was seen in U373 (Figure 41c). In T98G cells, mRNA expression of *NFκB1* was distinctly reduced at both time points (Figure 41c). *PD-L1* levels were strongly increased in BTL53 and U373 upon 24h

WP1066 incubation, while in T98G, more *PD-L1* was observed after 3h WP1066 treatment (Figure 41d).

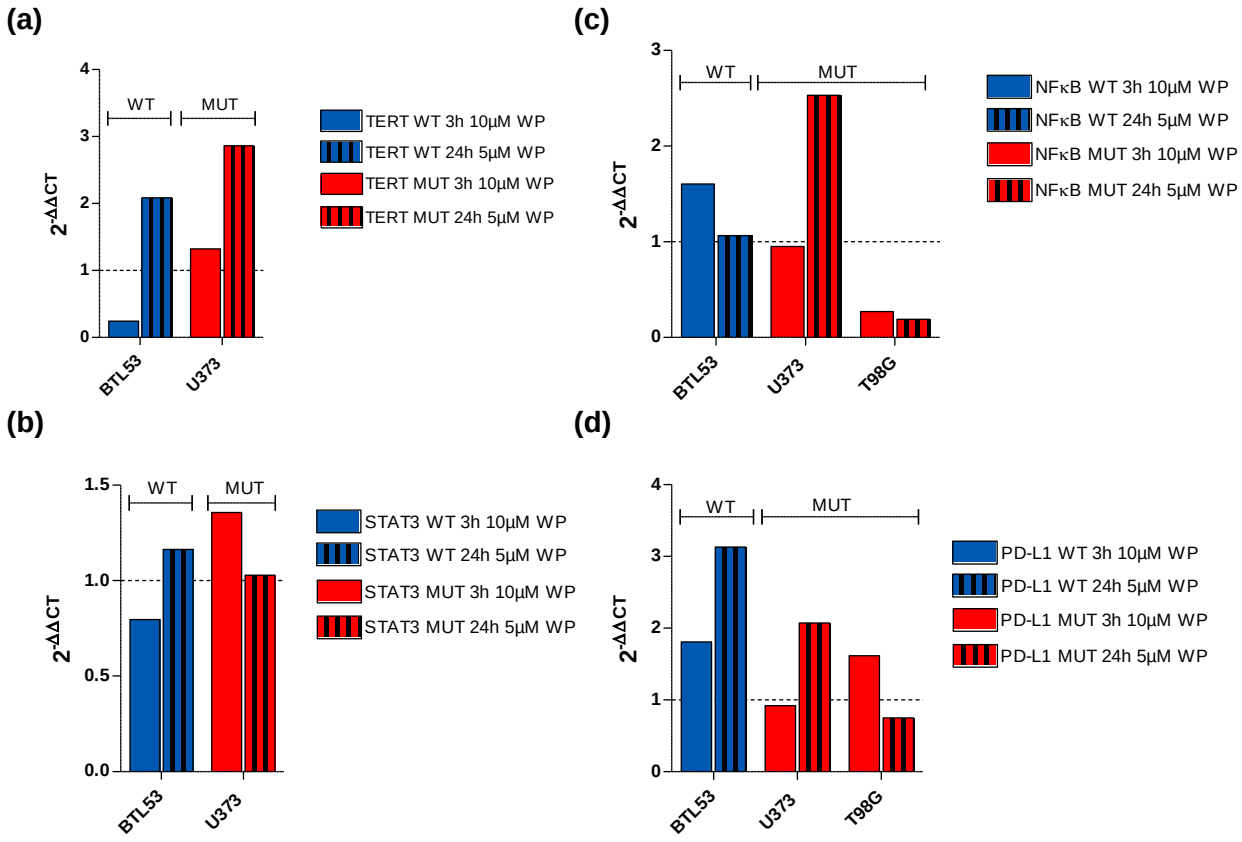

Figure 41. mRNA expression levels of depicted genes upon WP1066 treatment. The *TERT* promoter WT cell line BTL53 and the MUT models U373 and T98G were treated with WP1066 (3h 10μM and 24h 5μM). *TERT* **(a)**, *STAT3* **(b)**, *NFκB1* **(c)** and *PD-L1 (CD274)* **(d)** mRNA expression levels were tested with qRT-PCR. Expression values were normalized to the housekeeping gene β-Actin as well as to the untreated control (ΔΔCT), set as 1 (dotted line), and were converted to a linear form using $2^{-\Delta\Delta CT}$.

TERT promoter WT lines are marked with blue, and *TERT* promoter MUT cell lines are highlighted in red. Significance values are marked with stars: *** p<0.001, ** p<0.01, * p<0.05

3.8.6 The impact of WP1066 on the *TERT* promoter activity

The impact of WP1066 on *TERT* promoter activity was analyzed by luciferase reporter assays. The *TERT* promoter C250T MUT model T98G was transfected with plasmids containing either a WT or a MUT promoter sequence (C228T or C250T) in an rs2853669 SNP carrier or non-carrier background. After the transfection time for 8 hours, cells were treated with 10μM WP1066 for 24

hours. The results were expressed as the ratio of the two luciferase signals firefly to *Renilla*, serving as internal transfection control in each sample. Furthermore, every value was normalized to the promoter-less negative, auto-luminescence control, set as 1. Overall, in presence of the SNP, treatment with WP1066 caused enhanced activities irrespectively of the promoter sequence (Figure 41, C250T SNP, t-test: p=0.0469).

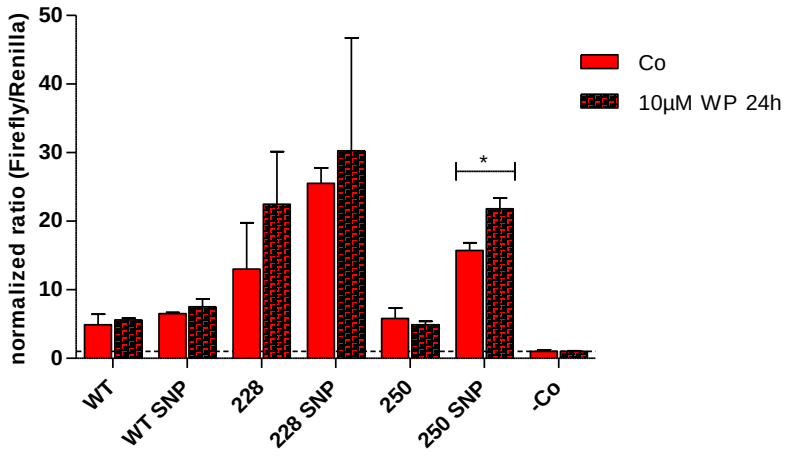

Figure 42. *TERT* promoter activities of different *TERT* promoter variants increase upon WP1066 treatment. The MUT cell model T98G was transfected with the following *TERT* promoter constructs: WT, WT sequence with the variant allele of the rs2853669 SNP (WT SNP), the C228T (228), and the C228T with the SNP (228 SNP) as well as the C250T sequence alone (250) and with the variant allele (250 SNP). After a transfection time of eight hours, cells were treated with 10µM WP1066 for 24h. Values are depicted as ratios between Firefly and *Renilla* and were additionally normalized to the negative control (-Co; promoter-less pGL3 vector), set as 1 (dotted line) (250 SNP, t-test: p=0.0469). Significance values are marked with stars: *** p<0.001, ** p<0.01, * p<0.05.

3.8.7 The impact of WP1066 on the telomerase activity

The telomerase activity has previously been correlated with increased TERT levels, especially with regard to *TERT* promoter mutations *(38, 101, 102, 105, 280)*. Herein, we were investigated the role of STAT3 inhibition in altering the telomerase activity in concern of the *TERT* promoter status in GBM. TRAP assay was conducted in order to analyze the telomerase activity in correspondence to the *TERT* promoter status. Therefore, the cells were treated with 10µM WP1066 for 24h under normal cell culture conditions. The results highlighted considerably higher telomerase activity in the *TERT* promoter MUT cell lines T98G and U373 (342.9 and 264.4 TPG units, respectively), compared to the WT cells BTL53 and BTL1333 (136.5 and 1.88 TPG units, respectively). Furthermore, treatment with WP1066 distinctly reduced the telomerase activity in all cell lines. (Figure 43)

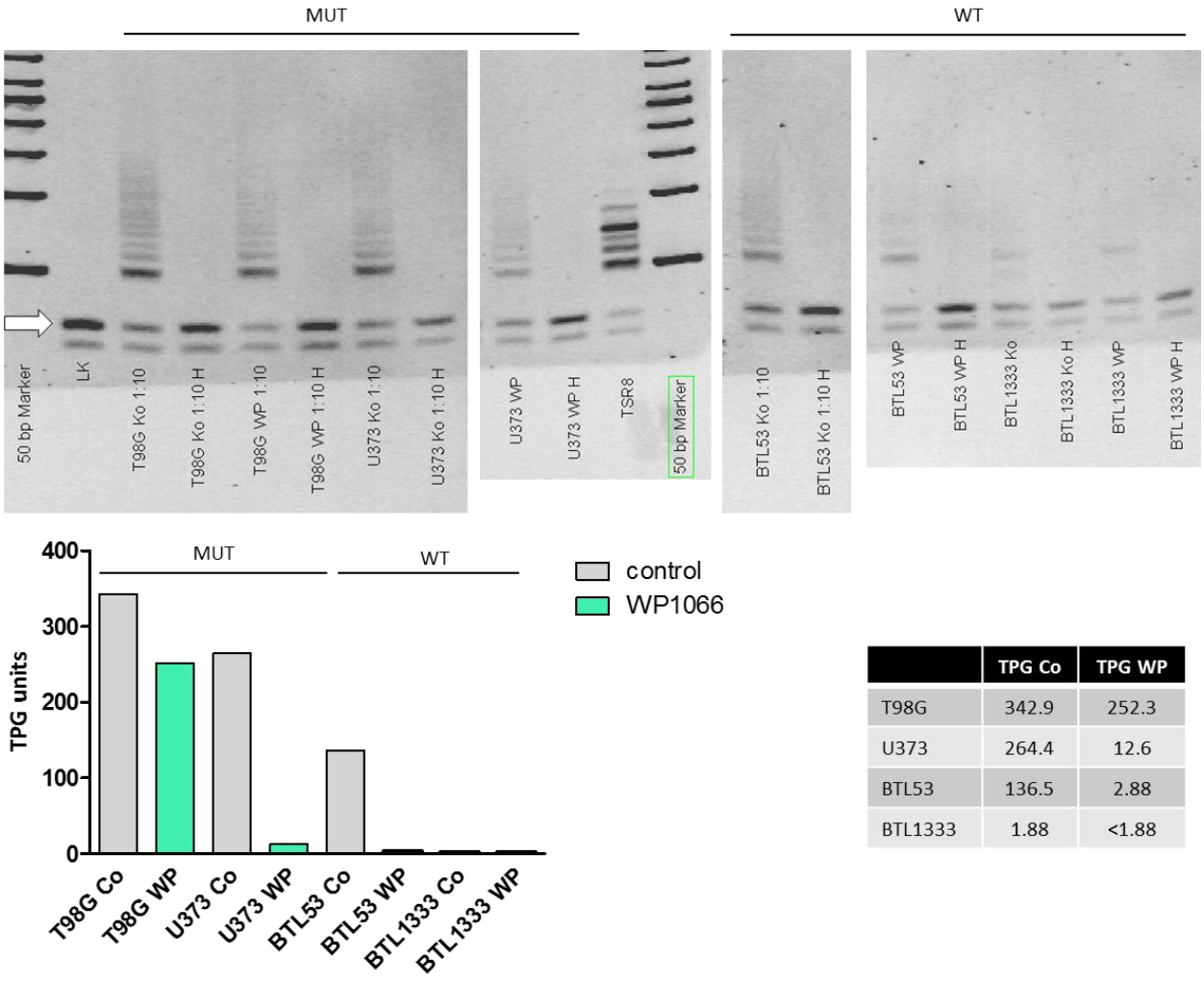

	TPG Co	TPG WP
T98G	342.9	252.3
U373	264.4	12.6
BTL53	136.5	2.88
BTL1333	1.88	<1.88

Figure 43. STAT3 inhibitor WP1066 reduces telomerase activity. Two *TERT* promoter WT (BTL53, BTL1333) and two MUT (T98G, U373) models were treated with 10mM WP1066 for 24h. The upper panel illustrates the gel of the TRAP assay, comparing the untreated cells (Ko) to the treated cells (WP). All samples were diluted 1:10. For every sample an internal control was included (white arrow). LK=control without sample, H=heat-inactivated, TSR8=defined oligonucleotide. The results were quantified according to the calculated TPG units (lower panel, histogram and table) WP1066 treatment is indicated with turquoise color.

3.9 *In vivo* analysis of PD-L1 and P-STAT3

IHC was conducted in order to confirm the presence of PD-L1 as well as P-STAT3 in patient-derived tumor samples.

3.9.1 PD-L1 expression in surgical GBM samples

One *TERT* promoter WT (BTL53) as well as one C250T MUT sample, both characterized by a TT rs2853669 SNP, was analyzed. Human placenta served as positive control for the PD-L1 immunostaining, specifically targeting tubular epithelial cells (Figure 44a). The tissue slides were stained with HE for histo-morphological analyses (Figure 44b/c). Figure 44 depicts representative immunostainings with antibodies against the immunosuppressor PD-L1 (Figure 44d/e). *TERT* promoter WT GBM specimen showed considerable PD-L1 expression (Figure 44d), confirming previous *in vitro* results on mRNA and protein levels (see section 3.5). On the contrary, in the *TERT* promoter C250T MUT sample only a small subgroup of cells was positive for PD-L1 (Figure 44e).

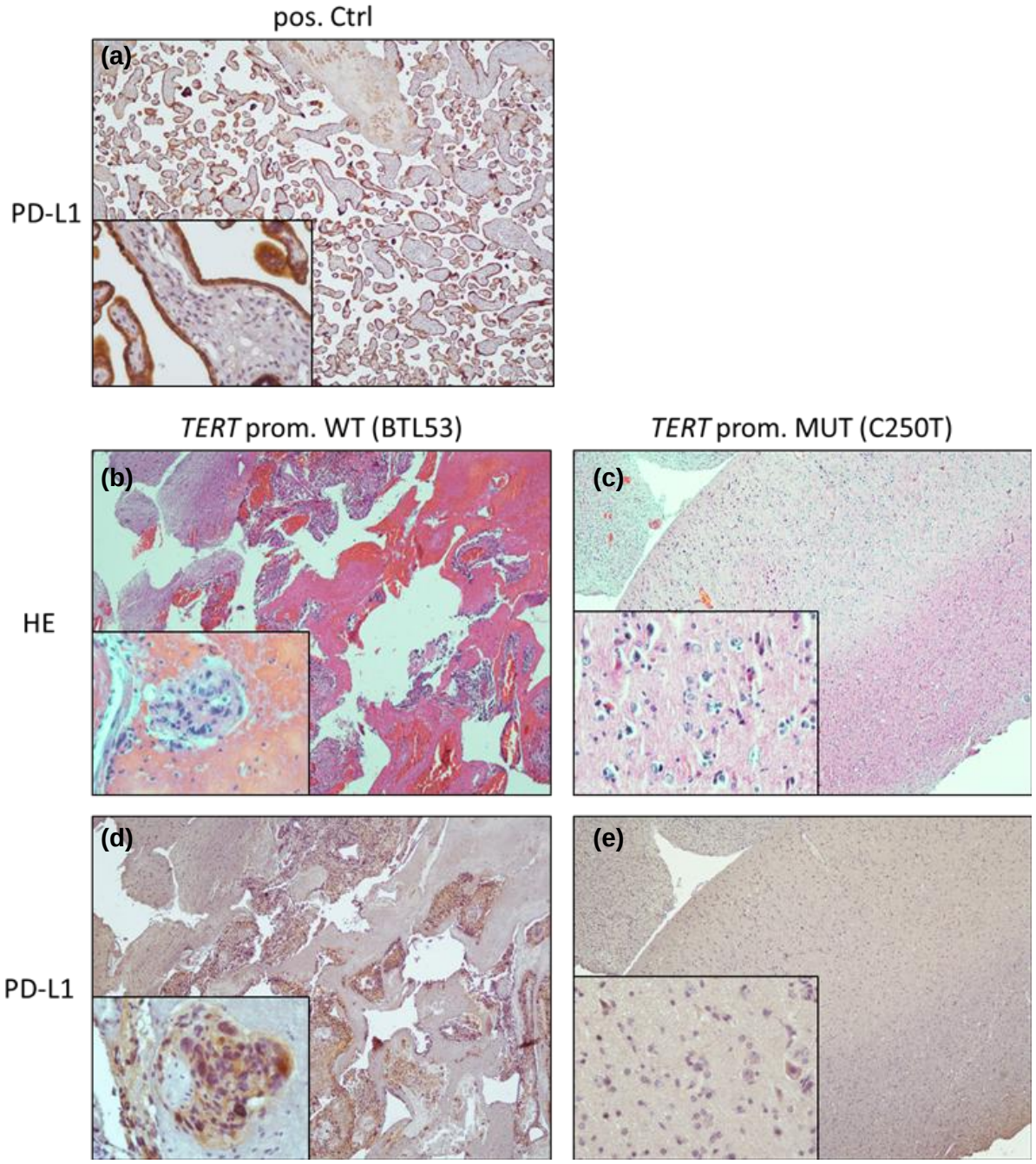

Figure 44. Immunohistochemistry analyses in human GBM tissues. One *TERT* promoter WT (BTL53) **(b and d)** and a C250T MUT cell line **(c and e)** are depicted representatively. Paraffin embedded GBM sections were stained using an antibody against PD-L1. **(a)** Normal human placenta served as positive control for the immunostaining showing positivity in tubular epithelial cells. Haematoxylin and eosin (HE) stain was performed for histopathologic analyses in a *TERT* promoter WT **(b)** as well as a MUT GBM **(c)**. The immunostaining targeting PD-L1 was respectively performed on a WT and MUT GBM **(d and e)**. All immunostainings were conducted according to the respective protocols, see Materials and Methods section 2.9.2. Microphotographs were taken with the Nikon Eclipse 80i microscope equipped with Nikon Plan Fluor 4x/0.13 or Nikon Plan Apo 40x/0.95 DIC M/N2 objectives for 4x (bigger pictures) or 40x (smaller sections) magnification respectively.

3.9.2 P-STAT3 expression in surgical GBM samples

In order to localize brain tumor tissue, the slides were stained with HE (Figure 45a/b). Interestingly, in the *TERT* promoter WT GBM sample (BTL53), P-STAT3 expression was observed in the majority of tumor cells (Figure 45c), while the C250T MUT tumor showed only weak P-STAT3 positivity (Figure 45d). These results are in accordance with previous *in vitro* experiments (see section 3.8.1), showing high P-STAT3 protein expression in BTL53 and low levels of P-STAT3 in *TERT* promoter MUT samples.

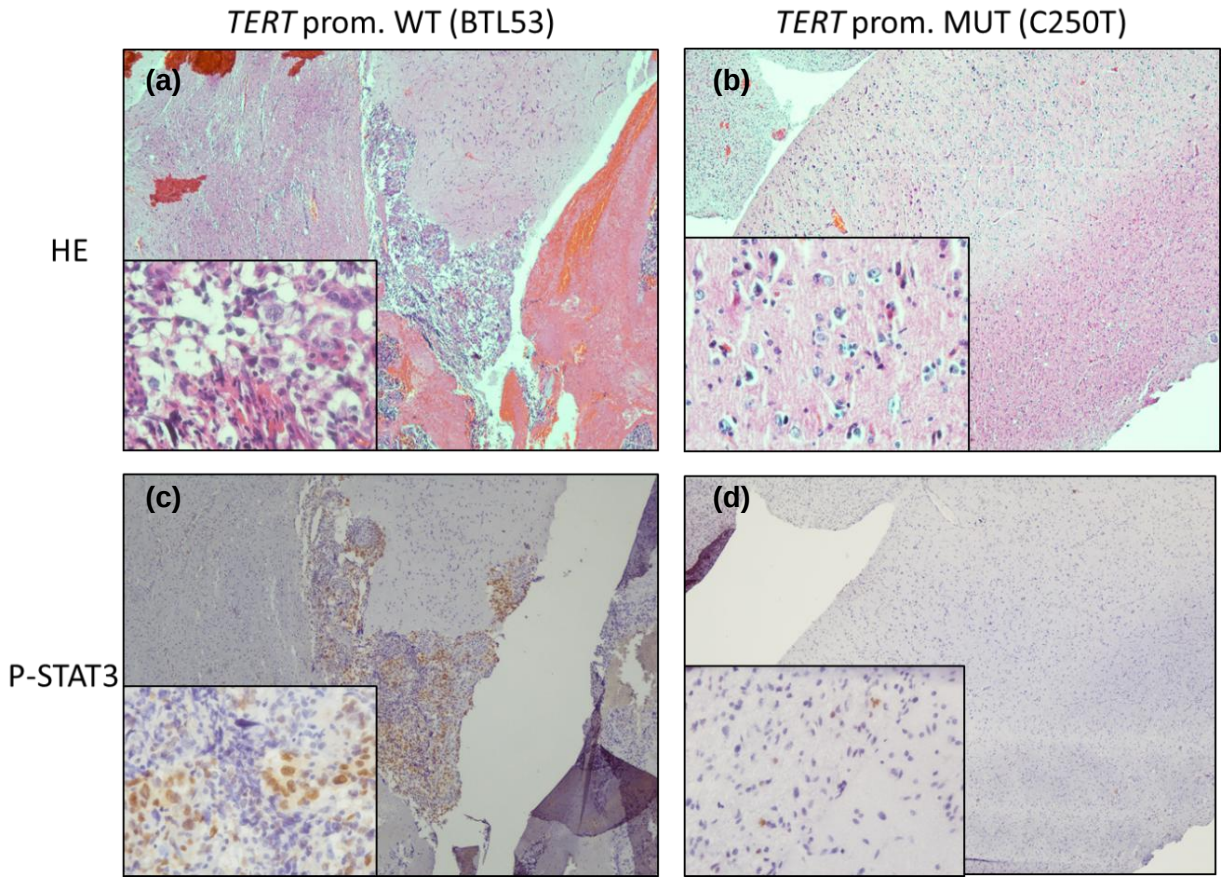

Figure 45. Immunohistochemistry analyses in human GBM tissues. One *TERT* promoter WT (BTL53) **(b and d)** and a C250T MUT cell line **(c and e)** are depicted representatively. Paraffin embedded GBM sections were stained using an antibody against phosphorylated STAT3 (P-STAT3). Haematoxylin and eosin (HE) stain was performed for histopathologic analyses in a *TERT* promoter WT **(a)** as well as a MUT GBM **(b)**. The immunostaining targeting P-STAT3 was respectively performed on a WT and MUT GBM **(c and d)**. All immunostainings were conducted according to the respective protocols, see Materials and Methods section 2.9.1. Microphotographs were taken with the Nikon Eclipse 80i microscope equipped with Nikon Plan Fluor 4x/0.13 or Nikon Plan Apo 40x/0.95 DIC M/N2 objectives for 4x (bigger pictures) or 40x (smaller sections) magnification respectively.

3.10 Additional data

3.10.1 EGFR protein expression and downstream signaling cascades

In addition to the previously described pathways, the EGFR protein expression as well as its downstream signaling pathways were analyzed in our GBM models. Accordingly, protein expression levels of members of the EGFR/MAPK (Figure 46) and PI3K/AKT (Figure 47) signaling cascades were investigated in a panel of TERT promoter MUT and WT cell lines.

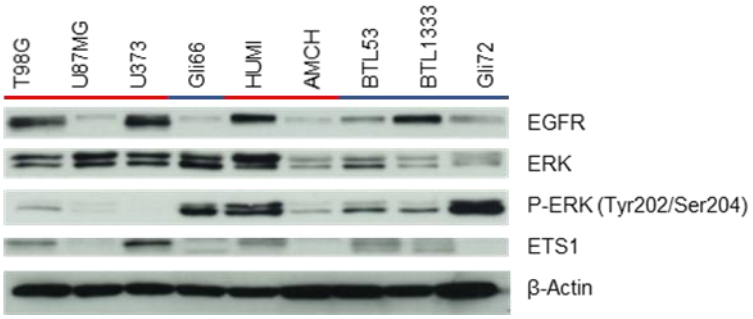

Figure 46. EGFR/MAPK signaling pathway in *TERT* promoter WT and MUT GBM cell lines. Total and phosphorylated protein levels of EGFR, ERK and ETS1 were analyzed by Western blots in the indicated cell lines. The blue bars mark WT and the red ones MUT cell lines. β-Actin served as loading control.

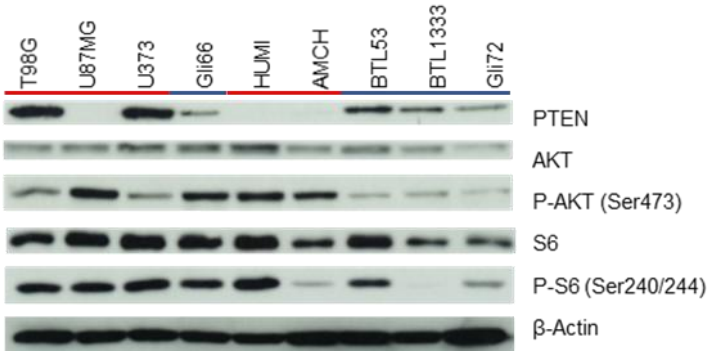

Figure 47. PI3K/AKT signaling pathway in *TERT* promoter WT and MUT GBM cell lines. Total and phosphorylated protein levels of PTEN, AKT and S6 were analyzed by Western blots in the indicated cell lines. The blue bars mark WT and the red ones MUT cell lines. β-Actin served as loading control.

3.10.2 Cell cycle analysis upon QNZ or WP1066 treatment

Different GBM cell lines were treated with the NFκB inhibitor QNZ or with the STAT3 inhibitor WP1066 for 24 hours as depicted in Figure 48a or Figure 48b, respectively. Summarized results for NFκB inhibition or STAT3 inhibition are outlined in sections 3.6.3 or 3.8.3, respectively.

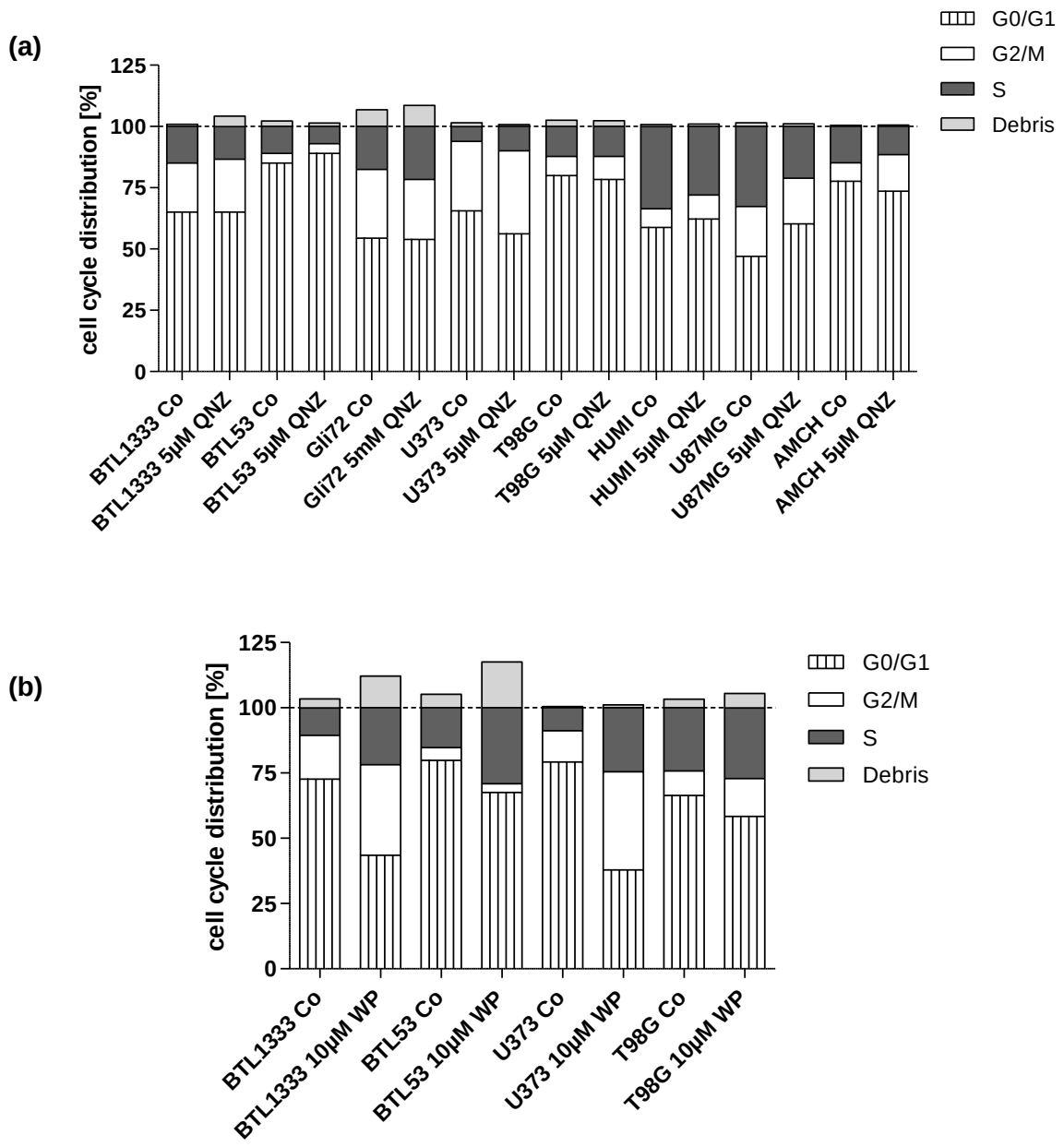

Figure 48. Cell cycle analysis upon drug treatment. (a) Three *TERT* promoter WT GBM and five MUT cell lines were incubated with 5µM QNZ for 24 hours. **(b)** Two *TERT* promoter WT and two MUT GBM cells were treated with 10µM WP for 24 hours. Cells were fixed, DNA was stained with PI and the cell cycle distribution was analyzed by flow cytometry.

4 Discussion

4.1 TERT expression drives tumor aggressiveness in GBM

Reactivation of telomerase, based on expression of TERT, is observed in a versatile variety of tumor entities *(93-95)*. TERT overexpression is often caused by genetic alterations of the *TERT* promoter, representing mostly two activating point mutation *(80)*. Occurrence of such mutations is documented in over 80% of primary GBM, making this tumor the highest ranking entity in this respect *(100)*. Recently, Killela *et al.* characterized C228T and C250T as the most abundant alterations, together accounting for over 90% of all *TERT* promoter mutations *(100)*. Presence of such an activating mutation leads to reactivation of TERT expression, thus reducing self-limiting replicative potential of the malignant cell *(61)*. The present study investigated the *TERT* promoter status in correspondence to TERT expression levels and telomerase as well as *TERT* promoter activity. Using qRT-PCR and Western blot analysis, we revealed that tumors harboring either a C228T or a C250T promoter mutation express significantly more TERT on mRNA as well as on protein levels, respectively, than did WT GBM. Comparable to previous studies *(38, 101, 102, 105, 280)*, in the present thesis we furthermore found that presence of a *TERT* promoter mutation results in higher enzymatic telomerase activity.

In 2015, Spiegl-Kreinecker *et al.* characterized *TERT* promoter mutations as a negative prognostic parameter linked to worse patients' overall survival in GBM *(38)*. Accordingly, they hypothesized that tumors harboring *TERT* promoter mutations exhibit more pronounced tumor aggressiveness as compared to WT GBM *(9, 38, 40, 100, 278)*. To confirm this hypothesis on the level of the malignant cell, we analyzed in the current study the sphere formation potential of *TERT* promoter WT versus MUT cells as a stemness parameter. We observed that all of the tested GBM models have the ability to form neurospheres under stem cell conditions. In accordance to previous hypotheses *(38)*, we indeed observed that *TERT* promoter MUT GBM cells exerted a significantly higher potential to re-adhere and re-differentiate after growing under stem cell conditions as compared to the WT GBM models. Chiba *et al.* introduced *TERT* promoter mutations into embryonic stem cells and analyzed the transcriptional activity of the promoter. They revealed that stem cells with such an introduced mutation overcome *TERT* expression silencing, which is conflicting with embryonic stem cells with an introduced WT sequence *(294)*. With regard to GBM, our present data affirmatively suggest that *TERT* promoter MUT GBM might have an enhanced potential for multi-lineage differentiation.

In addition to mutations in the *TERT* promoter, also the common SNP rs2853669 has been discussed to possess prognostic potential for GBM patients *(9, 38, 40, 278)*. Rachakonda *et al.*

analyzed the impact of this SNP on the *TERT* promoter activity in bladder cancer. Therein they found that promoters carrying the SNP are more transcriptionally active than those lacking this alteration. *(275)* In the current study, we also investigated the *TERT* promoter activity with respect to the promoter mutation status as well as to the SNP. Promoter activity was tested via luciferase reporter assays, introducing expression plasmids harboring different *TERT* promoter variants. Furthermore, we tested those constructs on different cellular backgrounds, hence, *TERT* promoter WT as well as MUT GBM models were transfected with the plasmids. Regarding the cellular background, we found distinct differences on the activities of the transgenic promoter constructs. Apparently, the cellular *TERT* promoter status highly influenced the outcome of the experiment, even after normalization to the transfection control. In accordance with several reports on *TERT* mRNA expression in GBM cell lines and tissues harboring such alterations *(101, 295)*, WT cell lines tended to express lower luciferase levels than those harboring *TERT* promoter mutations.

In 2014, Heidenreich *et al.* postulated the *de novo* generation of different ETS-factor binding sites mediated by C228T and C250T *TERT* promoter mutations *(80)*. Conversely, presence of the SNP rs2853669 has been reported to disrupt the binding site of such ETS-factors, thus decreasing the promoter activity in bladder cancer *(275, 296)*. In contrast to these findings in bladder cancer, in our GBM cell lines we found that SNP-carrying constructs possessed higher *TERT* promoter activity than non-carriers. Precisely, while presence of the SNP causes downregulation of *TERT* promoter activity in bladder cancer *(275)*, we observed an increased activity in GBM. Recently published data reported an association between presence of the mentioned SNP and an increased risk for breast cancer *(297, 298)*. Another publication suggests this SNP as feasible biomarker for adverse prognosis in melanoma patients *(39)*. With respect to GBM, Spiegl-Kreinecker *et al.* characterized the SNP as positive prognostic factor in tumors harboring a WT *TERT* promoter, while presence of the polymorphism predicts negative prognosis in patients with a *TERT* promoter MUT GBM *(38)*. Concerning the GBM background, our data indicate an increase of *TERT* promoter activity resulting from the SNP rs2853669, independent of the *TERT* promoter mutation status. All these findings lead us to the suspicion that there are conspicuous differences between tumor entities regarding the modulatory mechanisms of the SNP.

With respect to the luciferase reporter assays, the activity of the *TERT* promoter constructs was distinctly variable between the transfected cell models. Different transfection efficacies can not underlie this observation as *Renilla* was in all cases included as a transfection control. Hence, the basal ETS-factor expression levels of the respective cell model may be underlying the

different outcomes of the luciferase reporter assays. The endogenous *TERT* promoter status was not associated with the activity of the promoter constructs with both MUT and WT cell models exhibiting in selected cases low to very high activity levels. Interestingly, however only in cell lines harboring endogenous a WT *TERT* promoter status, especially the C228T mutation-containing construct exhibited distinctly enhanced activity as compared to the respective WT plasmid. In contrast, in MUT cell lines this effect was insignificant. The underlying mechanisms are unknown so far, but might be based on a squelching mechanism, due to enhanced binding of endogenously expressed transcription factors to the cellular MUT promoter sequence *(299)*. Alternatively, general changes in the expression pattern of ETS-transcription factors able to bind the respective motifs within the WT and MUT *TERT* promoter might underlie these observations. Interestingly, several previous studies suggested that GABPA might be the decisive ETS-family member, hyper-activating *TERT* expression based on activating promoter mutations *(101, 300, 301)*. However in a recent study, ETS1 was uncovered as key factor for MAPK-activated *TERT* expression in a BRAF MUT and *TERT* promoter MUT melanoma background *(302)*. One might hypothesize that such different expression patterns of ETS-transcription factors might be a consequence of different malignant transformation programs in a *TERT* promoter WT and MUT background. Hence, the occurrence of the *TERT* promoter mutation might be as an essential factor determining the malignant transformation process which might differ between cancer types harboring such mutations. To target this hypothesis, a MUT promoter could be introduced into a WT GBM and *vice versa* using the CRISPR/Cas9 system, thus creating isogenic cell models and allowing to dissect the impact of endogenous *TERT* promoter status. Such models would allow to separate direct impacts of the altered *TERT* promoter sequences or reflections of differing malignant transformation programs.

Taken together, our experiments led to the conclusion that *TERT* promoter MUT tumors are characterized by a more aggressive phenotype regarding their growth pattern and proliferation behavior as compared to WT GBM. This higher aggressiveness may also be due to higher TERT protein and mRNA expression levels and increased enzymatic telomerase activity in those tumors harboring a *TERT* promoter mutation.

4.2 The non-canonical crosstalk between TERT and NFκB

Recently, a plurality of non-canonical functions of telomerase has been described *(75, 78, 79, 81, 86, 87)*. Besides chromosomal end elongation, TERT is also involved in regulation of transcription especially with respect to the NFκB *(75)* and Wnt/β-Catenin pathways *(303)*. The NFκB signaling is considered to be of major importance in various types of

cancer and was also found to be highly upregulated in GBM *(304, 305)*. In terms of the canonical NFκB axis, nuclear TERT forms a protein complex via binding to the p65 subunit of NFκB, thus enhancing transcription of target genes like *IL6, TNFα or IL8 (75). Vice versa,* both NFκB as well as β-Catenin can act as *TERT* gene transcription factors in that case resulting in a positive feedback loop *(76, 77)*. Based on this knowledge, we analyzed a possible interconnection between the *TERT* promoter status and the canonical NFκB pathway in our GBM cell models, especially regarding more pronounced tumor aggressiveness in mutants. Accordingly, investigated expression and phosphorylation of several NFκB signaling proteins using Western blot analyses. Indeed, we elucidated that *TERT* promoter WT GBM models are characterized by distinctly higher levels of activated NFκB p65 as compared to the MUT lines. These enigmatic findings are in contrast to our working hypothesis. As various groups published a direct activation of *TERT* transcription by NFκB *(75-77)*, we had expected more pronounced NFκB activity in the MUT tumors.

To clarify the impact of NFκB signaling on *TERT* expression in the GBM background investigated in this thesis, we performed luciferase reporter assays using expression plasmids encoding for different *TERT* promoter variants and the NFκB inhibitor QNZ. Considering the direct interaction between NFκB and the *TERT* promoter *(75-77)*, we hypothesized that inhibition of the NFκB pathway by QNZ leads to decreased *TERT* promoter activity. Correspondingly, massive reduction of the promoter activity was detected in the WT cell line BTL53. The other WT GBM BTL1333 confirmed this inhibitory effect on the *TERT* promoter in most of the transfected plasmids. Unexpectedly, the MUT cells showed a completely different *TERT* promoter activity pattern upon NFκB inhibition. Treatment of the promoter MUT cell lines T98G and U373 with QNZ resulted in distinctly upregulated *TERT* promoter activity with regard to the majority of *TERT* promoter expression plasmid variants used. Especially the activity of the C228T mutated promoter and SNP carrier was massively stimulated upon QNZ treatment. These findings imply that presence of the SNP indeed results in increased *TERT* promoter activity in response to NFκB inhibition by QNZ especially in the C228T variant. This suggests that NFκB signaling might have an unexpected inhibitory function on the MUT version of the TERT promoter especially in connection with the investigated SNP in the GBM background. The exact mechanisms underlying this inhibitory function of NFκB need to be worked out in detail. However, the general higher levels of NFκB p65 phosphorylation in the WT as compared to the MUT GBM background would support such a scenario.

For the described set of experiments to dissect a role of NFκB in the regulation of TERT expression in GBM cells, we have blocked the pathway by use of QNZ. This inhibitor targets the

SOC entry into the cell and furthermore is capable to inhibit the IL6 and TNFα production *(256)*. Hence due to the SOC entry effect, QNZ inhibits both the canonical as well as the non-canonical NFκB pathways. Additionally to QNZ, we have also applied the inhibitor Bay-11-7082, specifically impeding the cytokine-induced phosphorylation of the negative regulator IkBα, thus inhibiting the release of canonical NFκB and inducing the respective transcriptional programs *(124, 259-261)*. The GBM models were treated with both single drugs for three and seven days in cell viability assays and clone formation assays, respectively. We observed a significantly higher sensitivity to both NFκB inhibitors in the *TERT* promoter MUT cell lines as compared to the WT GBMs. Considering the lower levels of activated NFκB in the MUT background described above, this suggest that a higher vulnerability of essential NFκB-mediated signals in the MUT background. We hypothesize that *TERT* promoter MUT cell lines may be more susceptible to both drugs since they are characterized by significantly lower levels of activated NFκB p65 as we observed in the Western blots. *Vice versa,* WT samples express more activated NFκB p65, thus there might be a need for higher concentrations of the drugs in order to inhibit the pathway.

As most of the data regarding the inhibitor QNZ are based on findings in Huntington's disease *(256-258)*, we attempted to investigate its mode of action also in GBM. QNZ did not show any impact on the cell cycle distribution of our GBM cell models after 24 hours using FACS-PI. Furthermore, we treated the GBM cell cultures for eight hours with QNZ and isolated nuclear as well as cytoplasmic protein fractions to investigate activation of NFκB signaling also in association with STAT3 activation. One of the most important activators for the JAK/STAT pathway is the cytokine IL6, which represents a major target of the NFκB pathway *(82-84)*. As expected, we observed upon QNZ treatment a distinct decrease of the canonical NFκB activation via p65 phosphorylation as well as of the downstream STAT3 pathway in the *TERT* promoter WT cell lines. U373 harboring a C228T mutation and T98G with a C250T mutation, both non-carriers for the SNP rs2853669, did not show any notable alterations in neither NFκB nor STAT3 activation signals upon QNZ treatment. Considering the general sensitivity against QNZ regarding viability and clonogenic potential of these mutated cell lines, these data are unexpected and suggest an NFκB-independent off-target activity of the inhibitor. Interestingly, the cell model HUMI with a C250T-mutated *TERT* promoter and homozygous for the SNP is highly sensitive to short-term QNZ treatment concerning downregulation of the canonical NFκB as well as of the STAT3 signals. Correspondingly, we assume that the *TERT* promoter status regarding mutation and SNP might have a major impact on the therapy response to QNZ probably integrating NFκB-specific and off-target effects. This mechanism need to be dissected in ongoing investigations.

Concerning our short-term NFκB inhibition with QNZ, we additionally proved specificity by analyzing the respective gene expression at the mRNA level. Consistent with the downregulation of the STAT3 pathway proteins upon QNZ treatment for eight hours, we also detected distinct decrease of *STAT3* mRNA levels using qRT-PCR. In contrast to the respective protein experiment identifying this STAT3 pathway inhibition solely in the *TERT* promoter WT cell lines as well as in the C250T mutant harboring a CC SNP, all analyzed GBM models showed a downregulation of *STAT3* mRNA expression suggesting an impact of post-transcriptional or protein stability effects.

To sum up, our data point towards an important role of the NFκB pathway in GBM cell growth *(304, 305)*. Nevertheless, our results suggest a complex and partially contradictory impact of the *TERT* promoter status on this non-canonical TERT effector signaling pathways *(75-80)*. Detailed molecular analyses are needed to dissect these complex interactions in detail. Recently, Li *et al.* stated that the non-canonical NFκB pathway is responsible for *TERT* promoter activation solely in the C250T MUT GBM. The authors detected an increase of p52 NFκB subunit which is able to interact with ETS-factors at the *TERT* promoter. Consequently, p52 correlated with an induction of telomerase activity in this subgroup. *(105)* Thus, also the non-canonical NFκB arm might be of major interest. Future projects planned in our lab will include co-culturing of our GBM models with immune cells or at least induction of the NFκB pathway via various proinflammatory cytokines.

4.3 The NFκB /STAT3/TERT interaction network

IL6 represents one of the most important cytokines in the human body, regulating inflammatory reactions. Furthermore, this cytokine interconnects the NFκB and the STAT3 signaling pathways as the *IL6* gene is one of the key target genes activated by NFκB signals. IL6 is released from the activated cell and can subsequently bind to its transmembrane IL6 receptor, hence activating the JAK/STAT pathway. *(82-84)* Yang *et al.* postulated a new interconnection between the JAK/STAT3 and the NFκB pathways *(287)*. This is based on the hyper-expression of the *STAT3* gene due to activation of the JAK-STAT pathway by IL6 leading to translation of high levels of unphosphorylated STAT3. The authors hypothesize that this unphosporylated STAT3 competes with IκBα for binding to the NFκB dimer (p65/p50) *(287)*. In addition, a physical interaction of canonical NFκB heterodimers and STAT3 has also been identified *(288-291)*. Unsphosphorylated STAT3 binds to NFκB forming a trimer, acting as transcription factor *(287)*. The transcription of numerous genes activated by these pathways including well-known

NFκB target genes require cooperation between the two transcription factors as reviewed in Grivennikov *et al. (84)*

IL6 was previously shown to be associated with the *TERT* promoter mutation status as well as by the common SNP rs2853669 within the *TERT* promoter *(40)*. In the present study, we stimulated our *TERT* promoter WT as well as the MUT GBM models with IL6 for increasing time periods and analyzed activation of both the NFκB as well as the STAT3 pathway using Western blots. We found distinct differences in the expression/activation patterns of both pathways between the WT and the MUT cell lines. In general, the *TERT* promoter WT cell line displayed markedly earlier response to IL6 treatment as compared to the MUT cell line. While the total STAT3 expression remained mainly unchanged in both cell lines, the activated form of the protein could be clearly stimulated with IL6. The total NFκB p65 expression was clearly stimulated with IL6 in all cell lines tested. With respect to the MUT cell line, the activated form of NFκB p65 directly followed the pattern of its inactive analog suggesting predominant regulation at protein expression but not activation. Taken together, the STAT3 pathway seems to be activated by IL6 at first as only IL6 stimulation for 15 minutes was sufficient for activating STAT3 in all cases. Also the canonical NFκB pathway was activatable upon IL6 stimulation. However, longer IL6 stimulation was necessary in order to activate the NFκB pathway, suggesting that STAT3-mediated signals act upstream in NFκB activation by IL6. Following previous findings *(84, 287-291)*, we hypothesize that STAT3 may form a complex including NFκB p65 possessing transcriptional potential.

Following the distinct interconnection between the NFκB and the JAK/STAT3 pathway, we analyzed a feasible relation between the *TERT* promoter status of our GBM cell lines and the STAT3 pathway activation. We were especially interested in a potential role of IL6-inducible STAT3 signals in the more pronounced aggressiveness of *TERT* promoter MUT GBM tumors. Total protein analysis of our GBM models revealed more activated STAT3 in the *TERT* promoter WT samples as compared to the mutants. These results were also confirmed in surgical samples using immunohistochemical detection of activated STAT3. Blockade of the pathway using the inhibitor WP1066 (a direct STAT3 inhibitor) or STATTIC (hindering STAT3 dimerization via interaction with the SH2 domains) led to interesting but unexpected results. As in cell viability assays blockade of the pathway for three days did not show differing results with the two inhibitors, we performed long-term treatment with the drugs for seven days in clone formation assay. Interestingly, *TERT* promoter MUT cell lines were significantly more sensitive against both inhibitors as compared to WT GBM models when applying higher drug concentrations.

Various studies have focused on STAT3 inhibition via WP1066 in different tumor entities including oral squamous cell carcinoma *(293)* and leukemia *(292)*. These studies have revealed an accumulation of the treated tumor cells in the G0-G1 phase of the cell cycle *(292, 293)*. In order to characterize the mode of action of the inhibitor WP-1066 in GBM, we also investigated the impact on cell cycle progression. Thus, we performed FACS-PI analysis and demonstrated induction of an S-phase arrest in all GBM models analyzed independent of the respective *TERT* promoter mutation status.

With regard to the more pronounced expression of activated STAT3 in the *TERT* promoter WT GBM, we analyzed the *TERT* promoter activity upon STAT3 inhibition. Therefore, luciferase assays using different *TERT* promoter constructs were transfected into a GBM cell line and promoter activities were determined. Interestingly, we observed higher promoter activities upon WP1066 treatment in all the constructs. This increase was a trend but reached significance in the C250T promoter mutant carrying the SNP. It is currently unclear whether this change might be related to the genomic background of the cell lines as the T98G cell line used harbored exactly the same *TERT* promoter variant concerning mutation and SNP. Telomerase activity upon STAT3 inhibition was also tested on two WT (BTL53, BTL1333) and on two MUT (T98G, U373) *TERT* promoter GBM samples. BTL1333 did not show any functional telomerase activity *per se.* However, the STAT3 inhibitor strongly inhibited telomerase activity independent of the *TERT* promoter status of the treated GBM lines. In brief, we hypothesize that there is a strong interconnection between *TERT* promoter activity, telomerase functionality and STAT3 inhibition. The paradoxical activation of the promoter after STAT3 inhibition points to activation of a feedback loop induced by telomerase inactivation. Chung *et al.* postulated a regulatory function of STAT3 on *TERT* transcription in breast cancer cells *(85)*. STAT3 may form a complex with NFκB, as already published by others *(287-291)*, which binds to the *TERT* promoter, thus regulating its transcriptional activity *(85)*. Our data would support such an interaction between STAT3 and the regulation of the *TERT* promoter also in GBM cells.

As we previously uncovered that inhibition of the NFκB pathway results in a concomitant downregulation of the JAK/STAT3 pathway, we additionally analyzed the opposite situation. Therefore, we inhibited the STAT3 pathway by use of WP1066 and analyzed protein expression/activation patterns of both the JAK/STAT3 pathway but also of canonical NFκB pathway members. Indeed, especially with respect to *TERT* promoter MUT GBM, we found indications for a STAT3 inhibition-mediated downregulation of the NFκB pathway as well. Regarding inhibition of the activated form of STAT3, the *TERT* promoter MUT GBM lines tended

to be more responsive to the drug as compared to the WT cells. This corresponded to the pronounced inhibition of NFκB pathway members by WP1066 in this GBM subgroup.

Zhang *et al.* identified the *PD-L1 (CD274)* promoter as transcriptional target of STAT3 *(285, 286)*. In the current study, the expression pattern of PD-L1 resembled that of STAT3 phosphorylation upon IL6 stimulation in a *TERT* promoter WT cell line overexpressing PD-L1. Hence, PD-L1 can be stimulated upon short-term treatment (15 minutes) with IL6 in the GBM background, while at longer treatment (1-2 h) times PD-L1 levels markedly declined. This indicates an interconnection between the STAT3 signals and PD-L1 expression in GBM. Accordingly, we found that IL6 does not only stimulate STAT3 pathway induction but also PD-L1 expression in GBM cells. Consequently, we inhibited STAT3 with WP1066 and followed the expression pattern of PD-L1. Interestingly, we detected a strong upregulation of the immune-regulator upon STAT3 inhibition in one of our *TERT* promoter WT cell lines (BTL53), while another one (BTL1333) did not show any response to the drug at the level of PD-L1.
Summing up, we observed a decline of PD-L1 expression after long-term IL6 stimulation. Correspondingly, PD-L1 was strongly upregulated upon long-term treatment with the STAT3 inhibitor WP1066. These findings suggest that PD-L1 expression can be induced by IL6, but only in the first phase of the cytokine stimulation, hence, in the early phase of inflammation. After long-term cytokine stimulation, the immune-regulator gets repressed probably due to a feedback loop. This signaling may be negatively regulated by the JAK/STAT3 signaling axes, as long-term inhibition of the STAT3 results in strong upregulation of PD-L1.

4.4 PD-L1 and its relation to the *TERT* promoter status

Recently, the tumor microenvironment including tumor-associated immune cells came into focus in cancer therapy. *(7, 179-182)* Especially GBM creates an immunosuppressive microenvironment, protecting the tumor from recognition and a combat by the body's immune system. *(306-308)* PD-L1 represents a major immune-modulator in humans, physiologically expressed on APC and regulatory immune cells to interact with its receptor PD-1 located on effector T-cells *(202, 309)*. Thereby, the PD-L1/PD-1 binding initiates inhibition of T-cell differentiation and activation, hence, inhibition of the adaptive immunity *(310)*. Interestingly, the immuno-suppressor PD-L1 is also expressed on the cellular surface of tumor cells in 60-80% of all GBM cases. *(239, 281)* The prognostic impact of PD-L1 positivity in GBM is intensively discussed in current literature *(311)*. While some researchers state that PD-L1-positive neurons co-localized to the tumor are connected with a better prognosis *(312)*, some others claim that PD-L1 expression in GBM tumors predicts worse prognosis as compared to case lacking tumor-

associated PD-L1 expression *(281-284)*. However, Berghoff et al. did not detect a prognostic or predictive impact of PD-L1 expression in GBM patients *(239)*.

TERT promoter mutations were also characterized as negative prognostic factor in GBM *(9, 38, 40, 100, 278)*. As suggest by a recent study from our group based on clinical observations *(38)*, this thesis work proves that *TERT* promoter MUT GBM harbor enhanced tumor aggressiveness as compared to WT cell models. As presence of an activating *TERT* promoter mutation *(9, 38, 40, 100, 278)* as well as PD-L1 positivity *(281-284)* represent negative prognostic markers in GBM, we aimed to investigate a potential interconnection between those two parameters. Consequently, we analyzed the basal PD-L1 protein expression levels in our GBM cell models. Surprisingly, we identified PD-L1 to be highly expressed in tumors harboring a WT *TERT* promoter. On the contrary, *TERT* promoter MUT cell lines were characterized by significantly lower levels of the immune-suppressor. Corroboratively, *PD-L1 (CD274)* gene expression levels were significantly higher in GBM with a *TERT* promoter WT background as those harboring a mutation. Also immunohistochemistry targeting PD-L1 in the GBM cells confirmed these results, revealing PD-L1 overexpression solely in the *TERT* promoter WT tumors. These observations are somehow surprising considering previous data from Nduom *et al.* characterizing PD-L1 expression as negative prognostic parameter in GBM *(281)*. Our data suggest that PD-L1 over-expression is restricted to *TERT* promoter WT tumors, which are less aggressive as compared to the MUT ones *(9, 38, 40, 100, 278)*. These data definitely prove that the higher aggressiveness of TERT promoter MUT GBM cases is unlikely to be based on enhanced immunosuppression by PD-L1. Within this thesis work, we could not clarify the question whether PD-L1 expression is a direct consequence or only a bystander effect of the *TERT* promoter status. This is object of ongoing experiments. Additionally, Ponceau S staining of Western blot membranes indicated overexpression of an unknown 45kDa protein selectively in all *TERT* promoter MUT cell models (data not shown). In order to identify the specificity of those proteins, the respective proteins are currently identified using a shotgun proteomics approach.

Recently, researchers have described circulating forms of PD-1 as well as PD-L1 harboring full functionality making them especially interesting as biomarkers for tumor detection *(313, 314)*. Interestingly, soluble PD-1 unlike soluble PD-L1 has contradictory biological effects than the membrane-bound form of PD-1. Therefore, the circulating form exhibits T-cell stimulating effects after ligand binding. *(313, 314)* In the current study only endogenous PD-L1 levels were checked, thus, soluble forms of neither PD-L1 nor PD-1 were analyzed. Subsequent projects

may deal with the analysis of those markers in the supernatant of tumor cell models via enzyme-linked immunosorbent assay (ELISA).

With respect to the discovery of PD-L1/PD-1 checkpoint molecules, the development of onco-immunotherapy revolutionized the field of cancer therapy. Current immunotherapy follows the principle of targeting various immune-checkpoints, thus hyper-activating T-cells to target the cancer cells. One group of such immunestimulatory drugs are PD-L1/PD-1 checkpoint inhibitors *(240)*. Two clinically approved examples for PD-1 inhibitors are the therapeutic monoclonal antibodies Nivolumab or Pembrolizumab *(241)*, already used in NSCLC and malignant melanoma. As a consequence of our findings, concerning restriction of PD-L1 positivity to the *TERT* promoter WT GBM, we hypothesize that this subgroup of patients would stronger benefit from immunotherapeutic approaches using anti-PD-1 or anti-PD-L1 therapeutic antibodies like Nivolumab or Pembrolizumab. Of course, this hypothesis needs to be proven in future experiments using animal models and clinical studies.

5 Appendix

5.1 Vector maps for luciferase reporter assay

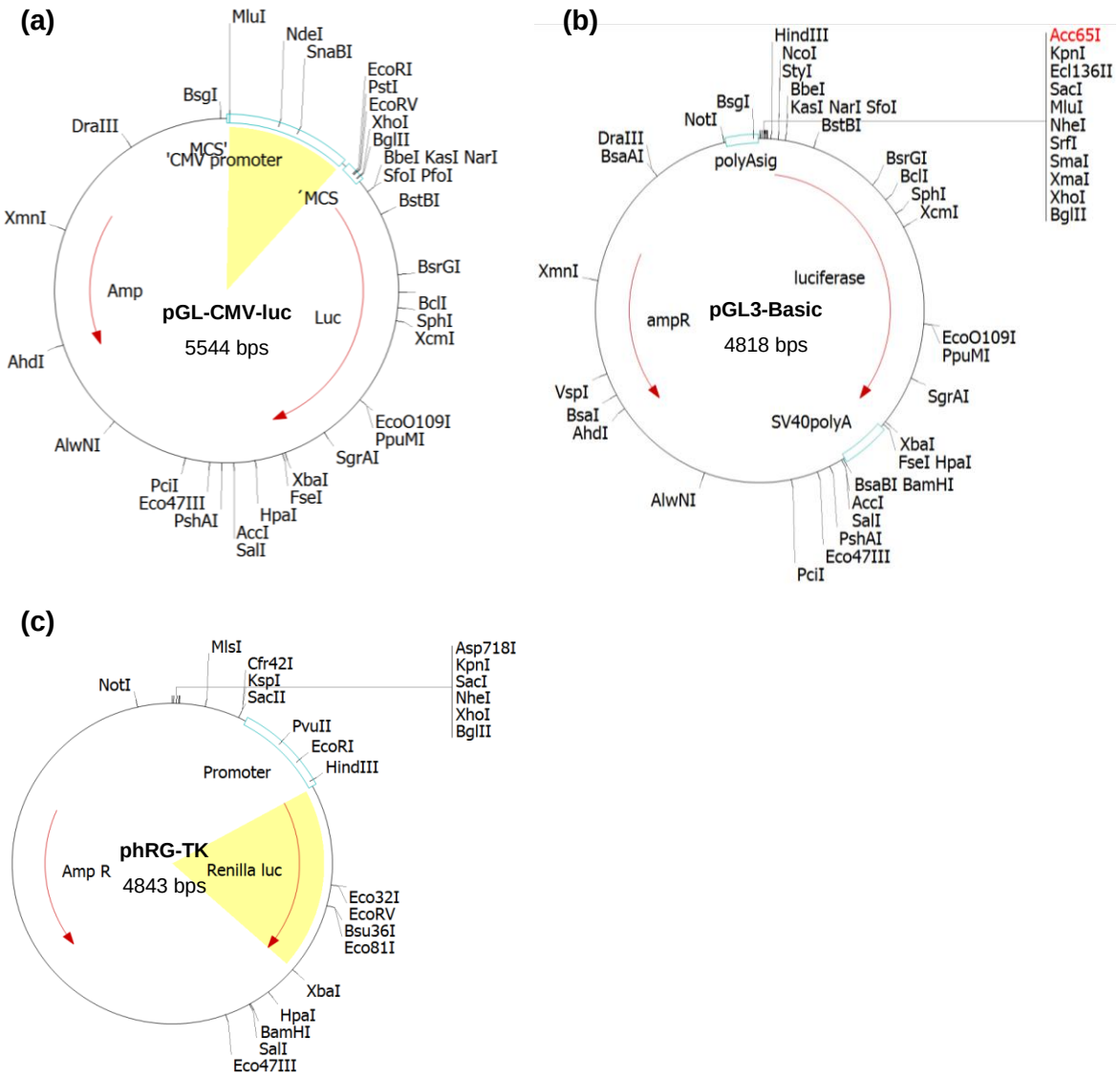

Figure 49. Vector maps of plasmids for luciferase reporter assay. (a) pGL-CMV-luc was used as positive control. The 5544 bp long plasmid harbors a highly active cytomegalovirus promoter and a luciferase reporter. **(b)** pGL3-Basic promoter-less plasmid is 4818bp long and served as negative control in order to normalize the unspecific background luminescence. **(c)** The phRG-TK plasmid is 4843 bp is characterized by reporter sequence encoding for *Renilla* luciferase, which represents another enzyme responsible for luminescence. This plasmid served as internal control in order to evaluate the transfection efficiency and further to normalize the luminescence values. *(275)*

Abbreviations

AKT=PKB	Protein kinase B
ANK	Ankyrin repeats
AP-1	Activator protein 1
APC	Antigen presenting cell
APS	Ammonium persulfate
ARG1	Arginase 1
BBB	Blood-brain barrier
Bcl-2	B-cell lymphoma 2
BER	Base excision repair
bFGF	Basal fibroblast growth factor
BRAF=C-Raf-1	Murine Sarcoma Viral Oncogene Homolog B
BSA	Bovine serum albumin
cAMP	Cyclic adenosine-monophosphate
CCL	Chemokine (C-C motif) ligand 2
CMV	Cytomegalovirus
CNS	Central nervous system
CSF1	Colony stimulating factor 1
CSF-1R	Colony stimulating factor 1 receptor
CTE	C-terminal extension domain
CTLA-4	Cytotoxic T-lymphocyte-associated antigen 4
CXCL	Chemokine (C-X-C motif) ligand
DD	Death domain
DKC1	Dyskerin
DMSO	Dimethyl sulfoxide
EBE	Ethyl-n-butyl ether
EDTA	Ethylenediaminetetraacetic acid
EGF	Epidermal growth factor
EGFR	Epidermal growth factor receptor
ELISA	Enzyme-linked immunosorbent assay
EMT	Epithelial-mesenchymal transition
ERK	Extracellular (signal-) regulated kinase
ETS	E-twenty six
FACS	Fluorescence-activated-cell-sorting

FBS	Fetal bovine serum
FOXP3	Forkhead box P3
GBM	Glioblastoma multiforme
GRB2	Growth factor receptor-bound protein 2
GRR	Glycine rich region
GS	Gliosarcoma
GSK3β	Glycogen synthase kinase 3β
HB-EGF	Heparin-binding EGF-like growth factor
HE	Haematoxilin and eosin
hTR=TERC	Telomerase RNA
IBD	Inflammatory bowel disease
IC50	Half maximal inhibitory concentration
ICAM	Intercellular adhesion molecules
IDH	Isocitrate dehydrogenase
IFN	Interferone
IHC	Immunohistochemistry
IKK	Inhibitor of kappa B kinase
IL	Interleukin
IL6Rα	Interleukin 6 receptor alpha chain
IκB	Inhibitor of kappa B
JAK	Janus kinase
Lef	Lymphoid Enhancer-Binding Factor
LOH	Loss of heterozygosity
LPS	Lipopolysaccharide
LRP	Low-density lipoprotein receptor-related protein
LZ	Leucine zipper
MAPK=ERK	mitogen activated protein kinase
MAPKK=MEK	mitogen activated protein kinase kinase
MAPKKK=RAF	mitogen activated protein kinase kinase kinase
MGMT	O6-methylguanine-DNA methyltransferase
MHC	Major histocompatibility complex
MMR	Mismatch repair
Mrc1	Mannose receptor
MTT	3-(4,5-Dimethylthiazol-2-yl)-2,5-diphenyltetrazolium bromide
MUT	mutated

NAF1	Nuclear Assembly Factor 1
NAK	TRAF-associated NFκB activator (TANK) binding kinase
NEMO	NFκB essential modulator
NFκB	Nuclear factor ‘immunoglobulin κ-light-chain-enhancer' restricted to activated B-cells
NK	Natural killer
NO	Nitric oxide
NOP10	Neurospora crassa 10
NOS	Not otherwise specified
NOS2	Nitric oxide synthase 2
NSCLC	Non-small cell lung cancer
NSC	Neuronal stem cells
PAGE	Poly-acrylamid-gel-electrophoresis
PAMP	Pathogen-associated molecular patterns
PBS	Phosphate buffered saline
PBST	Phosphate buffered saline with 0.1% Tween20
PD-1	Programmed death 1
PDGF	Platelet derived growth factor
PDGFR	Platelet derived growth factor receptor
PD-L1	Programmed death ligand 1
PGE_2	Prostaglandin E_2
PI	Propidium iodide
PI3K	Phosphatidylinositol bisphosphate 3 kinase
PKB	Protein kinase B
PTEN	Phosphatase and tensin homolog
PVDF	Polyvinylidefluorid
RAS	Rat sarcoma
RHD	Rel homology domain
ROS	Reactive oxygen species
RPL41	Ribosomal protein L41
RSK1	Ribosomal S6 kinase 1
RT	Reverse transcriptase
RTK	Receptor tyrosine kinases
SDS	Sodium dodecyl sulfate
sf	Serum-free

SH2	Src homology domain 2
SNP	Single nucleotide polymorphism
SOC	Store-operated calcium
SOS	Son of sevenless
SP1	Specificity protein 1
STAT	Signal transducer and activator of transcription
T2K	TRAF-associated NFκB activator (TANK) binding kinase
TAD	Transactivation domain
TAM	Tumor associated macrophages
TANK	TRAF-associated NFκB activator
TBK	TRAF-associated NFκB activator (TANK) binding kinase
TBST	Tris-buffered saline with 0.1% Tween20
TCF	Ternary complex factor
TCR	T-cell receptor
TEN	Telomerase N-terminal
TERT	Telomerase reverse transcriptase
TGF	Transforming growth factor
Th	T-helper
TK	Thymidine kinase
TLR	Toll-like receptors
TMZ	Temozolomide
TNF	Tumor necrosis factors
TPG	Total product generated
TRAP	Telomerase repeat amplification protocol
TRBD	TR-binding domain
Treg	T-regulatory
TS	Telomerase substrate
TSR8	Thrombospondin type 1 repeat 8
TYK2	Tyrosine kinase 2
VEGF	Vascular endothelial growth factor
WHO	World Health Organization
WT	Wild-type
α-Catenin	α-catenin
β-Catenin	β-catenin

References

1. Statistik Austria, Krebserkrankungen/Todesursachen. *http://www.statistik.at/web_de/statistiken/menschen_und_gesellschaft/gesundheit/* download: 07/**2016**.

2. J. Ferlay *et al.*, Cancer incidence and mortality worldwide: sources, methods and major patterns in GLOBOCAN 2012. *Int. J. Cancer.* **136**, E359-86 (2015).

3. World Health Organisation. *http://www.who.int/* download: 11/2016

4. D. Hanahan, R. A. Weinberg, The hallmarks of cancer. *Cell.* **100**, 57-70 (2000).

5. D. B. Couch, Carcinogenesis: basic principles. *Drug Chem. Toxicol.* **19**, 133-148 (1996).

6. C. M. Croce, Oncogenes and cancer. *N. Engl. J. Med.* **358**, 502-511 (2008).

7. D. Hanahan, R. A. Weinberg, Hallmarks of cancer: the next generation. *Cell.* **144**, 646-674 (2011).

8. Q. T. Ostrom *et al.*, American Brain Tumor Association Adolescent and Young Adult Primary Brain and Central Nervous System Tumors Diagnosed in the United States in 2008-2012. *Neuro Oncol.* **18 Suppl 1**, i1-i50 (2016).

9. U. Nencha *et al.*, TERT promoter mutations and rs2853669 polymorphism: prognostic impact and interactions with common alterations in glioblastomas. *J. Neurooncol.* **126**, 441-446 (2016).

10. A. Wohrer *et al.*, The Austrian Brain Tumour Registry: a cooperative way to establish a population-based brain tumour registry. *J. Neurooncol.* **95**, 401-411 (2009).

11. Q. T. Ostrom *et al.*, CBTRUS Statistical Report: Primary Brain and Central Nervous System Tumors Diagnosed in the United States in 2008-2012. *Neuro Oncol.* **17 Suppl 4**, iv1-iv62 (2015).

12. D. R. Johnson, D. J. Ma, J. C. Buckner, J. E. Hammack, Conditional probability of long-term survival in glioblastoma: a population-based analysis. *Cancer.* **118**, 5608-5613 (2012).

13. N. R. Smoll, K. Schaller, O. P. Gautschi, Long-term survival of patients with glioblastoma multiforme (GBM). *J. Clin. Neurosci.* **20**, 670-675 (2013).

14. D. N. Louis *et al.*, The 2016 World Health Organization Classification of Tumors of the Central Nervous System: a summary. *Acta Neuropathol.* **131**, 803-820 (2016).

15. H. Ohgaki *et al.*, Genetic pathways to glioblastoma: a population-based study. *Cancer Res.* **64**, 6892-6899 (2004).

16. H. Ohgaki, P. Kleihues, Genetic pathways to primary and secondary glioblastoma. *Am. J. Pathol.* **170**, 1445-1453 (2007).

17. D. N. Louis *et al.*, The 2007 WHO classification of tumours of the central nervous system. *Acta Neuropathol.* **114**, 97-109 (2007).

18. K. Zhang, X. Q. Wang, B. Zhou, L. Zhang, The prognostic value of MGMT promoter methylation in Glioblastoma multiforme: a meta-analysis. *Fam. Cancer.* **12**, 449-458 (2013).

19. E. S. Newlands, M. F. Stevens, S. R. Wedge, R. T. Wheelhouse, C. Brock, Temozolomide: a review of its discovery, chemical properties, pre-clinical development and clinical trials. *Cancer Treat. Rev.* **23**, 35-61 (1997).

20. E. S. Newlands *et al.*, Phase I trial of temozolomide (CCRG 81045: M&B 39831: NSC 362856). *Br. J. Cancer.* **65**, 287-291 (1992).

21. J. Zhang, M. F. Stevens, T. D. Bradshaw, Temozolomide: mechanisms of action, repair and resistance. *Curr. Mol. Pharmacol.* **5**, 102-114 (2012).

22. M. Preusser *et al.*, Anti-O6-methylguanine-methyltransferase (MGMT) immunohistochemistry in glioblastoma multiforme: observer variability and lack of association with patient survival impede its use as clinical biomarker. *Brain Pathol.* **18**, 520-532 (2008).

23. F. Ohka *et al.*, The global DNA methylation surrogate LINE-1 methylation is correlated with MGMT promoter methylation and is a better prognostic factor for glioma. *PLoS One.* **6**, e23332 (2011).

24. M. Mellai *et al.*, MGMT promoter hypermethylation and its associations with genetic alterations in a series of 350 brain tumors. *J. Neurooncol.* **107**, 617-631 (2012).

25. R. Stupp *et al.*, Radiotherapy plus concomitant and adjuvant temozolomide for glioblastoma. *N. Engl. J. Med.* **352**, 987-996 (2005).

26. S. E. Combs *et al.*, Prognostic significance of IDH-1 and MGMT in patients with glioblastoma: one step forward, and one step back? *Radiat. Oncol.* **6**, 115-717X-6-115 (2011).

27. M. E. Hegi *et al.*, Correlation of O6-methylguanine methyltransferase (MGMT) promoter methylation with clinical outcomes in glioblastoma and clinical strategies to modulate MGMT activity. *J. Clin. Oncol.* **26**, 4189-4199 (2008).

28. V. Suri, P. Jha, M. C. Sharma, C. Sarkar, O6 -methylguanine DNA methyltransferase gene promoter methylation in high-grade gliomas: a review of current status. *Neurol. India.* **59**, 229-235 (2011).

29. Sang Y. Lee, Temozolomide resistance in glioblastoma multiforme. *Genes and Diseases.*, 198-210 (2016).

30. M. E. Hegi *et al.*, MGMT gene silencing and benefit from temozolomide in glioblastoma. *N. Engl. J. Med.* **352**, 997-1003 (2005).

31. R. A. Olson, P. K. Brastianos, D. A. Palma, Prognostic and predictive value of epigenetic silencing of MGMT in patients with high grade gliomas: a systematic review and meta-analysis. *J. Neurooncol.* **105**, 325-335 (2011).

32. M. E. Hegi *et al.*, Clinical trial substantiates the predictive value of O-6-methylguanine-DNA methyltransferase promoter methylation in glioblastoma patients treated with temozolomide. *Clin. Cancer Res.* **10**, 1871-1874 (2004).

33. A. A. Yin *et al.*, The predictive but not prognostic value of MGMT promoter methylation status in elderly glioblastoma patients: a meta-analysis. *PLoS One.* **9**, e85102 (2014).

34. D. W. Parsons *et al.*, An integrated genomic analysis of human glioblastoma multiforme. *Science.* **321**, 1807-1812 (2008).

35. H. Yan *et al.*, IDH1 and IDH2 mutations in gliomas. *N. Engl. J. Med.* **360**, 765-773 (2009).

36. S. Borah *et al.*, Cancer. TERT promoter mutations and telomerase reactivation in urothelial cancer. *Science.* **347**, 1006-1010 (2015).

37. J. Min, J. W. Shay, TERT Promoter Mutations Enhance Telomerase Activation by Long-Range Chromatin Interactions. *Cancer. Discov.* **6**, 1212-1214 (2016).

38. S. Spiegl-Kreinecker *et al.*, Prognostic quality of activating TERT promoter mutations in glioblastoma: interaction with the rs2853669 polymorphism and patient age at diagnosis. *Neuro Oncol.* **17**, 1231-1240 (2015).

39. R. Batista *et al.*, The prognostic impact of TERT promoter mutations in glioblastomas is modified by the rs2853669 single nucleotide polymorphism. *Int. J. Cancer.* **139**, 414-423 (2016).

40. M. A. Mosrati *et al.*, TERT promoter mutations and polymorphisms as prognostic factors in primary glioblastoma. *Oncotarget.* **6**, 16663-16673 (2015).

41. J. D. Griffith *et al.*, Mammalian telomeres end in a large duplex loop. *Cell.* **97**, 503-514 (1999).

42. C. M. Counter *et al.*, Telomere shortening associated with chromosome instability is arrested in immortal cells which express telomerase activity. *Embo j.* **11**, 1921-1929 (1992).

43. M. A. Blasco *et al.*, Telomere shortening and tumor formation by mouse cells lacking telomerase RNA. *Cell.* **91**, 25-34 (1997).

44. E. H. Blackburn, Switching and signaling at the telomere. *Cell.* **106**, 661-673 (2001).

45. T. de Lange, How telomeres solve the end-protection problem. *Science.* **326**, 948-952 (2009).

46. T. de Lange, How shelterin solves the telomere end-protection problem. *Cold Spring Harb. Symp. Quant. Biol.* **75**, 167-177 (2010).

47. S. Burge, G. N. Parkinson, P. Hazel, A. K. Todd, S. Neidle, Quadruplex DNA: sequence, topology and structure. *Nucleic Acids Res.* **34**, 5402-5415 (2006).

48. A. Sfeir, T. de Lange, Removal of shelterin reveals the telomere end-protection problem. *Science.* **336**, 593-597 (2012).

49. Y. Lu, B. Wei, T. Zhang, Z. Chen, J. Ye, How will telomeric complex be further contributed to our longevity? - the potential novel biomarkers of telomere complex counteracting both aging and cancer. *Protein Cell.* **4**, 573-581 (2013).

50. J. Nandakumar, T. R. Cech, Finding the end: recruitment of telomerase to telomeres. *Nat. Rev. Mol. Cell Biol.* **14**, 69-82 (2013).

51. M. Z. Levy, R. C. Allsopp, A. B. Futcher, C. W. Greider, C. B. Harley, Telomere end-replication problem and cell aging. *J. Mol. Biol.* **225**, 951-960 (1992).

52. J. Campisi, Senescent cells, tumor suppression, and organismal aging: good citizens, bad neighbors. *Cell.* **120**, 513-522 (2005).

53. J. Campisi, The biology of replicative senescence. *Eur. J. Cancer.* **33**, 703-709 (1997).

54. J. Campisi, Aging and cancer: the double-edged sword of replicative senescence. *J. Am. Geriatr. Soc.* **45**, 482-488 (1997).

55. L. HAYFLICK, P. S. MOORHEAD, The serial cultivation of human diploid cell strains. *Exp. Cell Res.* **25**, 585-621 (1961).

56. L. HAYFLICK, The Limited in Vitro Lifetime of Human Diploid Cell Strains. *Exp. Cell Res.* **37**, 614-636 (1965).

57. J. Campisi, F. d'Adda di Fagagna, Cellular senescence: when bad things happen to good cells. *Nat. Rev. Mol. Cell Biol.* **8**, 729-740 (2007).

58. G. I. Evan, K. H. Vousden, Proliferation, cell cycle and apoptosis in cancer. *Nature.* **411**, 342-348 (2001).

59. J. Gil, G. Peters, Regulation of the INK4b-ARF-INK4a tumour suppressor locus: all for one or one for all. *Nat. Rev. Mol. Cell Biol.* **7**, 667-677 (2006).

60. D. T. Eisenberg, An evolutionary review of human telomere biology: the thrifty telomere hypothesis and notes on potential adaptive paternal effects. *Am. J. Hum. Biol.* **23**, 149-167 (2011).

61. S. Kyo, M. Takakura, T. Fujiwara, M. Inoue, Understanding and exploiting hTERT promoter regulation for diagnosis and treatment of human cancers. *Cancer. Sci.* **99**, 1528-1538 (2008).

62. C. W. Greider, E. H. Blackburn, A telomeric sequence in the RNA of Tetrahymena telomerase required for telomere repeat synthesis. *Nature.* **337**, 331-337 (1989).

63. Y. S. Cong, W. E. Wright, J. W. Shay, Human telomerase and its regulation. *Microbiol. Mol. Biol. Rev.* **66**, 407-25, table of contents (2002).

64. G. Sarek, P. Marzec, P. Margalef, S. J. Boulton, Molecular basis of telomere dysfunction in human genetic diseases. *Nat. Struct. Mol. Biol.* **22**, 867-874 (2015).

65. C. A. Theimer, J. Feigon, Structure and function of telomerase RNA. *Curr. Opin. Struct. Biol.* **16**, 307-318 (2006).

66. X. Darzacq *et al.*, Stepwise RNP assembly at the site of H/ACA RNA transcription in human cells. *J. Cell Biol.* **173**, 207-218 (2006).

67. I. Dokal, Fanconi's anaemia and related bone marrow failure syndromes. *Br. Med. Bull.* **77-78**, 37-53 (2006).

68. E. H. Blackburn, K. Collins, Telomerase: an RNP enzyme synthesizes DNA. *Cold Spring Harb Perspect. Biol.* **3**, 10.1101/cshperspect.a003558 (2011).

69. J. Jurczyluk *et al.*, Direct involvement of the TEN domain at the active site of human telomerase. *Nucleic Acids Res.* **39**, 1774-1788 (2011).

70. A. R. Robart, K. Collins, Human telomerase domain interactions capture DNA for TEN domain-dependent processive elongation. *Mol. Cell.* **42**, 308-318 (2011).

71. R. A. Wu, K. Collins, Sequence specificity of human telomerase. *Proc. Natl. Acad. Sci. U. S. A.* **111**, 11234-11235 (2014).

72. C. K. Lai, J. R. Mitchell, K. Collins, RNA binding domain of telomerase reverse transcriptase. *Mol. Cell. Biol.* **21**, 990-1000 (2001).

73. J. Lingner *et al.*, Reverse transcriptase motifs in the catalytic subunit of telomerase. *Science.* **276**, 561-567 (1997).

74. C. K. Garcia, W. E. Wright, J. W. Shay, Human diseases of telomerase dysfunction: insights into tissue aging. *Nucleic Acids Res.* **35**, 7406-7416 (2007).

75. A. Ghosh *et al.*, Telomerase directly regulates NF-kappaB-dependent transcription. *Nat. Cell Biol.* **14**, 1270-1281 (2012).

76. L. Yin, A. K. Hubbard, C. Giardina, NF-kappa B regulates transcription of the mouse telomerase catalytic subunit. *J. Biol. Chem.* **275**, 36671-36675 (2000).

77. Y. Zhang, L. Toh, P. Lau, X. Wang, Human telomerase reverse transcriptase (hTERT) is a novel target of the Wnt/beta-catenin pathway in human cancer. *J. Biol. Chem.* **287**, 32494-32511 (2012).

78. S. Mukherjee, E. J. Firpo, Y. Wang, J. M. Roberts, Separation of telomerase functions by reverse genetics. *Proc. Natl. Acad. Sci. U. S. A.* **108**, E1363-71 (2011).

79. Y. Li, V. Tergaonkar, Noncanonical functions of telomerase: implications in telomerase-targeted cancer therapies. *Cancer Res.* **74**, 1639-1644 (2014).

80. B. Heidenreich, P. S. Rachakonda, K. Hemminki, R. Kumar, TERT promoter mutations in cancer development. *Curr. Opin. Genet. Dev.* **24**, 30-37 (2014).

81. M. Akiyama *et al.*, Nuclear factor-kappaB p65 mediates tumor necrosis factor alpha-induced nuclear translocation of telomerase reverse transcriptase protein. *Cancer Res.* **63**, 18-21 (2003).

82. R. Catlett-Falcone *et al.*, Constitutive activation of Stat3 signaling confers resistance to apoptosis in human U266 myeloma cells. *Immunity.* **10**, 105-115 (1999).

83. J. Bollrath *et al.*, gp130-mediated Stat3 activation in enterocytes regulates cell survival and cell-cycle progression during colitis-associated tumorigenesis. *Cancer. Cell.* **15**, 91-102 (2009).

84. S. Grivennikov *et al.*, IL-6 and Stat3 are required for survival of intestinal epithelial cells and development of colitis-associated cancer. *Cancer. Cell.* **15**, 103-113 (2009).

85. S. S. Chung, C. Aroh, J. V. Vadgama, Constitutive activation of STAT3 signaling regulates hTERT and promotes stem cell-like traits in human breast cancer cells. *PLoS One.* **8**, e83971 (2013).

86. L. Konnikova, M. C. Simeone, M. M. Kruger, M. Kotecki, B. H. Cochran, Signal transducer and activator of transcription 3 (STAT3) regulates human telomerase reverse transcriptase (hTERT) expression in human cancer and primary cells. *Cancer Res.* **65**, 6516-6520 (2005).

87. L. Konnikova, M. Kotecki, M. M. Kruger, B. H. Cochran, Knockdown of STAT3 expression by RNAi induces apoptosis in astrocytoma cells. *BMC Cancer.* **3**, 23 (2003).

88. Y. S. Cong, J. Wen, S. Bacchetti, The human telomerase catalytic subunit hTERT: organization of the gene and characterization of the promoter. *Hum. Mol. Genet.* **8**, 137-142 (1999).

89. E. Gonzalez-Suarez, J. M. Flores, M. A. Blasco, Cooperation between p53 mutation and high telomerase transgenic expression in spontaneous cancer development. *Mol. Cell. Biol.* **22**, 7291-7301 (2002).

90. K. J. Wu *et al.*, Direct activation of TERT transcription by c-MYC. *Nat. Genet.* **21**, 220-224 (1999).

91. H. Li, T. H. Lee, H. Avraham, A novel tricomplex of BRCA1, Nmi, and c-Myc inhibits c-Myc-induced human telomerase reverse transcriptase gene (hTERT) promoter activity in breast cancer. *J. Biol. Chem.* **277**, 20965-20973 (2002).

92. A. Cerezo, H. Kalthoff, M. Schuermann, B. Schafer, P. Boukamp, Dual regulation of telomerase activity through c-Myc-dependent inhibition and alternative splicing of hTERT. *J. Cell. Sci.* **115**, 1305-1312 (2002).

93. J. W. Shay, Y. Zou, E. Hiyama, W. E. Wright, Telomerase and cancer. *Hum. Mol. Genet.* **10**, 677-685 (2001).

94. J. W. Shay, S. Bacchetti, A survey of telomerase activity in human cancer. *Eur. J. Cancer.* **33**, 787-791 (1997).

95. K. C. Low, V. Tergaonkar, Telomerase: central regulator of all of the hallmarks of cancer. *Trends Biochem. Sci.* **38**, 426-434 (2013).

96. W. C. Hahn, M. Meyerson, Telomerase activation, cellular immortalization and cancer. *Ann. Med.* **33**, 123-129 (2001).

97. J. Zhu, Y. Zhao, S. Wang, Chromatin and epigenetic regulation of the telomerase reverse transcriptase gene. *Protein Cell.* **1**, 22-32 (2010).

98. R. M. Marion, M. A. Blasco, Telomere rejuvenation during nuclear reprogramming. *Curr. Opin. Genet. Dev.* **20**, 190-196 (2010).

99. K. Masutomi *et al.*, Telomerase maintains telomere structure in normal human cells. *Cell.* **114**, 241-253 (2003).

100. P. J. Killela *et al.*, TERT promoter mutations occur frequently in gliomas and a subset of tumors derived from cells with low rates of self-renewal. *Proc. Natl. Acad. Sci. U. S. A.* **110**, 6021-6026 (2013).

101. S. Horn *et al.*, TERT promoter mutations in familial and sporadic melanoma. *Science.* **339**, 959-961 (2013).

102. D. S. Huang *et al.*, Recurrent TERT promoter mutations identified in a large-scale study of multiple tumour types are associated with increased TERT expression and telomerase activation. *Eur. J. Cancer.* **51**, 969-976 (2015).

103. R. J. Bell *et al.*, Cancer. The transcription factor GABP selectively binds and activates the mutant TERT promoter in cancer. *Science.* **348**, 1036-1039 (2015).

104. M. M. Makowski *et al.*, An interaction proteomics survey of transcription factor binding at recurrent TERT promoter mutations. *Proteomics.* **16**, 417-426 (2016).

105. Y. Li *et al.*, Non-canonical NF-kappaB signalling and ETS1/2 cooperatively drive C250T mutant TERT promoter activation. *Nat. Cell Biol.* **17**, 1327-1338 (2015).

106. Deutsches Krebsforschungszentrum *https://www.nct-heidelberg.de/forschung/nct-clinical-and-translational-research-programs-groups/cancer-prevention-early-detection-and-outcomes/molecular-genetic-epidemiology-hermminiki.html* download: 07/**2016**

107. E. Hodis *et al.*, A landscape of driver mutations in melanoma. *Cell.* **150**, 251-263 (2012).

108. M. Uhlen *et al.*, Towards a knowledge-based Human Protein Atlas. *Nat. Biotechnol.* **28**, 1248-1250 (2010).

109. P. C. Burger *et al.*, Small cell architecture--a histological equivalent of EGFR amplification in glioblastoma multiforme? *J. Neuropathol. Exp. Neurol.* **60**, 1099-1104 (2001).

110. H. Ohgaki, P. Kleihues, Genetic pathways to primary and secondary glioblastoma. *Am. J. Pathol.* **170**, 1445-1453 (2007).

111. A. J. Ekstrand *et al.*, Genes for epidermal growth factor receptor, transforming growth factor alpha, and epidermal growth factor and their expression in human gliomas in vivo. *Cancer Res.* **51**, 2164-2172 (1991).

112. F. Azuaje, K. Tiemann, S. P. Niclou, Therapeutic control and resistance of the EGFR-driven signaling network in glioblastoma. *Cell. Commun. Signal.* **13**, 23-015-0098-6 (2015).

113. M. A. Lemmon, J. Schlessinger, K. M. Ferguson, The EGFR family: not so prototypical receptor tyrosine kinases. *Cold Spring Harb Perspect. Biol.* **6**, a020768 (2014).

114. X. Zhang, J. Gureasko, K. Shen, P. A. Cole, J. Kuriyan, An allosteric mechanism for activation of the kinase domain of epidermal growth factor receptor. *Cell.* **125**, 1137-1149 (2006).

115. T. Pawson, Specificity in signal transduction: from phosphotyrosine-SH2 domain interactions to complex cellular systems. *Cell.* **116**, 191-203 (2004).

116. M. A. Lemmon, J. Schlessinger, Cell signaling by receptor tyrosine kinases. *Cell.* **141**, 1117-1134 (2010).

117. G. F. Xu *et al.*, The catalytic domain of the neurofibromatosis type 1 gene product stimulates ras GTPase and complements ira mutants of S. cerevisiae. *Cell.* **63**, 835-841 (1990).

118. A. F. Ward, B. S. Braun, K. M. Shannon, Targeting oncogenic Ras signaling in hematologic malignancies. *Blood.* **120**, 3397-3406 (2012).

119. R. Sen, D. Baltimore, Multiple nuclear factors interact with the immunoglobulin enhancer sequences. *Cell.* **46**, 705-716 (1986).

120. R. M. Waterhouse *et al.*, Evolutionary dynamics of immune-related genes and pathways in disease-vector mosquitoes. *Science.* **316**, 1738-1743 (2007).

121. S. Ghosh, M. J. May, E. B. Kopp, NF-kappa B and Rel proteins: evolutionarily conserved mediators of immune responses. *Annu. Rev. Immunol.* **16**, 225-260 (1998).

122. B. Tian, D. E. Nowak, A. R. Brasier, A TNF-induced gene expression program under oscillatory NF-kappaB control. *BMC Genomics.* **6**, 137 (2005).

123. B. Tian, D. E. Nowak, M. Jamaluddin, S. Wang, A. R. Brasier, Identification of direct genomic targets downstream of the nuclear factor-kappaB transcription factor mediating tumor necrosis factor signaling. *J. Biol. Chem.* **280**, 17435-17448 (2005).

124. H. L. Pahl, Activators and target genes of Rel/NF-kappaB transcription factors. *Oncogene.* **18**, 6853-6866 (1999).

125. M. Karin, Y. Ben-Neriah, Phosphorylation meets ubiquitination: the control of NF-[kappa]B activity. *Annu. Rev. Immunol.* **18**, 621-663 (2000).

126. A. S. Baldwin Jr, The NF-kappa B and I kappa B proteins: new discoveries and insights. *Annu. Rev. Immunol.* **14**, 649-683 (1996).

127. T. D. Gilmore, NF-kappa B, KBF1, dorsal, and related matters. *Cell.* **62**, 841-843 (1990).

128. H. Zhong, M. J. May, E. Jimi, S. Ghosh, The phosphorylation status of nuclear NF-kappa B determines its association with CBP/p300 or HDAC-1. *Mol. Cell.* **9**, 625-636 (2002).

129. P. Dobrzanski, R. P. Ryseck, R. Bravo, Both N- and C-terminal domains of RelB are required for full transactivation: role of the N-terminal leucine zipper-like motif. *Mol. Cell. Biol.* **13**, 1572-1582 (1993).

130. A. Oeckinghaus, S. Ghosh, The NF-kappaB family of transcription factors and its regulation. *Cold Spring Harb Perspect. Biol.* **1**, a000034 (2009).

131. M. Karin, The beginning of the end: IkappaB kinase (IKK) and NF-kappaB activation. *J. Biol. Chem.* **274**, 27339-27342 (1999).

132. U. Senftleben *et al.*, Activation by IKKalpha of a second, evolutionary conserved, NF-kappa B signaling pathway. *Science.* **293**, 1495-1499 (2001).

133. S. Ghosh, M. Karin, Missing pieces in the NF-kappaB puzzle. *Cell.* **109 Suppl**, S81-96 (2002).

134. S. Akira, S. Uematsu, O. Takeuchi, Pathogen recognition and innate immunity. *Cell.* **124**, 783-801 (2006).

135. S. Akira, K. Takeda, Toll-like receptor signalling. *Nat. Rev. Immunol.* **4**, 499-511 (2004).

136. L. A. O'Neill, A. G. Bowie, The family of five: TIR-domain-containing adaptors in Toll-like receptor signalling. *Nat. Rev. Immunol.* **7**, 353-364 (2007).

137. R. Schauvliege, S. Janssens, R. Beyaert, Pellino proteins: novel players in TLR and IL-1R signalling. *J. Cell. Mol. Med.* **11**, 453-461 (2007).

138. E. Zandi, D. M. Rothwarf, M. Delhase, M. Hayakawa, M. Karin, The IkappaB kinase complex (IKK) contains two kinase subunits, IKKalpha and IKKbeta, necessary for IkappaB phosphorylation and NF-kappaB activation. *Cell.* **91**, 243-252 (1997).

139. P. Viatour, M. P. Merville, V. Bours, A. Chariot, Phosphorylation of NF-kappaB and IkappaB proteins: implications in cancer and inflammation. *Trends Biochem. Sci.* **30**, 43-52 (2005).

140. N. D. Perkins, Integrating cell-signalling pathways with NF-kappaB and IKK function. *Nat. Rev. Mol. Cell Biol.* **8**, 49-62 (2007).

141. A. R. Brasier, The NF-kappaB regulatory network. *Cardiovasc. Toxicol.* **6**, 111-130 (2006).

142. R. F. Schwabe, D. A. Brenner, Role of glycogen synthase kinase-3 in TNF-alpha-induced NF-kappaB activation and apoptosis in hepatocytes. *Am. J. Physiol. Gastrointest. Liver Physiol.* **283**, G204-11 (2002).

143. F. Fujita *et al.*, Identification of NAP1, a regulatory subunit of IkappaB kinase-related kinases that potentiates NF-kappaB signaling. *Mol. Cell. Biol.* **23**, 7780-7793 (2003).

144. H. Buss *et al.*, Constitutive and interleukin-1-inducible phosphorylation of p65 NF-{kappa}B at serine 536 is mediated by multiple protein kinases including I{kappa}B kinase (IKK)-{alpha}, IKK{beta}, IKK{epsilon}, TRAF family member-associated (TANK)-binding kinase 1 (TBK1), and

an unknown kinase and couples p65 to TATA-binding protein-associated factor II31-mediated interleukin-8 transcription. *J. Biol. Chem.* **279**, 55633-55643 (2004).

145. Y. Lee, J. K. Lee, S. H. Ahn, J. Lee, D. H. Nam, WNT signaling in glioblastoma and therapeutic opportunities. *Lab. Invest.* **96**, 137-150 (2016).

146. R. Nusse, H. E. Varmus, Many tumors induced by the mouse mammary tumor virus contain a provirus integrated in the same region of the host genome. *Cell.* **31**, 99-109 (1982).

147. M. V. Semenov, R. Habas, B. T. Macdonald, X. He, SnapShot: Noncanonical Wnt Signaling Pathways. *Cell.* **131**, 1378 (2007).

148. J. L. Stamos, W. I. Weis, The beta-catenin destruction complex. *Cold Spring Harb Perspect. Biol.* **5**, a007898 (2013).

149. M. B. Major *et al.*, Wilms tumor suppressor WTX negatively regulates WNT/beta-catenin signaling. *Science.* **316**, 1043-1046 (2007).

150. M. Hart *et al.*, The F-box protein beta-TrCP associates with phosphorylated beta-catenin and regulates its activity in the cell. *Curr. Biol.* **9**, 207-210 (1999).

151. J. Behrens *et al.*, Functional interaction of beta-catenin with the transcription factor LEF-1. *Nature.* **382**, 638-642 (1996).

152. M. Molenaar *et al.*, XTcf-3 transcription factor mediates beta-catenin-induced axis formation in Xenopus embryos. *Cell.* **86**, 391-399 (1996).

153. G. R. Sareddy, M. Panigrahi, S. Challa, A. Mahadevan, P. P. Babu, Activation of Wnt/beta-catenin/Tcf signaling pathway in human astrocytomas. *Neurochem. Int.* **55**, 307-317 (2009).

154. C. Liu *et al.*, Wnt/beta-Catenin pathway in human glioma: expression pattern and clinical/prognostic correlations. *Clin. Exp. Med.* **11**, 105-112 (2011).

155. B. Rubinfeld, B. Souza, I. Albert, S. Munemitsu, P. Polakis, The APC protein and E-cadherin form similar but independent complexes with alpha-catenin, beta-catenin, and plakoglobin. *J. Biol. Chem.* **270**, 5549-5555 (1995).

156. A. Kikuchi, Tumor formation by genetic mutations in the components of the Wnt signaling pathway. *Cancer. Sci.* **94**, 225-229 (2003).

157. H. Zheng *et al.*, PLAGL2 regulates Wnt signaling to impede differentiation in neural stem cells and gliomas. *Cancer. Cell.* **17**, 497-509 (2010).

158. R. Sekiya *et al.*, PLAGL2 regulates actin cytoskeletal architecture and cell migration. *Carcinogenesis.* **35**, 1993-2001 (2014).

159. N. Zhang *et al.*, FoxM1 promotes beta-catenin nuclear localization and controls Wnt target-gene expression and glioma tumorigenesis. *Cancer. Cell.* **20**, 427-442 (2011).

160. X. Jin *et al.*, Frizzled 4 regulates stemness and invasiveness of migrating glioma cells established by serial intracranial transplantation. *Cancer Res.* **71**, 3066-3075 (2011).

161. D. S. Aaronson, C. M. Horvath, A road map for those who don't know JAK-STAT. *Science.* **296**, 1653-1655 (2002).

162. C. Schindler, D. E. Levy, T. Decker, JAK-STAT signaling: from interferons to cytokines. *J. Biol. Chem.* **282**, 20059-20063 (2007).

163. A. Ziemiecki, A. G. Harpur, A. F. Wilks, JAK protein tyrosine kinases: their role in cytokine signalling. *Trends Cell Biol.* **4**, 207-212 (1994).

164. J. E. Darnell Jr, I. M. Kerr, G. R. Stark, Jak-STAT pathways and transcriptional activation in response to IFNs and other extracellular signaling proteins. *Science.* **264**, 1415-1421 (1994).

165. J. E. Darnell Jr, Phosphotyrosine signaling and the single cell:metazoan boundary. *Proc. Natl. Acad. Sci. U. S. A.* **94**, 11767-11769 (1997).

166. H. Yu, R. Jove, The STATs of cancer--new molecular targets come of age. *Nat. Rev. Cancer.* **4**, 97-105 (2004).

167. K. Takeda, S. Akira, STAT family of transcription factors in cytokine-mediated biological responses. *Cytokine Growth Factor Rev.* **11**, 199-207 (2000).

168. R. Buettner, L. B. Mora, R. Jove, Activated STAT signaling in human tumors provides novel molecular targets for therapeutic intervention. *Clin. Cancer Res.* **8**, 945-954 (2002).

169. H. Yu, R. Jove, The STATs of cancer--new molecular targets come of age. *Nat. Rev. Cancer.* **4**, 97-105 (2004).

170. E. B. Haura, J. Turkson, R. Jove, Mechanisms of disease: Insights into the emerging role of signal transducers and activators of transcription in cancer. *Nat. Clin. Pract. Oncol.* **2**, 315-324 (2005).

171. H. Yu, D. Pardoll, R. Jove, STATs in cancer inflammation and immunity: a leading role for STAT3. *Nat. Rev. Cancer.* **9**, 798-809 (2009).

172. A. Yoshimura, T. Naka, M. Kubo, SOCS proteins, cytokine signalling and immune regulation. *Nat. Rev. Immunol.* **7**, 454-465 (2007).

173. T. Hirano, K. Ishihara, M. Hibi, Roles of STAT3 in mediating the cell growth, differentiation and survival signals relayed through the IL-6 family of cytokine receptors. *Oncogene.* **19**, 2548-2556 (2000).

174. F. Balkwill, A. Mantovani, Inflammation and cancer: back to Virchow? *Lancet.* **357**, 539-545 (2001).

175. A. Mantovani, C. Garlanda, P. Allavena, Molecular pathways and targets in cancer-related inflammation. *Ann. Med.* **42**, 161-170 (2010).

176. P. A. Thompson *et al.*, Environmental immune disruptors, inflammation and cancer risk. *Carcinogenesis.* **36 Suppl 1**, S232-53 (2015).

177. L. Vannucci *et al.*, Colorectal carcinoma: Importance of colonic environment for anti-cancer response and systemic immunity. *J. Immunotoxicol.* **6**, 217-226 (2009).

178. P. M. Rothwell *et al.*, Effect of daily aspirin on long-term risk of death due to cancer: analysis of individual patient data from randomised trials. *Lancet.* **377**, 31-41 (2011).

179. H. F. Dvorak, Tumors: wounds that do not heal-redux. *Cancer. Immunol. Res.* **3**, 1-11 (2015).

180. R. Noy, J. W. Pollard, Tumor-associated macrophages: from mechanisms to therapy. *Immunity.* **41**, 49-61 (2014).

181. P. J. Murray, T. A. Wynn, Protective and pathogenic functions of macrophage subsets. *Nat. Rev. Immunol.* **11**, 723-737 (2011).

182. A. Mantovani, P. Allavena, A. Sica, F. Balkwill, Cancer-related inflammation. *Nature.* **454**, 436-444 (2008).

183. B. Ruffell *et al.*, Leukocyte composition of human breast cancer. *Proc. Natl. Acad. Sci. U. S. A.* **109**, 2796-2801 (2012).

184. B. Z. Qian, J. W. Pollard, Macrophage diversity enhances tumor progression and metastasis. *Cell.* **141**, 39-51 (2010).

185. R. Ostuni, F. Kratochvill, P. J. Murray, G. Natoli, Macrophages and cancer: from mechanisms to therapeutic implications. *Trends Immunol.* **36**, 229-239 (2015).

186. G. K. Gray, B. C. McFarland, S. E. Nozell, E. N. Benveniste, NF-kappaB and STAT3 in glioblastoma: therapeutic targets coming of age. *Expert Rev. Neurother.* **14**, 1293-1306 (2014).

187. S. I. Grivennikov, F. R. Greten, M. Karin, Immunity, inflammation, and cancer. *Cell.* **140**, 883-899 (2010).

188. S. Schwitalla *et al.*, Intestinal tumorigenesis initiated by dedifferentiation and acquisition of stem-cell-like properties. *Cell.* **152**, 25-38 (2013).

189. L. S. Ojalvo, W. King, D. Cox, J. W. Pollard, High-density gene expression analysis of tumor-associated macrophages from mouse mammary tumors. *Am. J. Pathol.* **174**, 1048-1064 (2009).

190. S. K. Biswas, A. Mantovani, Macrophage plasticity and interaction with lymphocyte subsets: cancer as a paradigm. *Nat. Immunol.* **11**, 889-896 (2010).

191. D. G. DeNardo *et al.*, CD4(+) T cells regulate pulmonary metastasis of mammary carcinomas by enhancing protumor properties of macrophages. *Cancer. Cell.* **16**, 91-102 (2009).

192. M. Torroella-Kouri *et al.*, Identification of a subpopulation of macrophages in mammary tumor-bearing mice that are neither M1 nor M2 and are less differentiated. *Cancer Res.* **69**, 4800-4809 (2009).

193. W. Zou, N. P. Restifo, T(H)17 cells in tumour immunity and immunotherapy. *Nat. Rev. Immunol.* **10**, 248-256 (2010).

194. S. K. Biswas *et al.*, A distinct and unique transcriptional program expressed by tumor-associated macrophages (defective NF-kappaB and enhanced IRF-3/STAT1 activation). *Blood.* **107**, 2112-2122 (2006).

195. B. Ruffell *et al.*, Macrophage IL-10 blocks CD8+ T cell-dependent responses to chemotherapy by suppressing IL-12 expression in intratumoral dendritic cells. *Cancer. Cell.* **26**, 623-637 (2014).

196. A. L. Doedens *et al.*, Macrophage expression of hypoxia-inducible factor-1 alpha suppresses T-cell function and promotes tumor progression. *Cancer Res.* **70**, 7465-7475 (2010).

197. B. Molon *et al.*, Chemokine nitration prevents intratumoral infiltration of antigen-specific T cells. *J. Exp. Med.* **208**, 1949-1962 (2011).

198. L. J. Hofseth *et al.*, Nitric oxide-induced cellular stress and p53 activation in chronic inflammation. *Proc. Natl. Acad. Sci. U. S. A.* **100**, 143-148 (2003).

199. T. Lu *et al.*, Tumor-infiltrating myeloid cells induce tumor cell resistance to cytotoxic T cells in mice. *J. Clin. Invest.* **121**, 4015-4029 (2011).

200. S. Fu *et al.*, TGF-beta induces Foxp3 + T-regulatory cells from CD4 + CD25 - precursors. *Am. J. Transplant.* **4**, 1614-1627 (2004).

201. Z. Li *et al.*, PD-L1 Expression Is Associated with Tumor FOXP3(+) Regulatory T-Cell Infiltration of Breast Cancer and Poor Prognosis of Patient. *J. Cancer.* **7**, 784-793 (2016).

202. L. M. Francisco *et al.*, PD-L1 regulates the development, maintenance, and function of induced regulatory T cells. *J. Exp. Med.* **206**, 3015-3029 (2009).

203. B. Malissen, P. Bongrand, Early T cell activation: integrating biochemical, structural, and biophysical cues. *Annu. Rev. Immunol.* **33**, 539-561 (2015).

204. A. H. Sharpe, E. J. Wherry, R. Ahmed, G. J. Freeman, The function of programmed cell death 1 and its ligands in regulating autoimmunity and infection. *Nat. Immunol.* **8**, 239-245 (2007).

205. M. Collins, V. Ling, B. M. Carreno, The B7 family of immune-regulatory ligands. *Genome Biol.* **6**, 223 (2005).

206. C. J. Nirschl, C. G. Drake, Molecular pathways: coexpression of immune checkpoint molecules: signaling pathways and implications for cancer immunotherapy. *Clin. Cancer Res.* **19**, 4917-4924 (2013).

207. O. Bloch *et al.*, Gliomas promote immunosuppression through induction of B7-H1 expression in tumor-associated macrophages. *Clin. Cancer Res.* **19**, 3165-3175 (2013).

208. A. T. Parsa *et al.*, Loss of tumor suppressor PTEN function increases B7-H1 expression and immunoresistance in glioma. *Nat. Med.* **13**, 84-88 (2007).

209. S. P. Patel, R. Kurzrock, PD-L1 Expression as a Predictive Biomarker in Cancer Immunotherapy. *Mol. Cancer. Ther.* **14**, 847-856 (2015).

210. P. Wu, D. Wu, L. Li, Y. Chai, J. Huang, PD-L1 and Survival in Solid Tumors: A Meta-Analysis. *PLoS One.* **10**, e0131403 (2015).

211. X. Meng, Z. Huang, F. Teng, L. Xing, J. Yu, Predictive biomarkers in PD-1/PD-L1 checkpoint blockade immunotherapy. *Cancer Treat. Rev.* **41**, 868-876 (2015).

212. Z. Chen, B. D. Trapp, Microglia and neuroprotection. *J. Neurochem.* **136 Suppl 1**, 10-17 (2016).

213. M. J. Carson, J. C. Thrash, B. Walter, The cellular response in neuroinflammation: The role of leukocytes, microglia and astrocytes in neuronal death and survival. *Clin. Neurosci. Res.* **6**, 237-245 (2006).

214. B. Engelhardt, Molecular mechanisms involved in T cell migration across the blood-brain barrier. *J. Neural Transm. (Vienna).* **113**, 477-485 (2006).

215. G. Driessens, J. Kline, T. F. Gajewski, Costimulatory and coinhibitory receptors in anti-tumor immunity. *Immunol. Rev.* **229**, 126-144 (2009).

216. D. S. Chen, I. Mellman, Oncology meets immunology: the cancer-immunity cycle. *Immunity.* **39**, 1-10 (2013).

217. M. Preusser, M. Lim, D. A. Hafler, D. A. Reardon, J. H. Sampson, Prospects of immune checkpoint modulators in the treatment of glioblastoma. *Nat. Rev. Neurol.* **11**, 504-514 (2015).

218. M. Weller *et al.*, EANO guideline for the diagnosis and treatment of anaplastic gliomas and glioblastoma. *Lancet Oncol.* **15**, e395-403 (2014).

219. F. Bokstein *et al.*, Stereotactic radiosurgery (SRS) in high-grade glioma: judicious selection of small target volumes improves results. *J. Neurooncol.* **126**, 551-557 (2016).

220. A. Quick, D. Patel, M. Hadziahmetovic, A. Chakravarti, M. Mehta, Current therapeutic paradigms in glioblastoma. *Rev. Recent. Clin. Trials.* **5**, 14-27 (2010).

221. C. Herbert *et al.*, Treatment of glioblastoma multiforme with radiotherapy and concomitant and adjuvant temozolomide: translation of randomised controlled trial evidence into routine clinical practice. *Clin. Oncol. (R. Coll. Radiol).* **23**, 372-373 (2011).

222. J. Clarke, N. Butowski, S. Chang, Recent advances in therapy for glioblastoma. *Arch. Neurol.* **67**, 279-283 (2010).

223. R. Stupp, J. C. Tonn, M. Brada, G. Pentheroudakis, ESMO Guidelines Working Group, High-grade malignant glioma: ESMO Clinical Practice Guidelines for diagnosis, treatment and follow-up. *Ann. Oncol.* **21 Suppl 5**, v190-3 (2010).

224. S. Ryu *et al.*, The role of radiotherapy in the management of progressive glioblastoma : a systematic review and evidence-based clinical practice guideline. *J. Neurooncol.* **118**, 489-499 (2014).

225. W. Wick *et al.*, MGMT testing--the challenges for biomarker-based glioma treatment. *Nat. Rev. Neurol.* **10**, 372-385 (2014).

226. M. R. Gilbert *et al.*, A randomized trial of bevacizumab for newly diagnosed glioblastoma. *N. Engl. J. Med.* **370**, 699-708 (2014).

227. J. L. Munoz *et al.*, Temozolomide resistance in glioblastoma cells occurs partly through epidermal growth factor receptor-mediated induction of connexin 43. *Cell. Death Dis.* **5**, e1145 (2014).

228. G. Perazzoli *et al.*, Temozolomide Resistance in Glioblastoma Cell Lines: Implication of MGMT, MMR, P-Glycoprotein and CD133 Expression. *PLoS One.* **10**, e0140131 (2015).

229. S. Kohsaka *et al.*, STAT3 inhibition overcomes temozolomide resistance in glioblastoma by downregulating MGMT expression. *Mol. Cancer. Ther.* **11**, 1289-1299 (2012).

230. C. Alifieris, D. T. Trafalis, Glioblastoma multiforme: Pathogenesis and treatment. *Pharmacol. Ther.* **152**, 63-82 (2015).

231. F. Atif, N. R. Patel, S. Yousuf, D. G. Stein, The Synergistic Effect of Combination Progesterone and Temozolomide on Human Glioblastoma Cells. *PLoS One.* **10**, e0131441 (2015).

232. M. Schuster, A. Nechansky, R. Kircheis, Cancer immunotherapy. *Biotechnol. J.* **1**, 138-147 (2006).

233. L. Yang, G. Guo, X. Y. Niu, J. Liu, Dendritic Cell-Based Immunotherapy Treatment for Glioblastoma Multiforme. *Biomed. Res. Int.* **2015**, 717530 (2015).

234. A. M. Sonabend, G. M. McKhann, Boosting Dendritic Cell Vaccination for Glioblastoma Using Tetanus Toxoid. *Neurosurgery.* **77**, N20-1 (2015).

235. T. Weiss, M. Weller, P. Roth, Immunotherapy for glioblastoma: concepts and challenges. *Curr. Opin. Neurol.* **28**, 639-646 (2015).

236. J. H. Sampson, D. A. Mitchell, Vaccination strategies for neuro-oncology. *Neuro Oncol.* **17 Suppl 7**, vii15-vii25 (2015).

237. J. P. Antonios *et al.*, PD-1 blockade enhances the vaccination-induced immune response in glioma. *JCI Insight.* **1**, e87059 (2016).

238. C. Jackson, J. Ruzevick, H. Brem, M. Lim, Vaccine strategies for glioblastoma: progress and future directions. *Immunotherapy.* **5**, 155-167 (2013).

239. A. S. Berghoff *et al.*, Programmed death ligand 1 expression and tumor-infiltrating lymphocytes in glioblastoma. *Neuro Oncol.* **17**, 1064-1075 (2015).

240. A. M. Dunn-Pirio, G. Vlahovic, Immunotherapy approaches in the treatment of malignant brain tumors. *Cancer.*(2016).

241. R. J. Motzer *et al.*, Nivolumab for Metastatic Renal Cell Carcinoma: Results of a Randomized Phase II Trial. *J. Clin. Oncol.* **33**, 1430-1437 (2015).

242. C. Karimkhani, R. Gonzalez, R. P. Dellavalle, A review of novel therapies for melanoma. *Am. J. Clin. Dermatol.* **15**, 323-337 (2014).

243. S. Carrel, N. de Tribolet, J. P. Mach, Expression of neuroectodermal antigens common to melanomas, gliomas, and neuroblastomas. I. Identification by monoclonal anti-melanoma and anti-glioma antibodies. *Acta Neuropathol.* **57**, 158-164 (1982).

244. C. H. Ries *et al.*, Targeting tumor-associated macrophages with anti-CSF-1R antibody reveals a strategy for cancer therapy. *Cancer. Cell.* **25**, 846-859 (2014).

245. S. M. Pyonteck *et al.*, CSF-1R inhibition alters macrophage polarization and blocks glioma progression. *Nat. Med.* **19**, 1264-1272 (2013).

246. M. J. van den Bent *et al.*, Randomized phase II trial of erlotinib versus temozolomide or carmustine in recurrent glioblastoma: EORTC brain tumor group study 26034. *J. Clin. Oncol.* **27**, 1268-1274 (2009).

247. J. J. Raizer *et al.*, A phase II trial of erlotinib in patients with recurrent malignant gliomas and nonprogressive glioblastoma multiforme postradiation therapy. *Neuro Oncol.* **12**, 95-103 (2010).

248. J. N. Rich *et al.*, Phase II trial of gefitinib in recurrent glioblastoma. *J. Clin. Oncol.* **22**, 133-142 (2004).

249. B. Thiessen *et al.*, A phase I/II trial of GW572016 (lapatinib) in recurrent glioblastoma multiforme: clinical outcomes, pharmacokinetics and molecular correlation. *Cancer Chemother. Pharmacol.* **65**, 353-361 (2010).

250. V. Vanaclocha *et al.*, Photodynamic therapy in the treatment of brain tumours. A feasibility study. *Photodiagnosis Photodyn Ther.* **12**, 422-427 (2015).

251. E. C. Burton, M. D. Prados, Malignant gliomas. *Curr. Treat. Options Oncol.* **1**, 459-468 (2000).

252. A. Giese, M. Westphal, Glioma invasion in the central nervous system. *Neurosurgery.* **39**, 235-50; discussion 250-2 (1996).

253. L. Nogueira *et al.*, Blockade of the NFkappaB pathway drives differentiating glioblastoma-initiating cells into senescence both in vitro and in vivo. *Oncogene.* **30**, 3537-3548 (2011).

254. L. Nogueira, P. Ruiz-Ontanon, A. Vazquez-Barquero, F. Moris, J. L. Fernandez-Luna, The NFkappaB pathway: a therapeutic target in glioblastoma. *Oncotarget.* **2**, 646-653 (2011).

255. S. Choi *et al.*, Nuclear factor-kappaB activated by capacitative Ca2+ entry enhances muscarinic receptor-mediated soluble amyloid precursor protein (sAPPalpha) release in SH-SY5Y cells. *J. Biol. Chem.* **281**, 12722-12728 (2006).

256. J. Wu *et al.*, Neuronal store-operated calcium entry pathway as a novel therapeutic target for Huntington's disease treatment. *Chem. Biol.* **18**, 777-793 (2011).

257. E. D. Nekrasov *et al.*, Manifestation of Huntington's disease pathology in human induced pluripotent stem cell-derived neurons. *Mol. Neurodegener.* **11**, 27-016-0092-5 (2016).

258. V. Vigont *et al.*, Both Orai1 and TRPC1 are Involved in Excessive Store-Operated Calcium Entry in Striatal Neurons Expressing Mutant Huntingtin Exon 1. *Front. Physiol.* **6**, 337 (2015).

259. T. D. Gilmore, The Rel/NF-kappaB signal transduction pathway: introduction. *Oncogene.* **18**, 6842-6844 (1999).

260. M. Karin, The beginning of the end: IkappaB kinase (IKK) and NF-kappaB activation. *J. Biol. Chem.* **274**, 27339-27342 (1999).

261. J. W. Pierce *et al.*, Novel inhibitors of cytokine-induced IkappaBalpha phosphorylation and endothelial cell adhesion molecule expression show anti-inflammatory effects in vivo. *J. Biol. Chem.* **272**, 21096-21103 (1997).

262. J. Schust, B. Sperl, A. Hollis, T. U. Mayer, T. Berg, Stattic: a small-molecule inhibitor of STAT3 activation and dimerization. *Chem. Biol.* **13**, 1235-1242 (2006).

263. J. S. McMurray, A new small-molecule Stat3 inhibitor. *Chem. Biol.* **13**, 1123-1124 (2006).

264. H. L. Grabenstatter *et al.*, The effect of STAT3 inhibition on status epilepticus and subsequent spontaneous seizures in the pilocarpine model of acquired epilepsy. *Neurobiol. Dis.* **62**, 73-85 (2014).

265. J. M. Daniel *et al.*, Inhibition of STAT3 signaling prevents vascular smooth muscle cell proliferation and neointima formation. *Basic Res. Cardiol.* **107**, 261-012-0261-9. Epub 2012 Mar 15 (2012).

266. A. Ferrajoli *et al.*, WP1066 disrupts Janus kinase-2 and induces caspase-dependent apoptosis in acute myelogenous leukemia cells. *Cancer Res.* **67**, 11291-11299 (2007).

267. A. Iwamaru *et al.*, A novel inhibitor of the STAT3 pathway induces apoptosis in malignant glioma cells both in vitro and in vivo. *Oncogene.* **26**, 2435-2444 (2007).

268. S. Ibrahem *et al.*, STAT3 paradoxically stimulates beta-catenin expression but inhibits beta-catenin function. *Int. J. Exp. Pathol.* **95**, 392-400 (2014).

269. S. F. Hussain *et al.*, A novel small molecule inhibitor of signal transducers and activators of transcription 3 reverses immune tolerance in malignant glioma patients. *Cancer Res.* **67**, 9630-9636 (2007).

270. Y. Zhang *et al.*, Noninvasive photoacoustic microscopy of living cells in two and three dimensions through enhancement by a metabolite dye. *Angew. Chem. Int. Ed Engl.* **50**, 7359-7363 (2011).

271. Motifolio Biology Bundle-Toolkit. *http://www.motifolio.com/* **2015**.

272. Chemicon international, TRAPEZE® Telomerase Detection Kit from Chemicon (Millipore, Billerica, MA, USA). *https://de.scribd.com/document/238427242/TRAPeze-Manual-S7700* download: 08/**2016**.

273. N. W. Kim, F. Wu, Advances in quantification and characterization of telomerase activity by the telomeric repeat amplification protocol (TRAP). *Nucleic Acids Res.* **25**, 2595-2597 (1997).

274. R. A. Weinberg, in (Garland Science, , ed. 1, 2007).

275. P. S. Rachakonda *et al.*, TERT promoter mutations in bladder cancer affect patient survival and disease recurrence through modification by a common polymorphism. *Proc. Natl. Acad. Sci. U. S. A.* **110**, 17426-17431 (2013).

276. P. Chomczynski, N. Sacchi, Single-step method of RNA isolation by acid guanidinium thiocyanate-phenol-chloroform extraction. *Anal. Biochem.* **162**, 156-159 (1987).

277. K. J. Livak, T. D. Schmittgen, Analysis of relative gene expression data using real-time quantitative PCR and the 2(-Delta Delta C(T)) Method. *Methods.* **25**, 402-408 (2001).

278. M. Simon *et al.*, TERT promoter mutations: a novel independent prognostic factor in primary glioblastomas. *Neuro Oncol.* **17**, 45-52 (2015).

279. B. Heidenreich *et al.*, TERT promoter mutations and telomere length in adult malignant gliomas and recurrences. *Oncotarget.* **6**, 10617-10633 (2015).

280. D. Lotsch *et al.*, Prognostic significance of telomerase-associated parameters in glioblastoma: effect of patient age. *Neuro Oncol.* **15**, 423-432 (2013).

281. E. K. Nduom *et al.*, PD-L1 expression and prognostic impact in glioblastoma. *Neuro Oncol.* **18**, 195-205 (2016).

282. L. Wang *et al.*, Immune sculpting of norepinephrine on MHC-I, B7-1, IDO and B7-H1 expression and regulation of proliferation and invasion in pancreatic carcinoma cells. *PLoS One.* **7**, e45491 (2012).

283. K. Abiko *et al.*, PD-L1 on tumor cells is induced in ascites and promotes peritoneal dissemination of ovarian cancer through CTL dysfunction. *Clin. Cancer Res.* **19**, 1363-1374 (2013).

284. D. Massi *et al.*, PD-L1 marks a subset of melanomas with a shorter overall survival and distinct genetic and morphological characteristics. *Ann. Oncol.* **25**, 2433-2442 (2014).

285. X. L. Zhang *et al.*, The tumor-stroma ratio is an independent predictor for survival in nasopharyngeal cancer. *Oncol. Res. Treat.* **37**, 480-484 (2014).

286. M. Marzec *et al.*, Oncogenic kinase NPM/ALK induces through STAT3 expression of immunosuppressive protein CD274 (PD-L1, B7-H1). *Proc. Natl. Acad. Sci. U. S. A.* **105**, 20852-20857 (2008).

287. J. Yang *et al.*, Unphosphorylated STAT3 accumulates in response to IL-6 and activates transcription by binding to NFkappaB. *Genes Dev.* **21**, 1396-1408 (2007).

288. Z. Yu, W. Zhang, B. C. Kone, Signal transducers and activators of transcription 3 (STAT3) inhibits transcription of the inducible nitric oxide synthase gene by interacting with nuclear factor kappaB. *Biochem. J.* **367**, 97-105 (2002).

289. Y. Yoshida *et al.*, Interleukin 1 activates STAT3/nuclear factor-kappaB cross-talk via a unique TRAF6- and p65-dependent mechanism. *J. Biol. Chem.* **279**, 1768-1776 (2004).

290. T. E. Battle, D. A. Frank, The role of STATs in apoptosis. *Curr. Mol. Med.* **2**, 381-392 (2002).

291. H. Lee *et al.*, Persistently activated Stat3 maintains constitutive NF-kappaB activity in tumors. *Cancer. Cell.* **15**, 283-293 (2009).

292. H. H. Assi *et al.*, Preclinical characterization of signal transducer and activator of transcription 3 small molecule inhibitors for primary and metastatic brain cancer therapy. *J. Pharmacol. Exp. Ther.* **349**, 458-469 (2014).

293. X. Zhou *et al.*, STAT3 inhibitor WP1066 attenuates miRNA-21 to suppress human oral squamous cell carcinoma growth in vitro and in vivo. *Oncol. Rep.* **31**, 2173-2180 (2014).

294. K. Chiba *et al.*, Cancer-associated TERT promoter mutations abrogate telomerase silencing. *Elife.* **4**, 10.7554/eLife.07918 (2015).

295. C. Chen *et al.*, TERT promoter mutations lead to high transcriptional activity under hypoxia and temozolomide treatment and predict poor prognosis in gliomas. *PLoS One.* **9**, e100297 (2014).

296. D. Xu, J. Dwyer, H. Li, W. Duan, J. P. Liu, Ets2 maintains hTERT gene expression and breast cancer cell proliferation by interacting with c-Myc. *J. Biol. Chem.* **283**, 23567-23580 (2008).

297. E. Oztas *et al.*, Association Between Human Telomerase Reverse Transcriptase Gene Variations and Risk of Developing Breast Cancer. *Genet. Test. Mol. Biomarkers.* **20**, 459-464 (2016).

298. Z. Y. Li, Y. L. Dong, Y. Feng, Z. Zhang, X. Z. Cao, Polymorphisms in the telomerase reverse transcriptase promoter are associated with risk of breast cancer: A meta-analysis. *J. Cancer. Res. Ther.* **12**, 1040-1044 (2016).

299. S. Natesan, V. M. Rivera, E. Molinari, M. Gilman, Transcriptional squelching re-examined. *Nature.* **390**, 349-350 (1997).

300. Y. Maida *et al.*, Direct activation of telomerase by EGF through Ets-mediated transactivation of TERT via MAP kinase signaling pathway. *Oncogene.* **21**, 4071-4079 (2002).

301. F. W. Huang *et al.*, TERT promoter mutations and monoallelic activation of TERT in cancer. *Oncogenesis.* **4**, e176 (2015).

302. A. F. Vallarelli *et al.*, TERT promoter mutations in melanoma render TERT expression dependent on MAPK pathway activation. *Oncotarget.*(2016).

303. J. I. Park *et al.*, Telomerase modulates Wnt signalling by association with target gene chromatin. *Nature.* **460**, 66-72 (2009).

304. H. Wang *et al.*, Analysis of the activation status of Akt, NFkappaB, and Stat3 in human diffuse gliomas. *Lab. Invest.* **84**, 941-951 (2004).

305. P. A. Robe *et al.*, In vitro and in vivo activity of the nuclear factor-kappaB inhibitor sulfasalazine in human glioblastomas. *Clin. Cancer Res.* **10**, 5595-5603 (2004).

306. A. B. Heimberger *et al.*, Incidence and prognostic impact of FoxP3+ regulatory T cells in human gliomas. *Clin. Cancer Res.* **14**, 5166-5172 (2008).

307. P. E. Fecci *et al.*, Increased regulatory T-cell fraction amidst a diminished CD4 compartment explains cellular immune defects in patients with malignant glioma. *Cancer Res.* **66**, 3294-3302 (2006).

308. A. El Andaloussi, M. S. Lesniak, An increase in CD4+CD25+FOXP3+ regulatory T cells in tumor-infiltrating lymphocytes of human glioblastoma multiforme. *Neuro Oncol.* **8**, 234-243 (2006).

309. L. M. Francisco, P. T. Sage, A. H. Sharpe, The PD-1 pathway in tolerance and autoimmunity. *Immunol. Rev.* **236**, 219-242 (2010).

310. A. M. Intlekofer, C. B. Thompson, At the bench: preclinical rationale for CTLA-4 and PD-1 blockade as cancer immunotherapy. *J. Leukoc. Biol.* **94**, 25-39 (2013).

311. M. Preusser, A. S. Berghoff, W. Wick, M. Weller, Clinical Neuropathology mini-review 6-2015: PD-L1: emerging biomarker in glioblastoma? *Clin. Neuropathol.* **34**, 313-321 (2015).

312. Y. Liu *et al.*, PD-L1 expression by neurons nearby tumors indicates better prognosis in glioblastoma patients. *J. Neurosci.* **33**, 14231-14245 (2013).

313. Y. Li *et al.*, Role of soluble programmed death-1 (sPD-1) and sPD-ligand 1 in patients with cystic echinococcosis. *Exp. Ther. Med.* **11**, 251-256 (2016).

314. Z. Zheng *et al.*, Level of circulating PD-L1 expression in patients with advanced gastric cancer and its clinical implications. *Chin. J. Cancer Res.* **26**, 104-111 (2014).

Abstract

Glioblastoma multiforme (GBM) is the most common malignant brain tumor in adults, characterized by a poor prognosis of about 15 months. Several genomic alterations including reactivation of *telomerase reverse transcriptase (TERT)* are responsible for telomerase reactivation GBM aggressiveness. In this respect, activating point mutations within the *TERT* promoter are detected in approximately 80% of GBM samples. Recent studies demonstrated that telomerase is not only restricted to chromosomal elongation, but may also have a broad variety of non-canonical functions. Accordingly, *TERT* promotes several signaling pathways including the nuclear factor (NFκB) axis, which in turn promotes activation of the signal transducer and activator of transcription 3 (STAT3) cascade. Moreover, 88% of all GBM cases are characterized by overexpression of the immune-regulator programmed death ligand 1 (PD-L1). Based on this knowledge, the present thesis focused on the association between non-canonical functions of TERT and suspected higher tumor aggressiveness of *TERT* promoter mutated (MUT) GBM.

This study analyzed differences in endogenous TERT expression levels of nine GBM cell culture models according to their *TERT* promoter mutation status. Furthermore, the expression profiles of the NFκB, STAT3 as well as PD-L1 signaling cascades were tested. Accordingly, the NFκB pathway was inhibited using QNZ or Bay-11-082, while STAT3 signaling was blocked with WP1066 or STATTIC. The inhibitory potential of these drugs towards their targets and connected pathways as well as towards telomerase reactivation was tested. mRNA and protein expression was analyzed by Western blots and quantitative real-time PCR, respectively. *TERT* promoter and telomerase activity was investigated performing luciferase reporter assays and TRAP assays, respectively. Finally, levels of PD-L1 and phosphorylated STAT3 were additionally evaluated in patient-derived tissue samples by immunohistochemistry analyses.

TERT promoter MUT cell lines were characterized by significantly higher *TERT* mRNA and protein levels. On the contrary, PD-L1 expression levels were distinctly increased in the wild-type (WT) as compared to MUT GBM cells. Furthermore, the results revealed a considerably more pronounced sensitivity towards NFκB and STAT3 pathway inhibitors in GBM harboring *TERT* promoter mutations than in WT cell lines. Surprisingly, blockade of either NFκB or STAT3 pathway resulted in concomitant inhibition of the respective other pathway as well. The inhibitory potential on the NFκB as well as on the STAT3 pathway is highly dependent on the *TERT* promoter mutation status in GBM. Inhibition of both pathways might represent promising therapeutic targets.

Zusammenfassung

Glioblastoma multiforme (GBM) zeichnet sich durch eine Prognose von nur 15 Monaten aus und ist demnach der bösartigste und außerdem der häufigste Gehirntumor in Erwachsenen. Reakivierung des *telomerase reverse transcriptase (TERT)* Gens geht oft mit Reaktivierung der Telomerase sowie erhöhter Tumoraggressivität einher. 80% der GBM liegen sogenannte aktivierende *TERT* Promoter Mutationen zugrunde. Neben ihrer Funktion in der Chromosomenverlängerung, hat Telomerase noch viele anderen Funktionen. Unter anderem spielt *TERT* in der Aktivierung verschiedener Signalwege, wie beispielsweise die nuclear factor kappa B (NFκB) Kaskade, eine Rolle. Ist die NFκB Achse wiederum aktiviert, stimuliert diese schließlich die signal transducer and activator of transcription 3 (STAT3) Kaskade. Des Weiteren exprimieren 88% aller GBM Fälle den Immunregulator programmed death ligand 1 (PD-L1). Davon ausgehend beschäftigt sich diese Studie mit den neu-definierten Funktionen von *TERT* und deren Zusammenhang mit der vermutlich erhöhten Tumoraggressivität in *TERT* Promoter mutierten (MUT) GBM.

Neun GBM Zelllinien wurden auf etwaige Unterschiede bezüglich TERT Expressionslevels in Bezug auf ihren *TERT* Promoter Status analysiert. Außerdem wurden die Expressionsmuster der entsprechenden NFκB, STAT3 und PD-L1 Signalwege getestet. Dementsprechend wurde QNZ oder Bay-11-082 als Inhibitor des NFκB Signalweges eingesetzt. Der STAT3 Signalachse wurde jedoch mit WP1066 oder STATTIC inhibiert. Schlussendlich wurden die inhibitorischen Effekte der Chemotherapeutika getestet. mRNA und protein Expression wurde durch Western Blot und quantitative real-time PCR getestet und die *TERT* Promoter und Telomerase Aktivität wurde durch Luciferase Reporter Assays und TRAP Assays analysiert. Unsere Resultate wurden abschließend zusätzlich immunohistochemisch überprüft.

GBM Zelllininen mit einem MUT *TERT* Promoter exprimierten signifikant mehr *TERT* mRNA und Protein. Die PD-L1 Expression war jedoch besonders in den Wildtyp (WT) Modellen erhöht. Die MUT Tumoren hatten außerdem ein auffallend hohes Toleranzlevel gegenüber den NFκB und STAT3 Inhibitoren. Überraschenderweise führte Blockade der NFκB oder der STAT3 Kaskade außerdem zur gleichzeitigen Inhibierung des jeweilig anderen Signalweges. Der *TERT* Promoter Status hat großen Einfluss auf die Inhibition des NFκB und STAT3 Signalachsen. Besonders eine Blockade beider Signalwege könnte zukünftige Therapiemöglichkeit darstellen.